



Speculative Study of Rotating Nanofluids Over a Stretching Surface



By

Aziz Ur Rehman

**Department of Mathematics
Quaid-i-Azam University, Islamabad
PAKISTAN
2017**



D
M.T
1423

Speculative Study of Rotating Nanofluids Over a Stretching Surface



By

Aziz Ur Rehman

Supervised

By

Prof. Dr. Sohail Nadeem

**Department of Mathematics
Quaid-i-Azam University, Islamabad
PAKISTAN
2017**



Speculative Study of Rotating Nanofluids Over a Stretching Surface



By

Aziz Ur Rehman

A Dissertation Submitted in the partial fulfillment of
the requirements for the degree of

DOCTOR OF PHILOSOPHY

IN

MATHEMATICS

Supervised By

Prof. Dr. Sohail Nadeem

**Department of Mathematics
Quaid-i-Azam University, Islamabad
PAKISTAN
2017**





Speculative Study of Rotating Nanofluids Over a Stretching Surface



By

Aziz Ur Rehman

**Department of Mathematics
Quaid-i-Azam University, Islamabad
PAKISTAN
2017**



P
MHT
1423

Speculative Study of Rotating Nanofluids Over a Stretching Surface



By

Aziz Ur Rehman

Supervised

By

Prof. Dr. Sohail Nadeem

**Department of Mathematics
Quaid-i-Azam University, Islamabad
PAKISTAN
2017**



Speculative Study of Rotating Nanofluids Over a Stretching Surface



By

Aziz Ur Rehman

*A Dissertation Submitted in the partial fulfillment of
the requirements for the degree of*

DOCTOR OF PHILOSOPHY

IN

MATHEMATICS

Supervised By

Prof. Dr. Sohail Nadeem

**Department of Mathematics
Quaid-i-Azam University, Islamabad
PAKISTAN
2017**



Infinite Hearty Dedications

To

*The Most Beloved, our Heart and Soul, the Last Prophet &
The only cause of creation of the whole Universe*

Hazrat Muhammad ﷺ

Due to Whom

The Creature was Disclosed

The Prime Secret of

The Universe that

Who is its

CREATOR



Acknowledgement

All admirations to *Almighty Allaah*, the most Gracious and the most Merciful, who created this universe, blessed us with His guidance and help in each and every step of my life and provided us with the idea to discover.

I am humbly grateful to Him who blessed us with the beloved and the last prophet, the only cause of creation of the whole universe, Sayyad ul Awwaleen and Sayyad ulAakhireen,

Sahib-e-Holy Quran *حَضْرَتِ مُحَمَّدٍ ﷺ* who is forever source of guidance and knowledge of secrets for humanity.

I express my deepest and heart-felt gratitudes to my loving parents who brought me up and filled my heart with the

true affection of *رَسُولِ اللَّهِ ﷺ* which made it easy for me to follow the true spirit of Islam.

I am really grateful to my respected teachers specially Mr. Abid Hussain whose cooperation and motivation geared me up to take admission in number one ranked university of Pakistan.

I am most thankful to my supervisor Prof. Dr. Sohail Nadeem for his guidance, patience, sympathetic behaviour and encouragement for me to work hard with keen interest.

I am thankful to the Chairman Department of Mathematics Prof. Dr. Muhammad Yousaf Malik for always caring me and providing necessary facilities to complete my thesis.

My love and gratitude from the core of my heart to all my class fellows and friends specially Dr. Rashid Mehmood Raja, Dr. Hashim, Dr. Aman Ullah, Dr. Hina Sadaf, Dr. Shagufta, Dr. Farzana, Dr. Tanveer Jamal Chishti and Dr. Zahoor Hussain.

I am thankful to my caring brothers, sisters and my life fellow Abdul Rahim, Khateeb Ur Rehman, Younas Rehman, Abdul Rehman , Nisar Fatima, Noor Fatima, Kaniz Fatima and Nasreen Akhtar for their prayers, support and encouragement.

I am thankful to my loving sons and daughters Muhammad Khalil Ur Rehman, Muhammad Mujeeb Ur Rehman, Muhammad Haseeb Ur Rehman, Samee Ur Rehman, Muhammad Ajmal, Abdul Nasir, Abdul Qadir, Abdullah Rahim, Saeeda, Hifza, Ghausia and Sobia who have always given me love, care and cheer and whose sustained hope in me led me to where I stand today.

May Almighty Allah shower His choicest blessing and prosperity on all those who assisted me in any way during completion of my thesis.

Author's Declaration

I **Aziz Ur Rehman** hereby state that my PhD thesis titled

“Speculative Study of Rotating Nanofluids Over a Stretching Surface”

is my own work and has not been submitted previously by me for taking any degree from this University

Quaid-i-Azam University Islamabad

Or anywhere else in the country/world.

At any time if my statement is found to be incorrect even after my Graduate the university has the right to withdraw my PhD degree.

Name of Student:



Aziz Ur Rehman

Date: 08-02-
-2017

Plagiarism Undertaking

I solemnly declare that research work presented in the thesis titled

“Speculative Study of Rotating Nanofluids Over a Stretching Surface”

is solely my research work with no significant contribution from any other person. Small contribution/help wherever taken has been duly acknowledged and that complete thesis has been written by me.

I understand the zero tolerance policy of the HEC and University

Quaid-I Azam University Islamabad

towards plagiarism. Therefore I as an Author of the above titled thesis declare that no portion of my thesis has been plagiarized and any material used as reference is properly referred/cited.

I undertake that if I am found guilty of any formal plagiarism in the above titled thesis even after award of PhD degree, the University reserves the rights to withdraw/revoke my PhD degree and that HEC and the University has the right to publish my name on the HEC/University Website on which names of students are placed who submitted plagiarized thesis.

Student /Author Signature : 

Name : **Aziz Ur Rehman**



CERTIFICATE

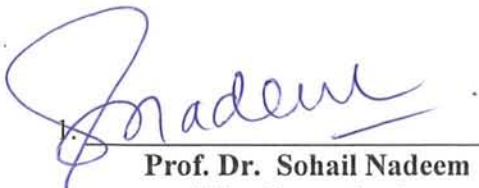
Speculative Study of Rotating Nanofluids Over a Stretching Surface

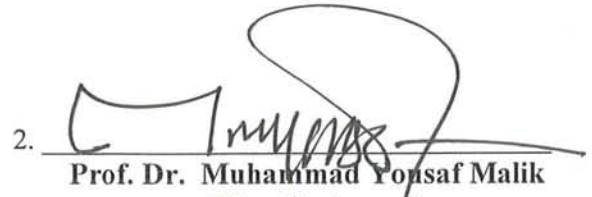
By


AZIZ UR REHMAN

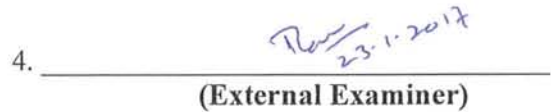
A DISSERTATION SUBMITTED IN THE PARTIAL FULFILLMENT OF THE
REQUIREMENTS FOR THE DEGREE OF
DOCTOR OF PHILOSOPHY

We accept this dissertation as conforming to the required standard

1. 
Prof. Dr. Sohail Nadeem
(The Supervisor)

2. 
Prof. Dr. Muhammad Yousaf Malik
(The Chairman)

3. 
(External Examiner)
Dr. Rahmat Ellahi
Associate Professor, I.I.U,
Islamabad

4. 
(External Examiner)
Dr. Tanvir Akbar Kiani
Assistant Professor, C.I.I.T,
Islamabad

**Department of Mathematics
Quaid-i-Azam University, Islamabad
PAKISTAN
2017**

Contents

Nomenclature	3
1 Introduction	6
1.1 Overview.....	6
1.2 Background.....	7
1.3 Methodology.....	10
1.4 Objectives.....	11
2 Boundary layer flow of rotating two phase nanofluid over a stretching surface	14
2.1 Introduction.....	14
2.2 Mathematical formulation.....	14
2.3 Physical quantities of interest.....	18
2.4 Solution method.....	18
2.5 Results and discussion.....	19
2.6 Conclusions	30
3 Partial slip effects on a rotating flow of two phase nanofluid over a stretching surface	31
3.1 Introduction.....	31
3.2 Mathematical formulation.....	31
3.3 Solution method	33
3.4 Results and discussion.....	34
3.5 Conclusions.....	48
4 Heat transfer analysis of a ferromagnetic rotating nanofluid over a stretching surface with viscous dissipation	49
4.1 Introduction.....	49
4.2 Mathematical formulation.....	49
4.3 Solution method	51
4.4 Physical quantities of interest	52
4.5 Results and discussion.....	53
4.6 Conclusions.....	68

5 Effects of single and multi-walled carbon nanotubes on water and engine oil based rotating fluids with internal heating	69
5.1 Introduction.....	69
5.2 Mathematical formulation.....	69
5.3 Solution method.....	71
5.4 Physical quantities of interest	74
5.5 Results and discussion.....	75
5.6 Conclusions.....	88
6 Entropy analysis of radioactive rotating nanofluid with thermal slip	90
6.1 Introduction.....	90
6.2 Mathematical formulation.....	90
6.3 Solution method	93
6.4 Physical quantities of interest.....	95
6.4.1 Skin friction and local heat transfer rate.....	95
6.4.2 Entropy generation and Bejan number.....	95
6.5 Results and discussion.....	97
6.6 Conclusions.....	114
7 Slip flow of a chemically reacting rotating hybrid nanofluid with uniform heat source/ sink	116
7.1 Introduction.....	116
7.2 Mathematical formulation.....	116
7.2.1 Governing Eqs.....	117
7.2.2 Relations of effective physical measures.....	117
7.2.3 Similarity relations.....	119
7.3 Physical quantities of interest	120
7.4 Solution method	121
7.5 Results and discussion.....	122
7.6 Conclusions.....	135
References	136

Nomenclature

Symbols	Meanings
Ag, Au	silver and gold nano particles,
a, b	stretching rates in directions of x - and y -axis,
Be	Bejan number,
Br	Brinkman number,
Gp	group parameter ($= Br/\omega$),
Cf_x, Cf_y	coefficients of skin friction in directions of x – axis and y – axis,
C_p	specific heat,
C_w, C_∞	fluid concentration at wall and ambient,
Cu, CuO	Copper, Copper Oxide nano particles,
D	Slip factor,
D_f, D_{nf}, D_{hnf}	mass diffusivity of base fluid, nano fluid and hybrid nano fluid,
$3D$	three dimensional,
Ec	Eckert number,
$f'(\eta), g'(\eta)$	dimensionless velocity modules in directions of x – axis and y – axis,
$H(\eta)$	dimensionless mass concentration,
$K,$	velocity slip,
K_1	chemical reaction of first order,
$K_s, K_f, K_{nf}, K_{hnf}$	thermal conductivity of solid nano particles, base fluid, nano fluid and hybrid nano fluid,
N_f	non-dimensional entropy due to frictions of fluid layers,
N_h	non-dimensional entropy generation due to heat transfer,
Ns	entire non-dimensional entropy,
Nu	Nusselt number,
Pr	Prandtl number,
q_w, q_m	flux at surface due to heat and mass,
Q_0	dimensional heat generation/absorption coefficient,
R	Thermal radiation parameter,
R_c	chemical reaction parameter,
Re	Reynolds number,
S_f	dimensional entropy generation due to fluid friction,



Sc	Schmidt number,
$S_{g,c}$	characteristic entropy rate,
$S_{g,t}$	dimensional entropy rate,
S_h	dimensional entropy due to heat transfer,
T, T_w, T_∞	Temperatures of fluid, surface and free stream,
u, v, w	Cartesian parts of velocity in directions of $x - axis, y - axis$ and $z - axis$,
u_w, v_w	velocity parts at wall,
V	velocity field,
x, y, z	Cartesian parts of velocity,
Greek Codes	
α	stretching ratio parameter ($= b/a$),
$\alpha_f, \alpha_{nf}, \alpha_{hnf}$	thermal diffusivity of base fluid, nanofluid and hybrid nano fluid respectively,
β_R	mean absorption coefficient,
γ	thermal slip parameter,
δ	heat source/sink parameter,
∇^2	Laplace operator,
ξ	the ratio y/x ,
ω	non-dimensional temperature ($= \frac{(T_w - T_\infty)}{T_\infty}$),
σ_e	Stefan-Boltzman constant,
η	dimensionless space variable,
$\theta(\eta)$	dimensionless temperature,
φ	nano particles volumetric fraction,
φ_1, φ_2	Particle volume fraction for nano and hybrid nano fluids,
λ	rotation parameter,
Ω	constant angular velocity,
$\rho_f, \rho_s, \rho_{nf}, \rho_{hnf}$	density of base fluid, solid nano particles, nanofluid and hybrid nano fluid respectively,
$\mu_f, \mu_{nf}, \mu_{hnf}$	dynamic viscosity of base fluid, nano fluid and hybrid nano fluid respectively,
$\nu_f, \nu_{nf}, \nu_{hnf}$	kinematic viscosities of base fluid, nanofluid and hybrid nano fluid,
$(\rho C_p)_s, (\rho C_p)_f, (\rho C_p)_{nf}, (\rho C_p)_{hnf}$	volumetric heat capacity of solid nano particles, base fluid, nanofluid and hybrid nano fluid respectively,
Subscripts	
w	condition at wall,
∞	condition at infinity,

f	base fluid,
nf	nano fluid,
hnf	hybrid nano fluid,
s	solid nano particles,
Superscripts	
$'$, $''$, and $'''$	1^{st} , 2^{nd} and 3^{rd} derivatives with respect to η .

Chapter 1

Introduction

1.1 Overview

A nanoparticle phenomenon is interesting due to the fact that it behaves like a bridge between substance and its atomic/molecular structure. As particles of a material break and approach their nano size, their intrinsic properties change quite dramatically. For example, platinum which is an inert element at macro scale becomes a catalyst at nano scale. Similarly silicon insulators become conductors and gold which is solid, inert and yellow, changes itself to a red liquid with unusual catalytic properties at nano scale. Thus nanoparticles have considerably different attributes as compared with particles of the same species and not in nanoscale.

Nanotechnology is a rising science of today. It is growing swiftly and has numerous applications in almost every discipline of our daily life e.g., in medicines, foodstuff, chemicals, automobiles and many more. Nanoparticle study is at present a part of focused and systematized notice due to a comprehensive range of its possible uses in biomedical, optical, material manufacturing, transportation, energy and electronic fields.

Since last two decades nanofluids have attracted the attention of scientists as an important research topic. Due to their intense use in extremely progressive technical and biomedical devices such as in nuclear reactors, microchips cooling, radiators and nano medications etc., nano particles are quite useful. Being comprised of low molecular mass but high thermal conductance, these fluids are considered to be vastly effective cooling managers.

Rotating fluids flow over elastic stretching sheets are fairly apparent in several industrial procedures such as material management conveyers, extrusion of elastic panes and cooling of an endless metal plate in a cooling bath. Furthermore in procedure of glass blowing, constant moulding, and turning of fibres also consist of the rotary flow over enlarging surface. The role of stretching is of vital importance as can be visualized in above procedures in which flow of heat and mass is produced by the stretching practice of surface. The properties preferred for a result of such a progression would mostly rest on two features. First is the rate of cooling of fluid and second is the rate of stretching surface boundary on which liquid is lying. During the engineering procedure, heat transmission level at the stretched surface is deeply perceived as it is much related with the quality of the ultimate product. Keeping in view this outstanding feature of the

modern day development engineering, numerous investigators have concentrated their attention on this precise area of study.

1.2 Background

Crane [1] originated by discussing over the fluid flowing over a stretching plate while Siddappa *et al.* [2] used the Rivlin-Ericksen flow of the fluid passing over an enlarging plate. Rajagopal *et al.* [3] investigated the exceptionality of flow due to Navier-Stokes fluid over a stretching surface. Wang [4] discussed three dimensional flow due to an infinite stretching flat surface. Rajagopal and co-workers [5] examined viscoelastic fluid flow due to stretching sheet. They considered second order fluid and concluded that skin friction co-efficient decreases with increasing elasticity of sheet. Ariel [6] discussed the same problem by stretching the sheet in two lateral directions and proposed that the homotopy perturbation method (HPM) can be applied even when flow is administered by a boundary value problem comprising of more than one differential Eq.. The same problem was solved by Ullah *et al.* [7]. They used extended optimal homotopy asymptotic method and concluded that results are better approximations of HPM.

Eastman and Choi [8] in 1995 introduced the concept of nanofluid. They involved Hamilton and Crosser model [9] to rise thermal conductance of fluid by using Copper nano subdivisions and concluded the fact that if a nanoparticle-based fluid with three times thermal conductance as compared to corresponding conventional base fluid is used, the heat transfer level will be doubled without an increase in pumping power. While to extract the same result with conventional fluid by the same equipment, the pumping power will have to increase by a factor of almost 10. This outstanding idea brought a revolution in manufacturing industries related with heat transferring phenomenon. The same author [10] explored the potential benefits of nanofluids in another study. The comprehensive work on convective transport in nanofluids was presented by Buongiorno [11]. Wong *et al.* [12] proposed applications of nano fluids in several fields in his novel study.

Cho *et al.* [13] deliberated convective transportation of dispersed liquids with submicron particles of metallic oxide. Wang [14] inclusively analysed thermal conductance of mixture of fluid and nanoparticles. Xuan *et al.* [15-17] experimentally inspected the heat transfer enhancement and transport properties of nanoparticle-based fluids. They exhibited the flow characteristics and convective heat transfer using Cu-nanoparticles with base fluid as water and discovered that inclusion of nanoparticles significantly enhances heat transfer and the

nanoparticle-based fluid has greater heat transfer compare to pure water for identical Reynolds number. Lee et al. [18] suggested the usage of nano particles in advanced cooling systems. "How heat transfer is enhanced by nanofluid?", The answer to this question was satisfactorily produced by Kakac et al. [19]. Convective endpoint conditioned Casson nanofluid was inspected by Nadeem et al. [20]. Aladag et al. [21] focused on viscosity of Al_2O_3 -water and Cu-water nano fluids at low concentration. Bachok et al. [22-24] considered the shrinking / stretching sheet to analyse the stagnation-point flow of nanofluid. Same authors extended their work for a moving plate and permeable stretching/shrinking sheet for nanofluids and also discussed the slip flow and heat transfer of nanofluid. Vajravelua et al. [25] adopted perturbation technique to examine non-linear coupled system for three dimensional rotating flow. An analysis of steady state rotating flow due to a stretching plane has been scrutinised by Nazar et al. [26]. Kumari et al. [27- 29] rationalized the transient rotating flow with MHD and power-law fluids over stretching plane and analysed the heat transmission in magneto hydro dynamic stagnation point flow. Zaimi et al. [30] focused on rotating viscoelastic fluid on a stretching surface. Wang [31] exposed stretching surface on a rotating fluid and concluded that perturbation solution for small and large rotation parameter λ meets well with the exact solution. In [32-34] computational techniques with their applications including midpoint integration with Richardson extrapolation are discussed in detail. Anderson [35] introduced the slip flow past a stretching surface. Aminreza and Sharma [36,37] analysed the variations in flow/ heat transfer due to partial slip of nano fluids. Rosensweig [38] involved alternating magnetic field to study the heating magnetic fluid. Nadeem et al. [39] used convective surface to numerically investigate Walter's B type nano fluid assuming MHD oblique flow. Debnath [40] scrutinized unsteady MHD boundary layers in a rotating flow. Sheikholeslami et al. [41] numerically discovered increasing capability of heat transfer of nano particles suspended in base fluid water within a finite domain while Takhar et al. [42] analysed the same flow for unsteady case. Subhas and Bataller [43,44] used non-uniform heating source in a viscoelastic flow caused by stretching sheet. Unsteady MHD flow/ heat transfer with viscous dissipation caused by a stretching surface was studied by Kumaran et al. [45]. Sheikholeslami et al. [46] used stretching and porous surfaces to investigate MHD rotating viscous flow and heat transfer in between the surfaces. Khan et al. [47] inspected stagnation point flow and heat transfer over stretching surface assumed by ferrofluid. In [48] Fehlberg introduced and explained his famous Runge-Kutta Fehlberg numerical method of order four five commonly known as RKF45 numerical scheme. In [49,50] various numerical methods including Runge-Kutta Fehlberg scheme with shooting process are introduced. Timofeeva et al. [51] used

alumina nanofluids to investigate how the shapes of a particle affect thermo physical properties of nanofluids. In [52-62] authors examined the effects on flow and heat transfer when traditional nano particles were replaced by carbon nano tubes. In [63-66] spectral Quasilinearisation method are introduced to solve the non-linear boundary value problems. Ishak et al. [67] discovered the effects of radiations on thermal boundary of micro polar fluid. While Aziz [68] analysed thermal slip boundary layer flow over a flat surface. Mukhopadhyay [69, 70] used exponential stretching sheet and found that slip and suction decrease velocity profile while thermal radiations increase the temperature profile. Kameswaran *et al.* [71] inspected nano fluid flows over a permeable surface with radiated heat transference. Nadeem et al. [72] thoroughly discussed the variations in stagnation point flow of MHD nano fluid due to slip and thermal radiations over a stretching plane.

During transfer of heat/ mass a system is considered to be an ideal and no energy losses are assumed. But in actual practice every system has a disorder and hence energy losses up to a certain degree. Quantifying the amount of this disorder is necessary and utmost in order to get our preferred results. The quantity representing absence of thermal energy of a system for transformation in to useful mechanical work is called entropy of the system which always rises with time according to second law of thermodynamics. Explanatory collection about entropy generation has been offered by Bejan [73]. Sheikholeslami *et al.* [74] engaged Lattice Boltzmann method to discuss the generation of entropy in MHD nanofluid. Mahmoodi *et al.* [75] considered thermal radiations to analyze the hydrothermal behaviour and entropy generation in a regenerative cooling channel.

Ellahi *et al.* [76] discussed the shape effects of copper nano particles on entropy generation. Recently, Butt *et al.* [77] studied MHD three-dimensional flow to dig out the effects of entropy generation and heat transference for viscous fluid caused by a stretching surface. Suriya et al. [78] explored the enigma of hybrid nano fluid flow for three dimensional stretching surfaces. Ferdows et al. [79] examined the facts how order of chemical reaction influences the flow produced by a linearly stretching sheet.



1.3 Methodology

The aim of present thesis is to study rotating nanoparticle-based fluids and explore their effects on flow, heat transfer, skin frictions and surface heat flux and analyse results in the presence and absence of magnetic field, partial slip, viscous dissipation etc. The analysis is carried out under the assumption of the fluid being steady, incompressible and in the absence of the pressure gradient. Suitable similarity transformations will be applied to convert the nonlinear system of partial differential Eqs. in to a nonlinear system of ordinary differential Eqs. along with boundary conditions. Nonlinear ordinary differential Eqs. thus obtained will be solved numerically through efficient software MAPLE and MATLAB by numerical schemes which are briefly introduced as follow:

1: *Midpoint scheme collaborated with Richardson extrapolation*

The scheme uses two approximations of an integral to compute a third more accurate estimate. It can refine the results swiftly when applied on even very erroneous basic schemes like rectangular or trapezoidal rule. The computational software Maple uses midpoint incorporation as base scheme and Richardson extrapolation as promptly enhancing pattern. In few solved problems, condition on semi-infinite domain $[0, \infty)$ has been replaced with domain $[0, L]$ where $L < \infty$ and 'L' is picked such that for $L < M < \infty$ no considerable change is observed in any result for any 'M'. A mesh size of 0.001 is fixed to achieve an accuracy of 10^{-6} . The method is well explained in [32-34].

2: *Runge – Kutta Fehlberg process with shooting technique*

The Runge-Kutta-Fehlberg process of fourth-fifth order belongs to well-known series of RK-methods. The scheme was developed by a German mathematician Ervin Fehlberg in his publication of 1969 and was labelled as RKF45 method i.e., Runge Kutta method of order $O(h^4)$ with an error estimate of order $O(h^5)$. This method is well described in [48] and its computer application are pronounced in [49, 50].

3: *Chebyshev pseudo – spectral method*

This numerical scheme is used after linearizing using the quasi-linearization method. The quasi-linearization method is a one term Taylor series expansion approach based on the assumption that the difference between values of approximate functions at successive iterations is small. This method is explained in [63-66].

Graphical results for velocity profile, temperature profile and other sundry parameters and tabular results for skin frictions and surface heat flux are computed and discussed with physical interpretation. At the end of various units a comparison has been observed between our results and those with already exist in published literature under the same physical conditions confirming authentication of our numerical results.

1.4 Objectives

In spite of the much significance of nanoparticle-based rotating fluids over stretching surfaces in vital scientific fields like biomedical, optical and electronics, these have not been focused a lot. The present study is an effort to explore theoretically the mysteries and enigmas concerned with these fields and to present a comprehensive and ideal model from the analysis. The current investigation will provide precise enquiry deducing the results for conventional fluid too. The controlling parameters of energy losses will be highlighted with their contribution in the system equipment.

The unit wise division of the thesis is presented as below.

Chapter 2 deals with the incompressible steady flow of a nano fluid. Two phase nanofluid model is engaged for the purpose. Copper and Titanium oxide are used in nano scale while pure water is used as base fluid. After involving scaling transformations, partial differential Eqs. of momentum and energy together with boundary conditions are converted in to coupled non-linear ordinary differential Eqs.. An extremely trusted numerical midpoint scheme collaborated with Richardson extrapolation is launched on *MAPLE* for the solution. *MAPLE* considers mid-point integration as base pattern and Richardson extrapolation as enhancing pattern. Velocity and temperature profiles of the flow are constituted. Physical quantities like tangential stress and local heat transfer rate are computed. All these are analyzed and the results have been compared with those of previously published literature to validate the numerical scheme. The outcomes of this unit are **published in Journal of Heat Transfer Asian Research. 2016, 45 (3), 285-298.**

In **chapter 3**, main theme is to explore effects of partial slip on flow/ heat transfer in rotating nano fluid. Mathematical differential Eqs. along with endpoints conditions characterizing the flow/ heat transfer are transformed from their partial status to ordinary status by invoking suitable similarity transformations. The solutions are extracted numerically by launching midpoint integration collaborated with Richardson extrapolation. The physical quantities of interest have been computed in the absence of each of slip, nano particle volume fraction and

rotation. This work is **published in Current Nanoscience. 2014, 10(6), 846-854.**

Chapter 4 is allied with the magnetohydrodynamic flow of a rotating nano fluid over a stretching surface with viscous dissipation. Two types of base fluids i.e., pure water and kerosene are involved. These base fluids are engaged one by one with nano particles of Barium Ferrite ($BaO.6Fe_2O_3$) in order to form a nano fluid. Solutions of nonlinear system of ordinary differential Eqs. are extracted by RKF45 Method with shooting technique. Effects of magnetism and viscous dissipation on the flow/ heat transfer and tangential stress for the steady rotating nano fluids are investigated. Results have been compared with those in previously published literature. **This problem is submitted for publication in Journal of Applied Nano Sciences.**

The main determination of **chapter 5** is to explore the effects of single and multi-walled carbon nano tubes on flow/ heat transfer in a rotating nano fluid over an enlarging sheet. The study also includes how heat source/sink affects the surface heat flux. Pure water and engine oil are considered as base fluids. Single walled and multiwalled carbon nano tubes are used thus to constitute four types of nano fluids. Related partial differential Eqs. of momentum/ energy are converted in to non-dimensional ordinary differential Eqs. together with boundary conditions. The non-dimensional ordinary differential Eqs. have been solved numerically by the *Chebyshev pseudo – spectral* process after linearizing using quasi-linearization method. The effects of necessary parameters on flow/ heat transfer are expressed through graphs/ tables for both single and multi-walled carbon nano tubes. **Reviews of this problem are submitted in Advanced Powder Technology.**

Chapter 6 is presented for entropy analysis of radioactive rotating nanofluid with thermal slip. Three types of nano particles namely Copper Oxide, Silver and Gold are used to constitute nano fluid along with base fluid water. Conforming Navier Stokes' Eqs. of mass, momentum and energy with essential limitations are transformed in to a set of differential Eqs. which are non-linear and ordinary in nature by employing suitable transformations. Richardson extrapolation is employed to enhance the solutions extracted by the midpoint integration numerical scheme. Effects of sundry parameters on flow, heat transfer, entropy generation/ Bejan number are presented via graphs/ tables. Further, the results are compared for validation. **This work is published in Journal of Applied Thermal Engineering.**

Chapter 7 is organized to study the effects of rotation, particle volume fractions, velocity slip, and chemical reaction on hybrid nano fluid flow due to a stretching surface. Differential Eqs. representing the flow, energy and concentration of the hybrid nano fluid flow are converted from



their partial status to ordinary status via similarity transformations. The numerical results are obtained using Runge-Kutta Fehlberg scheme coupled with shooting technique. Expressions for physical measures of interest like tangential stress, rates of heat/ mass transfer at the surface are arranged and tabulated and finally all results are discussed. **Matter of the study has been submitted for publication in Nonlinear Analysis: Real World Applications.**

Chapter 2

Boundary layer flow of rotating two phase nanofluid over a stretching surface

2.1 Introduction

An analysis is carried out to discover the influence on flow/ heat transfer of rotating nanofluid over a stretching surface. Two phase nanofluid model is engaged for the present study. Two types of nano particles, namely Copper (Cu) and Titanium Oxide TiO_2 are used in our analysis with water as the base fluid. The governing system of partial differential Eqs. along with the corresponding boundary conditions are presented and then transformed into a set of non-linear ordinary differential Eqs. by launching appropriate similarity transformations. The system of Eqs. is solved numerically by means of an iterative procedure called the midpoint integration scheme along with Richardson extrapolation [32 – 34]. The results for flow and heat transfer characteristics are presented through graphs against nanoparticle volume fraction and rotation parameter for both types of nanoparticles. Quantities of physical interest such as local skin friction coefficients and local heat flux rate at the stretching surface are computed and analyzed. Numerical values for skin frictions and local heat flux rate are computed in the absence of nano particle volume fraction and rotation. These are compared with existing published literature and are found to be in very good agreement.

2.2 Mathematical formulation

Consider an incompressible water based nanofluid lying in the region $Z \geq 0$. The boundary $Z = 0$ is elastic and is being linearly stretched by two equal and opposite forces in the direction of $x - axis$ with the condition that the origin remains fixed. The fluid is rotating about the $Z - axis$ with a constant angular velocity Ω .

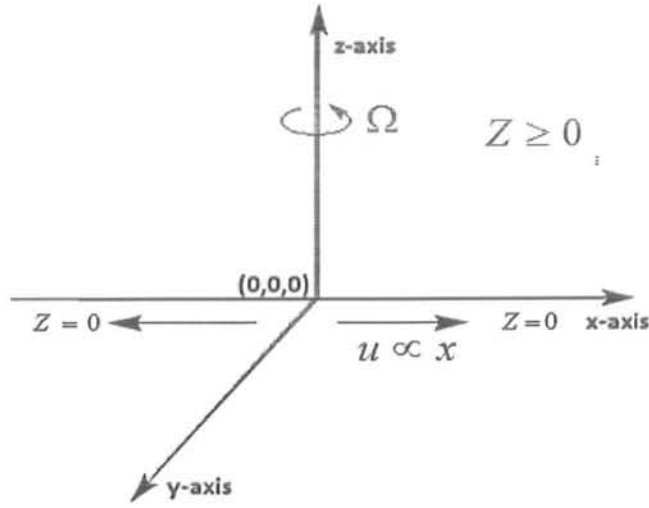


Fig. (2.1): A non-dimensional description of the problem

The velocity and temperature functions are defined as

$$\mathbf{V}(x, y, z) = (u(x, y, z), v(x, y, z), w(x, y, z)), \quad (2.1)$$

$$\mathbf{T} = \mathbf{T}(x, y, z). \quad (2.2)$$

The governing Eqs. of mass, momentum and energy are defined as

$$\text{div } \mathbf{V} = 0, \quad (2.3)$$

$$\rho_f \frac{d\mathbf{V}}{dt} = \text{div } \mathbf{S} + \mathbf{J} \times \mathbf{B}, \quad (2.4)$$

$$(\rho c)_f \frac{dT}{dt} = -\text{div } \mathbf{q}. \quad (2.5)$$

Here \mathbf{V} is the velocity, ρ_f is the fluid density, \mathbf{S} is the stress tensor, \mathbf{J} is the Lorentz's force, \mathbf{B} is magnetic field, \mathbf{T} is the temperature, $\mathbf{q} = -k\nabla T$ is the heat flux, k is the thermal conductivity.

The stress tensor \mathbf{S} for a Newtonian fluid can be written as

$$\mathbf{S} = -p\mathbf{I} + \mu\mathbf{A}_1, \quad (2.6a)$$

where p denotes the pressure, \mathbf{I} is the identity matrix and \mathbf{A}_1 is the first Rivlin Erickson tensor

given by

$$A_1 = \nabla V + (\nabla V)^t, \quad (2.6b)$$

where $(\nabla V)^t$ is the transpose of ∇V .

Invoking Eqs. (2.1), (2.2) and (2.6 a, b) in Eqs. (2.3)-(2.5), we have [23, 24, 31]

$$\frac{\partial u}{\partial x} + \frac{\partial v}{\partial y} + \frac{\partial w}{\partial z} = 0, \quad (2.7)$$

$$u \frac{\partial u}{\partial x} + v \frac{\partial u}{\partial y} + w \frac{\partial u}{\partial z} - 2\Omega v = \frac{\mu_{nf}}{\rho_{nf}} \nabla^2 u, \quad (2.8)$$

$$u \frac{\partial v}{\partial x} + v \frac{\partial v}{\partial y} + w \frac{\partial v}{\partial z} + 2\Omega u = \frac{\mu_{nf}}{\rho_{nf}} \nabla^2 v, \quad (2.9)$$

$$u \frac{\partial w}{\partial x} + v \frac{\partial w}{\partial y} + w \frac{\partial w}{\partial z} = \frac{\mu_{nf}}{\rho_{nf}} \nabla^2 w, \quad (2.10)$$

$$u \frac{\partial T}{\partial x} + v \frac{\partial T}{\partial y} + w \frac{\partial T}{\partial z} = \alpha_{nf} \frac{\partial^2 T}{\partial z^2}, \quad (2.11)$$

where u, v and w are usual velocity components in x, y and z directions respectively, Ω is constant angular velocity of the fluid, ρ_{nf} is density of the nanofluid, μ_{nf} is dynamic viscosity of nanofluid, α_{nf} is thermal diffusivity of nanofluid, T is the temperature of the fluid, K_{nf} is thermal conductivity of nanofluid, K_f is thermal conductivity of base fluid. All these are inter connected and related with particle volume fraction φ as defined below [22 – 24,75]

$$\left. \begin{aligned} \rho_{nf} &= \rho_f \left[1 - \varphi + \varphi \left(\frac{\rho_s}{\rho_f} \right) \right], \mu_{nf} = \frac{\mu_f}{(1-\varphi)^{2.5}}, \alpha_{nf} = \frac{K_{nf}}{(\rho C_p)_{nf}}, \\ (\rho C_p)_{nf} &= (\rho C_p)_f \left[1 - \varphi + \varphi \left(\frac{(\rho C_p)_s}{(\rho C_p)_f} \right) \right], \frac{K_{nf}}{K_f} = \frac{K_s + 2K_f - 2\varphi(K_f - K_s)}{K_s + 2K_f + 2\varphi(K_f - K_s)}. \end{aligned} \right\} \quad (2.12a, b)$$

Here $(\rho C_p)_s$ is the volumetric heat capacity of solid nano particles, $(\rho C_p)_f$, $(\rho C_p)_{nf}$ are volumetric heat capacities of base fluid and nanofluid respectively, φ is the particle volume fraction parameter of nano particles and ρ_f , μ_f are respectively the density and dynamic viscosity of base fluid, K_s is thermal conductivity of solid nano particles .

Suggested stretching velocity and surface temperature allocations are

$$\left. \begin{aligned} u &= ax, v = 0, w = 0 \text{ at } z = 0, \\ u &\rightarrow 0, v = 0 \text{ as } z \rightarrow \infty \\ T &= T_w \text{ at } z = 0 \\ T &\rightarrow T_\infty \text{ as } z \rightarrow \infty \end{aligned} \right\} \quad (2.13)$$

Here “ a ” is the constant of proportionality representing the stretching rate, T_w is wall temperature and T_∞ is free stream temperature.

Introducing similarity transformations [31, 37]

$$\left. \begin{aligned} u &= axf'(\eta), v = axh(\eta), w = -\sqrt{av}f(\eta), \\ \eta &= z\sqrt{\frac{a}{\nu}}, \quad \theta(\eta) = \frac{T-T_\infty}{T_w-T_\infty} \end{aligned} \right\} \quad (2.14)$$

Using definitions (2.12a, b) and similarity transformations (2.14), (2.7) is identically satisfied and the Eqs. (2.8) to (2.11) take the form

$$\frac{1}{(1-\varphi)^{2.5}}f'''' + \left(1 - \varphi + \varphi \frac{\rho_s}{\rho_{bf}}\right)(ff'' - f'^2 + 2\lambda h) = 0, \quad (2.15)$$

$$\frac{1}{(1-\varphi)^{2.5}}h'' + \left(1 - \varphi + \varphi \frac{\rho_s}{\rho_{bf}}\right)(fh' - f'h - 2\lambda f') = 0, \quad (2.16)$$

$$\frac{K_{nf}}{K_f}\theta''(\eta) + Pr\left[1 - \varphi + \varphi \frac{(\rho c_p)_s}{(\rho c_p)_f}\right]f\theta'(\eta) = 0. \quad (2.17)$$

In above Eqs., Pr is the Prandtl number and λ is the non-dimensional rotation parameter which are defined as

$$Pr = \frac{(\mu c_p)_f}{K_f}, \quad \lambda = \frac{\Omega}{a}, \quad (2.18)$$

here Ω is the constant angular velocity of rotating fluid with dimension $[T^{-1}]$. It is interesting to note that when we take particle volume fraction parameter of nano particles φ equal to zero, the above Eqs. (2.15) – (2.17) become identical with those of Wang [31].

The boundary conditions (2.13) by using the similarity transformations (2.14) take the following form

$$\left. \begin{aligned} f(0) = 0, \quad f'(0) = 1, \quad f'(\infty) = 0, \\ h(0) = 0, h(\infty) = 0, \theta(0) = 1, \theta(\infty) = 0. \end{aligned} \right\} \quad (2.19)$$

2.3 Physical quantities of interest

We are specifically interested in numerical values of the coefficients of skin frictions and heat flux [23, 37].

$$Cf_x = \frac{\tau_{xz}}{\rho(ax)^2}, \quad Cf_y = \frac{\tau_{yz}}{\rho(ax)^2}, \quad Nu = \frac{xq_w}{K_f(T_w - T_\infty)}, \quad (2.20)$$

where shear stresses τ_{xz} , τ_{yz} and heat flux q_w of the surface are given by

$$\tau_{xz} = \mu_{nf} \left(\frac{\partial u}{\partial z} \right)_{z=0}, \quad \tau_{yz} = \mu_{nf} \left(\frac{\partial v}{\partial z} \right)_{z=0}, \quad q_w = -K_{nf} \left(\frac{\partial T}{\partial z} \right)_{z=0}. \quad (2.21)$$

Using Eqs. (2.12a, b), (2.14) and (2.21) in Eq. (2.20), we get

$$(Re_x)^{\frac{1}{2}} Cf_x = \frac{1}{(1-\varphi)^{2.5}} f''(0), \quad (Re_x)^{\frac{1}{2}} Cf_y = \frac{1}{(1-\varphi)^{2.5}} h'(0), \quad (Re_x)^{-\frac{1}{2}} Nu = \frac{-K_{nf}}{K_f} \theta'(0), \quad (2.22)$$

where $Re_x = \frac{Ux}{\nu_f}$ is the local Reynolds number and Nu is the Nusselt number. Skin friction along x-axis i.e., $(Re_x)^{\frac{1}{2}} Cf_x$, skin friction along y-axis i.e., $(Re_x)^{\frac{1}{2}} Cf_y$ and heat flux $(Re_x)^{-\frac{1}{2}} Nu$ have been computed numerically for both type of nanofluids involved for various values of particle volume fraction φ and rotation parameter λ in Tables (2.2), (2.3) and (2.4).

2.4 Solution method

The governing system of coupled non-linear differential Eqs. (2.15) – (2.17) along with boundary conditions (2.19) have been solved numerically by using computational mathematical software Maple. Maple uses a combination of mid-point integration as a basic scheme and Richardson extrapolation as an enhancing scheme. The semi-infinite domain $[0, \infty)$ of the governing system has been replaced by a suitable finite domain $[0, L]$ where L must be large enough that after which no considerable variation in the velocity and temperature profiles can be observed. A mesh size of 0.001 is chosen to be satisfactory for a convergence criterion of 10^{-6}

in all numerical computations.

2.5 Results and discussion

This section is dedicated to interpret the graphical outputs of the unit. Figs. (2.2) to (2.14) have been developed to meet the purpose. Figs. (2.2) and (2.3) represent the x-component of non-dimensional velocity $f'(\eta)$ against nano particles volume fraction φ as well as rotation parameter λ for *Cu – water* and *TiO₂ – water* nanofluids respectively. It can be found from these Figs. that an increase in rotation parameter λ results in a prominent monotonic decrease in the similarity velocity $f'(\eta)$ for both types of nano fluids. Moreover it is observed that an increase in particle volume fraction φ , decreases the velocity component $f'(\eta)$ for *Cu – water* case but results in a small increase for the *TiO₂ – water* nanofluid case. This is because of the fact that *TiO₂* nano particles are smaller in density than the *Cu* nanoparticles, so their inclusion in the base fluid offers less resistance comparatively. Figs. (2.4) and (2.5) describe the relation between the similarity variable η and the non-dimensional z – component of velocity $f(\eta)$ against φ and λ . One can judge that increasing the rotation parameter λ decreases the z – component of velocity $f(\eta)$ for *Cu – water* as well as *TiO₂ – water* nanofluids. The physical reasoning behind it is that an increased rotation rate results in greater collision of the nanoparticles and base fluid particles which consequently opposes the velocity profile $f(\eta)$. The effect of particle volume fraction φ on z – component of velocity $f(\eta)$ is quite similar to as it has on the velocity profile $f'(\eta)$. Figs. (2.6) and (2.7) show that the y – component of similarity velocity $h(\eta)$ decreases with an increase in rotation parameter λ for both types of fluids. However increasing the particle volume fraction φ decreases the velocity profile $h(\eta)$ for the *Cu – water* case but the effects of particle volume fraction φ on *TiO₂ – water* are not very prominent. Figs. (2.8) and (2.9) illustrate that temperature profile $\theta(\eta)$ increases gradually with an increase in rotation parameter λ for *Cu* as well as *TiO₂ – water* nanofluids. Figs.

(2.10) and (2.11) show that temperature profile $\theta(\eta)$ increases with an increase in nano particle volume fraction φ . This is because of the fact that nano particles have higher thermal conductivity and lower specific heat compare to the base fluid water which results in an increase in the temperature profile $\theta(\eta)$. Here from Figs. (2.8) to (2.11) we observe that the Prandtl number Pr decreases the thermal boundary layer of both nanofluids. Quantities of physical interest such as local skin friction co-efficient along x and $y - axis$ and local heat flux are plotted through Figs. (2.12) to (2.14). It is found from these Figs. that local skin friction co-efficient along $x - axis$ i.e. $(-1/(1 - \varphi)^{2.5})f''(0)$, similarly along y -axis $(-1/(1 - \varphi)^{2.5})h'(0)$ and local heat flux rate i.e. $(-K_{nf}/K_f)\theta'(0)$ increases with an increase in particle volume fraction φ . This follows from the fact that inclusion of tiny nanoparticles within the fluid results in its thickening which leads to an increase in corresponding local skin friction co-efficient. Also more the inclusion of particle volume fraction φ is, greater the rate of local heat flux will be because of the greater thermal conductivity of the nanoparticles which better aids the fluid to transfer heat swiftly across the surface. It can also be observed from these Figs. that with an increase in rotation parameter λ , magnitude of the local skin friction along x as well as $y - axis$ increases but it has an opposite influence on local heat flux rate i.e. it causes a decrease in the local heat flux rate. Since it is observed that with an increase in rotation parameter λ , temperature profile $\theta(\eta)$ also increases so with this increase the corresponding heat flux rate at the wall obviously decreases. *Table (2.1)* gives the thermo physical properties of the constituents of the nanofluids discussed here in the study. These values are taken from the existing published literature. In *Table (2.2)*, it is obvious that for a fixed value of φ , absolute value of local skin friction $(-1/(1 - \varphi)^{2.5})f''(0)$ increases with an increase in λ . The behavior remains the same if we fix λ and change the values of particle volume fraction φ . However, for any fixed pair (φ, λ) , absolute local skin friction due to Cu is always greater than that due to TiO_2

which is because of the higher density of the Cu nanoparticles compared to TiO_2 nanoparticles. In *Table (2.3)* local skin friction $(-1/(1 - \varphi)^{2.5})h'(0)$ along the y -axis has been calculated for various distinct pairs of (φ, λ) . It is quite evident from this table that an increase in φ and λ absolutely increases the skin friction along $y - axis$. Noticeably, for any pair (φ, λ) , skin friction due to Cu is absolutely greater than that due to TiO_2 . From *Table (2.4)* we can see that the local heat flux decreases as the rotation parameter λ increases. On the other hand an increase in nanoparticle volume fraction φ increases the local heat flux rate because of the higher thermal conductivity and lower specific heat of the nano fluid compared to the base fluid. Moreover for any fixed pair (φ, λ) , local heat flux due to Cu is always greater than that due to TiO_2 . This is because TiO_2 has lower thermal conductivity as compared with Cu and hence allows the removal of heat rapidly. In *Table (2.5)*, comparison of skin frictions for $\varphi = 0$ with the previously existing literature has been presented. It is quite obvious from these results that current values of skin frictions $f''(0)$ and $h'(0)$ are in decent agreement with those obtained by Nazar et al. [26], and Kumari et al. [28] which authenticates the validity of our applied numerical scheme.



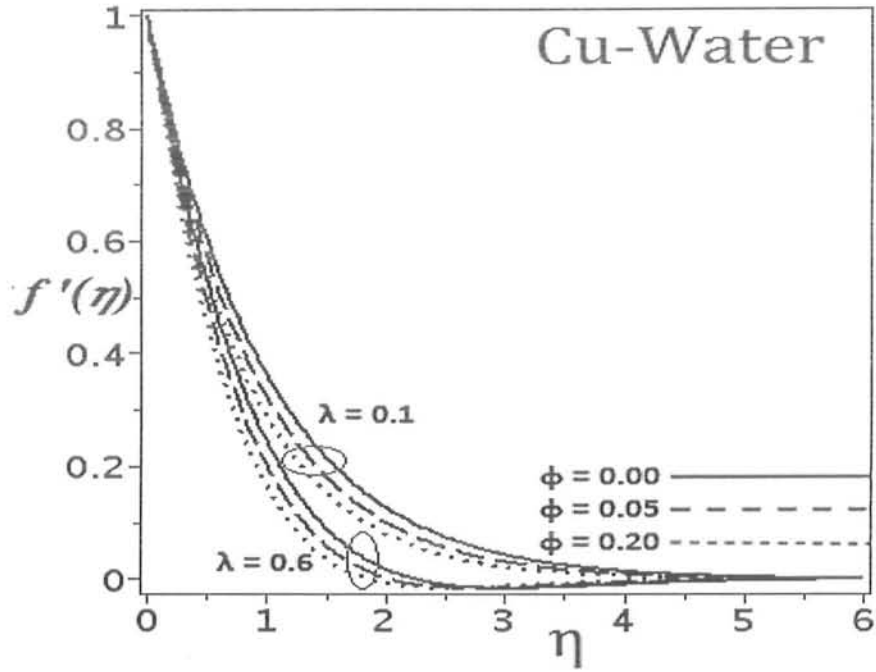


Fig. (2.2): Velocity profile $f'(\eta)$ against η with variations in ϕ and λ for *Cu – water* nanofluid

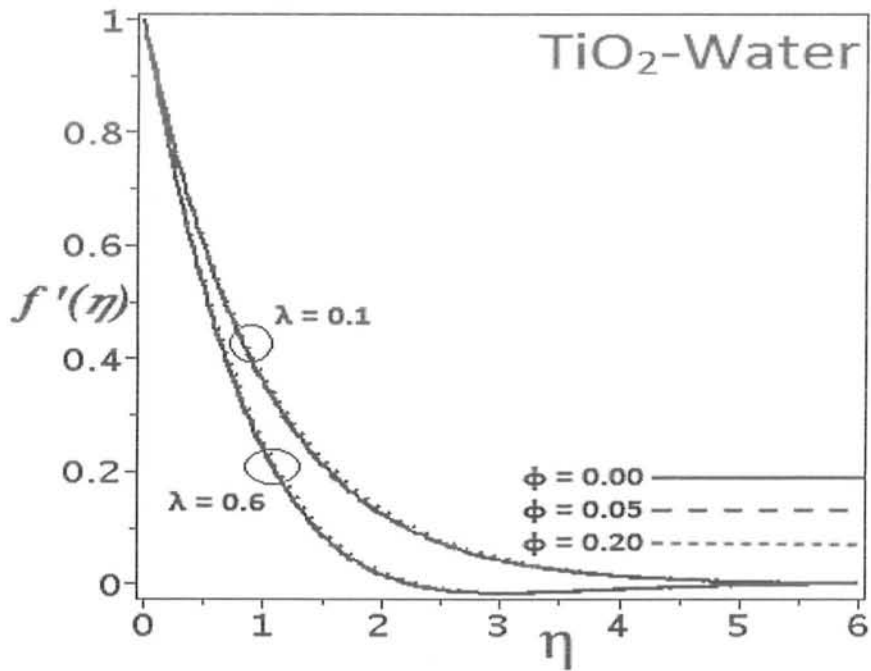


Fig. (2.3): Velocity profile $f'(\eta)$ against η with variations in ϕ and λ for *TiO₂ – water* nanofluid

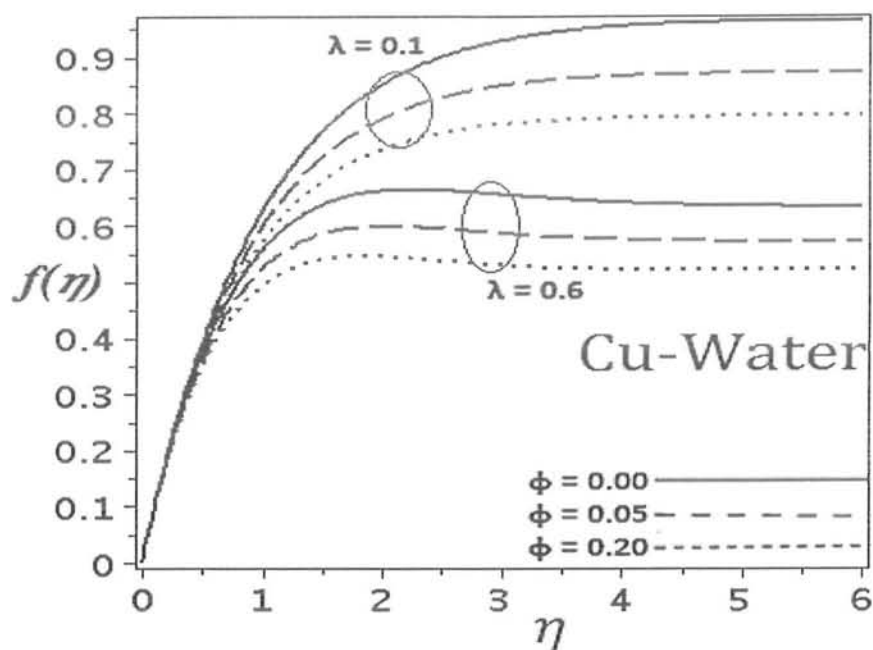


Fig. (2.4): Velocity profile $f(\eta)$ against η with variations in ϕ and λ for Cu – water nanofluid

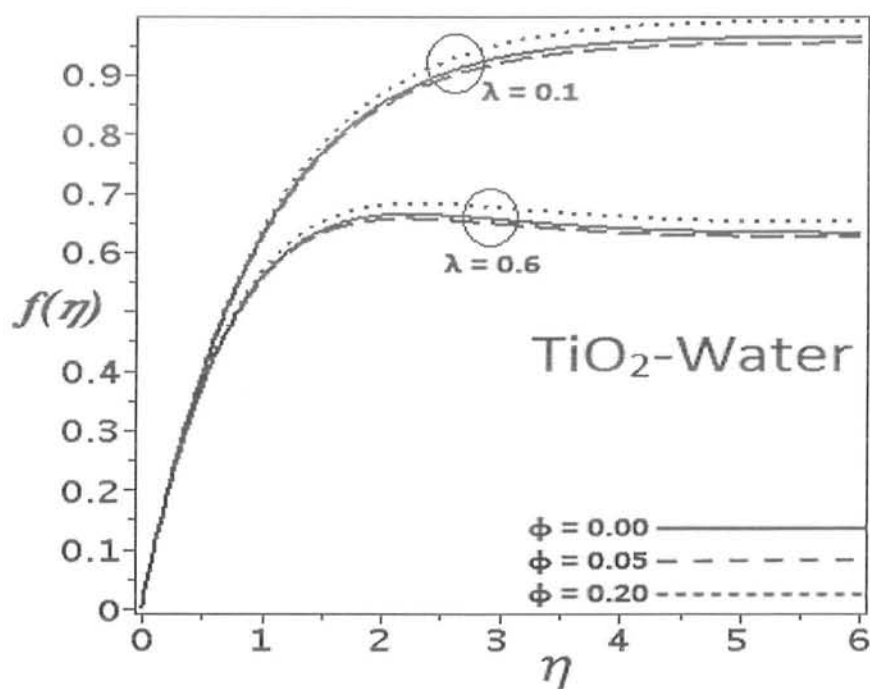


Fig. (2.5): Velocity profile $f(\eta)$ against η with variations in ϕ and λ for TiO₂ – water nanofluid

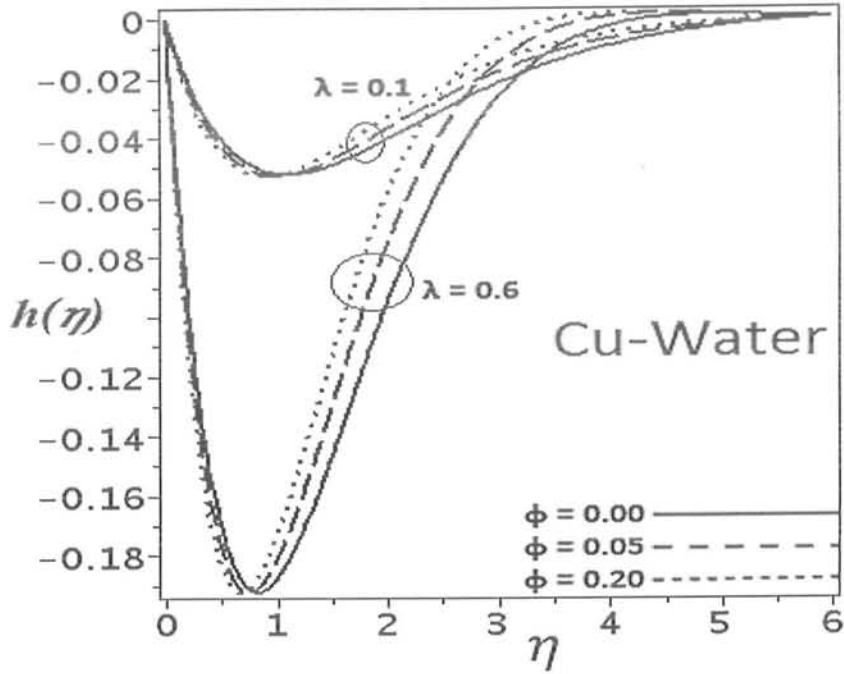


Fig. (2.6): Velocity profile $h(\eta)$ against η with variations in ϕ and λ for $\text{Cu} - \text{water}$ nanofluid

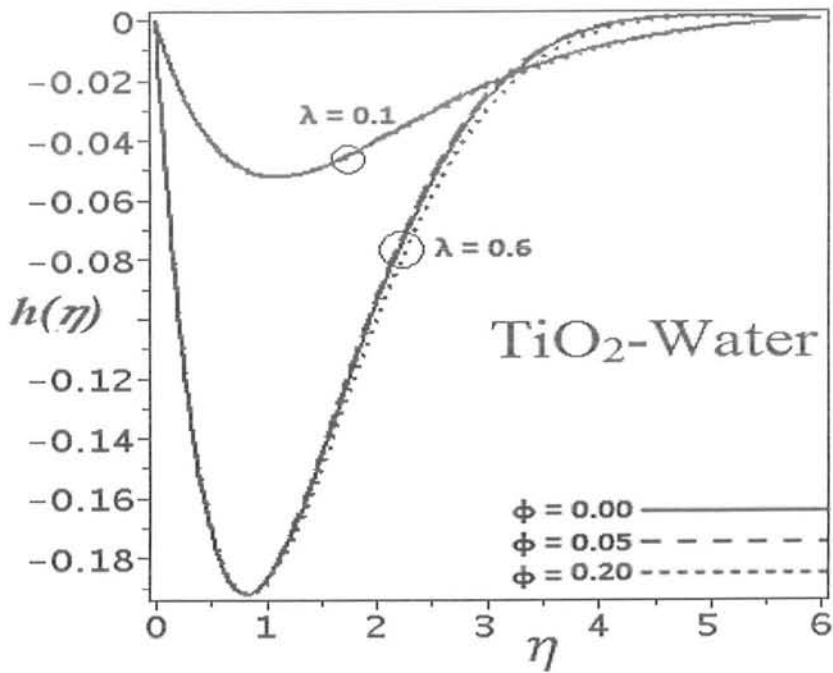


Fig. (2.7): Velocity profile $h(\eta)$ against η with variations in ϕ and λ for $\text{TiO}_2 - \text{water}$ nanofluid

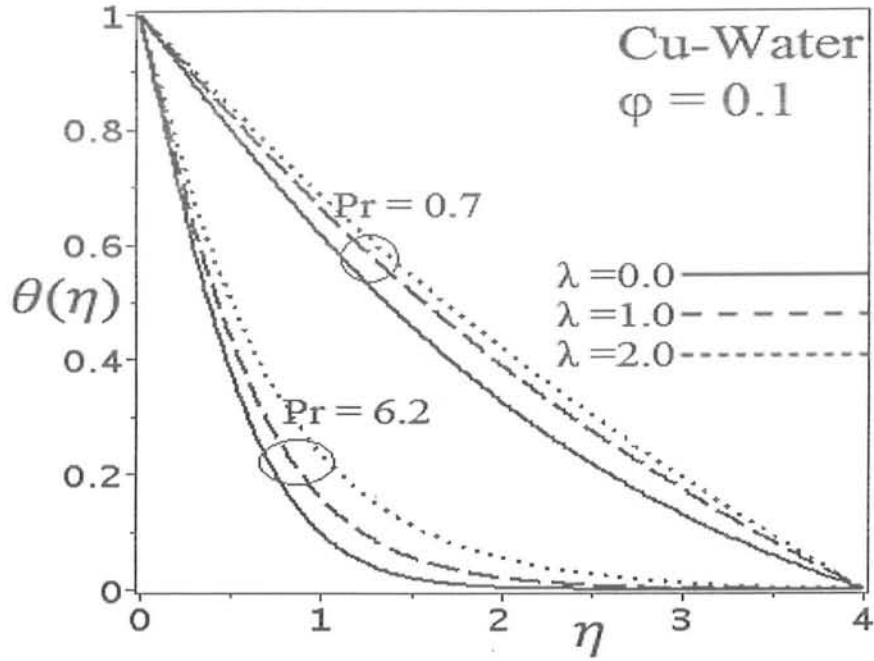


Fig. (2.8): Temperature profile $\theta(\eta)$ versus rotation parameter λ and Prandtl number Pr for $Cu - water$ nanofluid

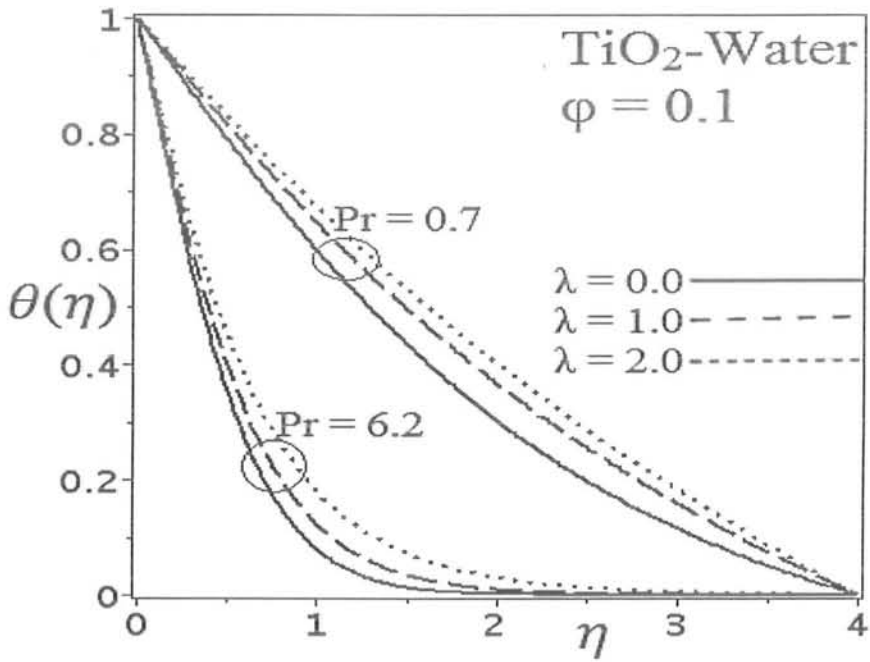


Fig. (2.9): Temperature profile $\theta(\eta)$ versus rotation parameter λ and Prandtl number Pr for $TiO_2 - water$ nanofluid

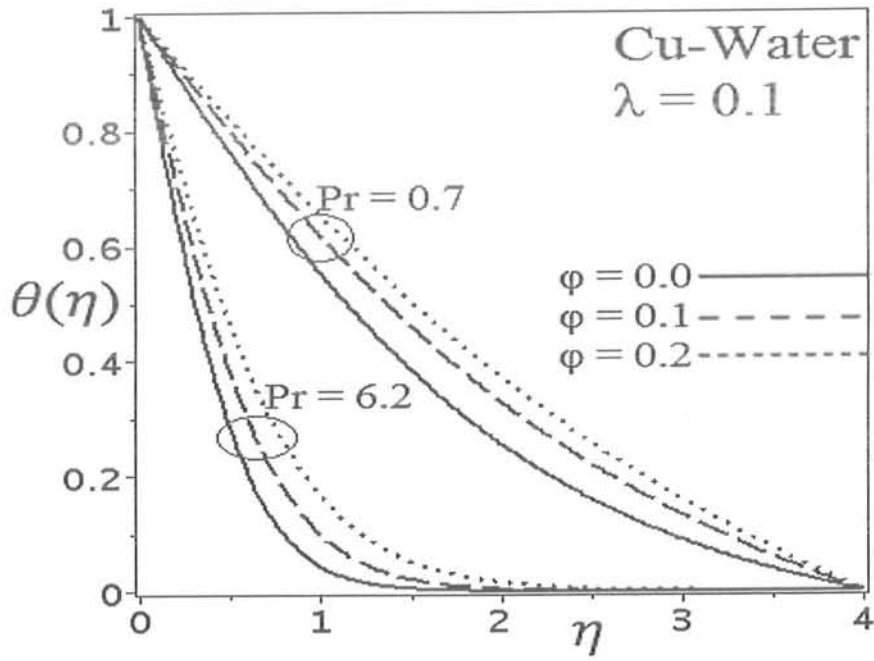


Fig. (2.10): Temperature profile $\theta(\eta)$ versus particle volume fraction ϕ and Prandtl number Pr for $Cu - water$ nanofluid

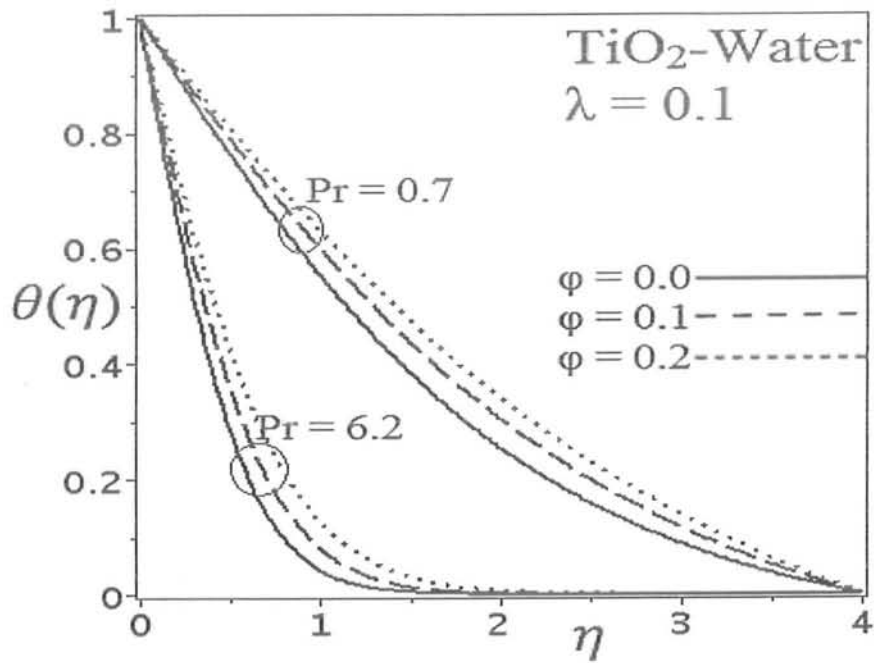


Fig. (2.11): Temperature profile $\theta(\eta)$ against particle volume fraction ϕ and Prandtl number Pr for $TiO_2 - water$ nanofluid

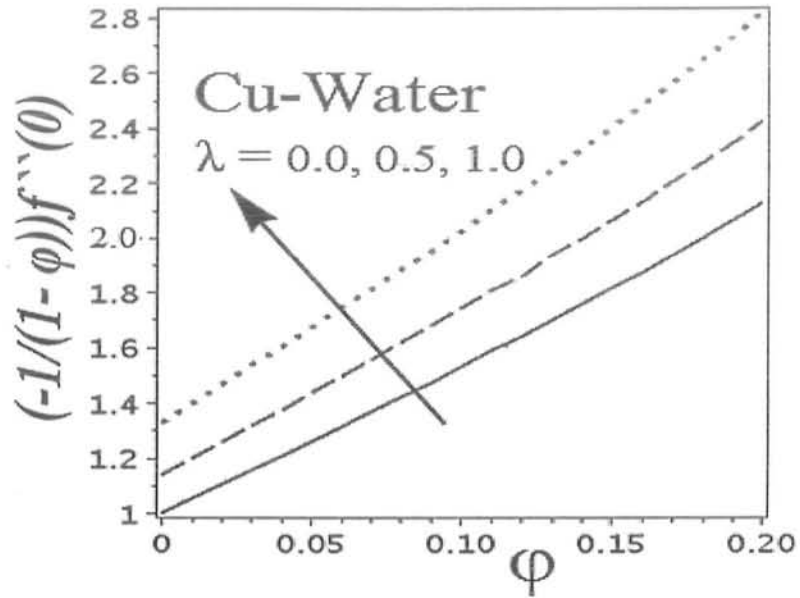


Fig. (2.12): Effects of particle volume fraction ϕ and rotation parameter λ on skin friction along x - axis for Cu - water nanofluid

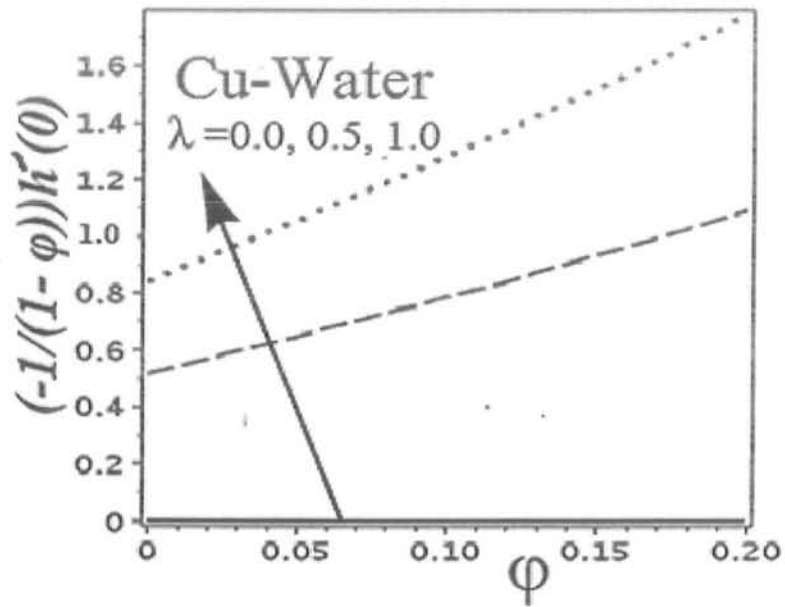


Fig. (2.13): Effects of particle volume fraction ϕ and rotation parameter λ on skin friction along y - axis for Cu - water nanofluid

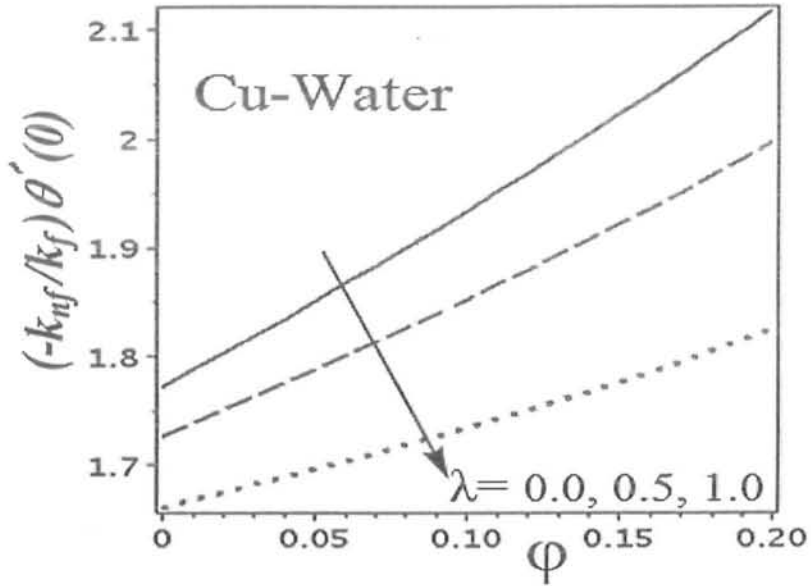


Fig. (2.14): Effects of particle volume fraction ϕ and rotation parameter λ on local heat flux for *Cu – water* nanofluid

Table 2.1: Thermo physical properties of constituents as used by *Bachok et al* [23]

Properties \ Constituents	H_2O	<i>Cu</i>	TiO_2
Density ρ (Kg/m^3)	997.1	8933	4250
Specific Heat C_p ($J/Kg.k$)	4179	385	686.2
Thermal Conductivity K ($W/m.K$)	0.613	400	8.9538

Table 2.2 : Numerical values of local skin friction $(-1/(1 - \phi)^{2.5})f''(0)$

ϕ	$\lambda = 0.0$	$\lambda = 0.5$	$\lambda = 1.0$	$\lambda = 2.0$
<i>Cu – water Nanofluid</i>				
0.00	1.000000	1.138381	1.325029	1.652352
0.01	1.052169	1.197769	1.394154	1.738553
0.10	1.528754	1.740304	2.025644	2.526040
0.20	2.127835	2.422286	2.819443	3.515932
<i>TiO₂ – Water Nanofluid</i>				
0.00	1.000000	1.138381	1.325029	1.652352
0.01	1.029028	1.171425	1.363491	1.700316
0.10	1.313734	1.495529	1.740735	2.170750
0.20	1.699044	1.934159	2.251282	2.807419

Table 2.3 : Numerical values of local skin friction $(-1/(1 - \varphi)^{2.5})h'(0)$

φ	$\lambda = 0.0$	$\lambda = 0.5$	$\lambda = 1.0$	$\lambda = 2.0$
<i>Cu – water Nanofluid</i>				
0.00	0.000000	0.512760	0.837098	1.287259
0.01	0.000000	0.539510	0.880769	1.354414
0.10	0.000000	0.783884	1.279718	1.967903
0.20	0.000000	1.091069	1.781207	2.739074
<i>TiO₂ – Water Nanofluid</i>				
0.00	0.000000	0.512760	0.837098	1.287259
0.01	0.000000	0.527644	0.861397	1.324625
0.10	0.000000	0.673630	1.099724	1.691115
0.20	0.000000	0.871202	1.422267	2.187109

Table 2.4 : Numerical values of local heat flux $(-K_{nf}/K_f) \theta'(0)$ ($Pr = 6.2$)

φ	$\lambda = 0.0$	$\lambda = 0.5$	$\lambda = 1.0$	$\lambda = 2.0$
<i>Cu – water Nanofluid</i>				
0.00	1.770948	1.725631	1.660286	1.533487
0.01	1.786502	1.737767	1.667333	1.530826
0.10	1.933636	1.851932	1.733394	1.515517
0.20	2.117373	1.996168	1.824178	1.534170
<i>TiO₂ – Water Nanofluid</i>				
0.00	1.770948	1.725631	1.660286	1.533487
0.01	1.786226	1.739291	1.671547	1.540139
0.10	1.926447	1.864745	1.775176	1.603259
0.20	2.093007	2.015334	1.902422	1.689698

Table 2.5: Comparison of absolute values of $f''(0)$ and $h'(0)$ extracted for conventional fluid ($\varphi = 0$)

λ	<i>Nazar et al [26]</i>		<i>Kumari et al [28]</i>		<i>Present Results</i>	
	$f''(0)$	$h'(0)$	$f''(0)$	$h'(0)$	$f''(0)$	$h'(0)$
0.0	1.0000	0.0000	1.00000	0.00000	1.00000	0.00000
0.5	1.1384	0.5128	1.13838	0.51275	1.138381	0.512760
1.0	1.3250	0.8371	1.32503	0.83709	1.325029	0.837098
2.0	1.6523	1.2873	1.65235	1.28724	1.652352	1.287259



2.6 Conclusions

The steady flow over a stretching surface of rotating *Cu – water* nanofluid and *TiO₂ – water* nanofluid is investigated. Some of the main conclusions are indicated here underneath:

- Rotation decreases the linear velocity of both nano fluids.
- Rotation and particle volume fraction both uplift the thermal boundary of both fluids. This propagation is prominent for *Cu – water* compared to *TiO₂ – water* fluid.
- Skin friction for $\varphi = 0$ exhibits good agreement for the case of viscous fluid which confirms the precise accuracy of our current computations.
- Local skin frictions increase with increase in angular velocity Ω and particle volume fraction of nano particles φ . This increase due to *Cu – water* nanofluid is absolutely greater than the respective growth due to *TiO₂ – water* nanofluid.
- In both nanofluids, absolute heat flux of the surface rises up with a rise in particle volume fraction φ but it drops with rotation increased.
- Prandtl number Pr decreases thermal boundary of both nanofluids.
- Category of nanofluid selected for heat transfer purpose is of crucial importance. To achieve the optimal results, *Cu – water* nanofluid is preferred.

Chapter 3

Partial slip effects on a rotating flow of two phase nanofluid over a stretching surface

3.1 Introduction

In this unit an analysis is performed to discuss the slip-flow of a rotating nanofluid over a stretching sheet. The two phase nanofluid model is used for the physical modeling of the system. By means of similarity transformations governing partial differential equations are reduced into three coupled ordinary differential equations. These are then solved numerically using mid-point integration scheme along with Richardson extrapolation via Maple. Influence of non-dimensional slip parameter K , rotation parameter λ and nanoparticle volume fraction φ on velocity, temperature and skin frictions have been tabularized, demonstrated graphically and discussed. In order to validate our numerical scheme, skin friction coefficients and local heat flux are computed in the absence of slip and rotation and they are found to be in very good agreement with the previously published literature.

3.2 Mathematical formulation

Let us consider an incompressible nanofluid lying on flat elastic sheet in the region $Z \geq 0$ and is rotating about $z - axis$ with constant angular velocity Ω . Two equal and opposite forces are applied along the $x - axis$ so that the sheet is being stretched with a speed $U(x)$ proportional to the distance from the origin $x = 0$. The nanofluid is only partially imitating the stretching sheet, and the fluid motion is thus subjected to the slip – flow conditions.

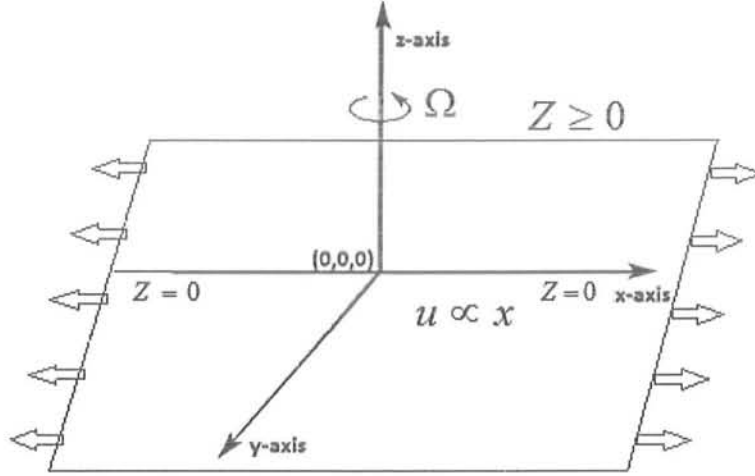


Fig. (3.1): Geometry of the problem

The Eqs. governing the system after neglecting pressure gradient and viscous dissipation are

$$\frac{\partial u}{\partial x} + \frac{\partial v}{\partial y} + \frac{\partial w}{\partial z} = 0, \quad (3.1)$$

$$u \frac{\partial u}{\partial x} + v \frac{\partial u}{\partial y} + w \frac{\partial u}{\partial z} - 2\Omega v = \frac{\mu_{nf}}{\rho_{nf}} \nabla^2 u, \quad (3.2)$$

$$u \frac{\partial v}{\partial x} + v \frac{\partial v}{\partial y} + w \frac{\partial v}{\partial z} + 2\Omega u = \frac{\mu_{nf}}{\rho_{nf}} \nabla^2 v, \quad (3.3)$$

$$u \frac{\partial w}{\partial x} + v \frac{\partial w}{\partial y} + w \frac{\partial w}{\partial z} = \frac{\mu_{nf}}{\rho_{nf}} \nabla^2 w, \quad (3.4)$$

$$u \frac{\partial T}{\partial x} + v \frac{\partial T}{\partial y} + w \frac{\partial T}{\partial z} = \alpha_{nf} \frac{\partial^2 T}{\partial z^2}, \quad (3.5)$$

Thermo physical properties of base fluid and nano fluid are interconnected via nano particle volume fraction φ as [21, 23, 24, 37, 51]

$$\left. \begin{aligned} \rho_{nf} &= \rho_f \left[1 - \varphi + \varphi \left(\frac{\rho_s}{\rho_f} \right) \right], & \mu_{nf} &= \frac{\mu_f}{(1-\varphi)^{2.5}}, & \alpha_{nf} &= \frac{K_{nf}}{(\rho C_p)_{nf}}, \\ (\rho C_p)_{nf} &= (\rho C_p)_f \left[1 - \varphi + \varphi \left(\frac{(\rho C_p)_s}{(\rho C_p)_f} \right) \right], & \frac{K_{nf}}{K_f} &= \frac{K_s + 2K_f - 2\varphi(K_f - K_s)}{K_s + 2K_f + 2\varphi(K_f - K_s)}. \end{aligned} \right\} \quad (3.6a, b)$$

where ρ_s is density of solid nano particles.

The corresponding boundary conditions are

$$\left. \begin{aligned} u(x, y, 0) - U &= k v \frac{\partial u}{\partial z}(x, y, 0), \\ v(x, y, 0) &= k v \frac{\partial v}{\partial z}(x, y, 0), \\ w(x, y, 0) &= k v \frac{\partial w}{\partial z}(x, y, 0), \end{aligned} \right\} \quad (3.7)$$

where $U = ax$ is sheet velocity, k is slip length and ν is kinematic viscosity of base fluid.

Utilizing similarity solution of the form [31]

$$\left. \begin{aligned} u &= axf'(\eta), \quad v = axh(\eta), \quad w = -\sqrt{av} f(\eta), \\ \eta &= z \sqrt{\frac{a}{\nu}}, \quad \theta(\eta) = \frac{T - T_\infty}{T_w - T_\infty}, \end{aligned} \right\} \quad (3.8)$$

where η is similarity space parameter.

By using Eq. (3.8) in Eq. (3.1) we observe that mass is conserved.

Invoking Eqs. (3.6a, b) and (3.8) in Eqs. (3.2) - (3.5) we get a system of coupled ordinary differential Eqs. as

$$\frac{1}{(1-\varphi)^{2.5}} f'''' + \left(1 - \varphi + \varphi \frac{\rho_s}{\rho_{bf}}\right) (ff'' - f'^2 + 2\lambda h) = 0, \quad (3.9)$$

$$\frac{1}{(1-\varphi)^{2.5}} h'' + \left(1 - \varphi + \varphi \frac{\rho_s}{\rho_{bf}}\right) (fh' - f'h - 2\lambda f') = 0, \quad (3.10)$$

$$\frac{K_{nf}}{K_f} \theta''(\eta) + Pr \left[1 - \varphi + \varphi \frac{(\rho C_p)_s}{(\rho C_p)_f}\right] f \theta'(\eta) = 0. \quad (3.11)$$

In above Eqs. Rotation parameter λ signifies the relative importance of rotation rate to stretching rate.

Transformed boundary conditions are

$$\left. \begin{aligned} f(0) &= 0, \quad f'(0) = 1 + Kf''(0), \quad f'(\infty) = 0, \\ h(0) &= Kh'(0), \quad h(\infty) = 0, \quad \theta(0) = 1, \quad \theta(\infty) = 0, \end{aligned} \right\} \quad (3.12)$$

where $K = k\sqrt{av}$ is the slip parameter. If $K = 0$, there is no slip i.e., velocity of the fluid and that of the sheet is the same and then boundary conditions (3.12) are reduced to those of Wang [31] and Sharma et al. [37]. If $K \rightarrow \infty$, the surface is stress-free indicating no flow at all.

3.3 Solution method

The system of coupled ordinary differential Eqs. (3.9) to (3.11) along with (3.12) is highly non-linear and has been solved numerically by applying midpoint scheme with Richardson extrapolation via Maple dsolve command. This scheme involves a highly stable numerical algorithm which gives grid independent solutions [32 – 34]. The semi-infinite domain $[0, \infty)$ is replaced with a proper finite domain i.e. $[0, L]$ where $L < \infty$ and must be so properly chosen that the numerical solutions would approach the asymptotic behaviour at infinity. A mesh size of

0.001 was supposed satisfactory for a convergence criterion of 10^{-6} in almost all computations. Pictorial solutions and numerical tables have been produced by launching the above said technique on mathematical software known as "Maple" to achieve all the preferred results.

Physical quantities of our distinctive interest are skin frictions Cf_x along x – axis, Cf_y along y – axis and Nusselt number Nu . These are given by [23,24] as follows

$$Cf_x = \frac{\tau_{xz}}{\rho(ax)^2}, Cf_y = \frac{\tau_{yz}}{\rho(ax)^2}, Nu = \frac{xq_w}{K_f(T_w - T_\infty)}, \quad (3.13)$$

where shear stresses τ_{xz}, τ_{yz} and heat flux q_w of the surface are given by

$$\tau_{xz} = \mu_{nf} \left(\frac{\partial u}{\partial z} + \frac{\partial w}{\partial x} \right)_{z=0}, \quad \tau_{yz} = \mu_{nf} \left(\frac{\partial v}{\partial z} + \frac{\partial w}{\partial y} \right)_{z=0}, \quad q_w = -K_{nf} \left(\frac{\partial T}{\partial z} \right)_{z=0}. \quad (3.14)$$

Using Eqs. (3.8) and (3.14) in (3.13), we obtain

$$(Re_x)^{\frac{1}{2}} Cf_x = \frac{1}{(1-\varphi)^{2.5}} f''(0), (Re_x)^{\frac{1}{2}} Cf_y = \frac{1}{(1-\varphi)^{2.5}} h'(0), (Re_x)^{-\frac{1}{2}} Nu = \frac{-K_{nf}}{K_f} \theta'(0). \quad (3.15)$$

Where $Re_x = \frac{Ux}{\nu_f}$ is the local Reynolds number. Skin friction $(-1/(1-\varphi)^{2.5})f''(0)$ and heat flux $(-K_{nf}/K_f)\theta'(0)$ have been computed numerically for both types of nanofluid using various values of nanoparticle volume fraction φ , slip parameter K and rotation parameter λ in Tables (3.2) and (3.3).

3.4 Results and discussion

This section describes the influence of some important physical parameters such as partial slip parameter K and rotation parameter λ on the velocities and temperature profiles for Cu – water as well as Al_2O_3 – water nano fluids. Graphical results are obtained simultaneously in the presence and absence of nano particles in order to discover their actual influence on these physical quantities. Figs. (3.2) to (3.17) are plotted to meet the purpose. Figs. (3.2) to (3.5) are planned to discover the effects of slip parameter K and rotation parameter λ on velocity profile $f'(\eta)$ for Cu – water and Al_2O_3 – water. It can be perceived from Figs. (3.2) and (3.3)

that increasing the slip parameter K results in a significant drop in the horizontal velocity profile $f'(\eta)$ for both $\text{Cu} - \text{water}$ and $\text{Al}_2\text{O}_3 - \text{water}$ nano fluids. This is due to the fact that in the presence of slip, velocity of the fluid near the sheet does not remain the same as the velocity of the stretching sheet. So with an increase in slip parameter K , slip velocity also increases. This consequently decreases the fluid velocity because in this case pulling of the stretching sheet can only contribute in a partial sense due to the presence of slip factor. The boundary layer thickness also decreases as the slip parameter increases. However on the other hand it is interesting to note here that inclusion of Cu nanoparticles leads to a decrease in the velocity profile $f'(\eta)$ whereas the behavior is opposite for the case of Al_2O_3 nano particles (see Figs. (3.2) and (3.3)). This follows from the fact that Al_2O_3 nano particles are smaller in density when compared with the Cu nanoparticles, so their inclusion in the base fluid offers less resistance comparatively. Similarly it can be noted from Figs. (3.4) and (3.5) that increasing the rotation parameter λ decreases the velocity profile $f'(\eta)$ for both types of nanoparticles. This is due to the presence of velocity slip factor which dominates over the fluid motion compared to its increasing rotation. The impact of partial slip parameter K and rotation parameter λ on vertical velocity component $h(\eta)$ is shown through Figs. (3.6) to (3.9) for $\text{Cu} - \text{water}$ and $\text{Al}_2\text{O}_3 - \text{water}$ nano fluids. From Figs. (3.6) and (3.7) it is quite clear that when the slip parameter K is increased, velocity profile $h(\eta)$ decreases near the wall. It is also noticed that the influence of particle volume fraction is opposite on $h(\eta)$ for $\text{Cu} - \text{water}$ and $\text{Al}_2\text{O}_3 - \text{water}$ fluid. Figs. (3.8) and (3.9) show that in the absence of rotation parameter λ , no variation in the vertical velocity component $h(\eta)$ is observed and with increasing λ , velocity $h(\eta)$ drops significantly. This type of decaying behavior is observed to be similar for both $\text{Cu} - \text{water}$ and $\text{Al}_2 - \text{O}_3 \text{ water}$ nano fluids. From Figs. (3.10) to (3.13) it can be manifested that in the absence of nano particles, flow profile $f(\eta)$ decays with increasing slip parameter K and rotation parameter λ . Moreover, with the

inclusion of *Cu* nanoparticles flow profile $f(\eta)$ decreases (see Figs. (3.10), (3.12)) whereas it increases for the case of Al_2O_3 - *water* nanoparticles (see Figs. (3.11), (3.13)). Variation in temperature profile $\theta(\eta)$ against slip parameter K and rotation parameter λ for *Cu* - *water* and Al_2O_3 - *water* nano fluid is presented through Figs. (3.14) to (3.17). We can conclude from these Figs. that temperature profile $\theta(\eta)$ significantly raises with an increase in slip parameter K and rotation parameter λ for *Cu* - *water* and Al_2O_3 - *water* nano fluids. Furthermore it is also noticed that higher temperature profile $\theta(\eta)$ is recorded in the presence of nanoparticles (*Cu* and Al_2O_3) when compared with the simple pure fluid with $\varphi = 0$. This is due to the fact that nanofluid has comparatively higher thermal conductivity compare to the pure fluid which leads to a higher temperature. To see the variations of interesting physical parameters on the local skin friction coefficient and local Nusselt number, *Tables 3.1 to 3.5* are presented. *Table (3.1)* represents the thermo physical properties of constituents of nanofluids. From *Table (3.2)* it can be seen that for fixed values of λ , local skin friction $(-1/(1 - \varphi)^{2.5})f''(0)$ and local heat flux $(-K_{nf}/K_f)\theta'(0)$ increase with an increase in φ for *Cu* - *Water* as well as Al_2O_3 - *water* nano fluids. This follows from the fact that with the inclusion of solid nanoparticles the fluid becomes thicker and consequently provides more friction at the surface. On the other hand since the nanoparticles possess a lot higher thermal conductivity than their corresponding base fluid, so as a result heat transfer rate at the wall increases compared to the pure base fluid. It is noteworthy to mention here that respective values of skin friction and heat flux are different for *Cu*-*water* and Al_2O_3 - *water* fluid which signifies the importance of type of nano particles. Moreover for any fixed φ , increasing the slip parameter K decreases the local skin friction and heat flux at the stretching surface for both types of nanofluids. This is in good agreement with the fact that an increase in the slip leads to a reduction in the surface friction and ultimately decays the local heat flux at the wall. We can also notice here that local skin friction due to

Cu – water is always greater than that *Al₂O₃ – water* because of the high density of *Cu* nano particles compared to the density of *Al₂O₃* nano particles. On the other hand, *Al₂O₃* nano particles proved to be more promising in rapid transfer of heat from the wall because they have lower thermal conductivity and greater specific heat capacity compared to *Cu*-nano particles. Effect of rotation parameter λ on local skin friction and heat flux at the wall is presented through *Table (3.3)* for both types of nano particles. We can notice that, increasing the rotation parameter λ causes an increase in the local skin friction and a decrease in local heat flux at the wall. This behavior is quite similar for *Cu – water* as well as *Al₂O₃ – water* nano fluids. The physical reasoning behind it is that an increase in the rotation parameter λ for a fixed value of slip parameter K results into more resistance at the surface. Finally *Table (3.4)* and *Table (3.5)* are prepared to confirm the accuracy of present numerical scheme. It is found that our results for local skin friction coefficient and local Nusselt number are in a decent agreement with the previously published literature in the absence of slip and rotation.

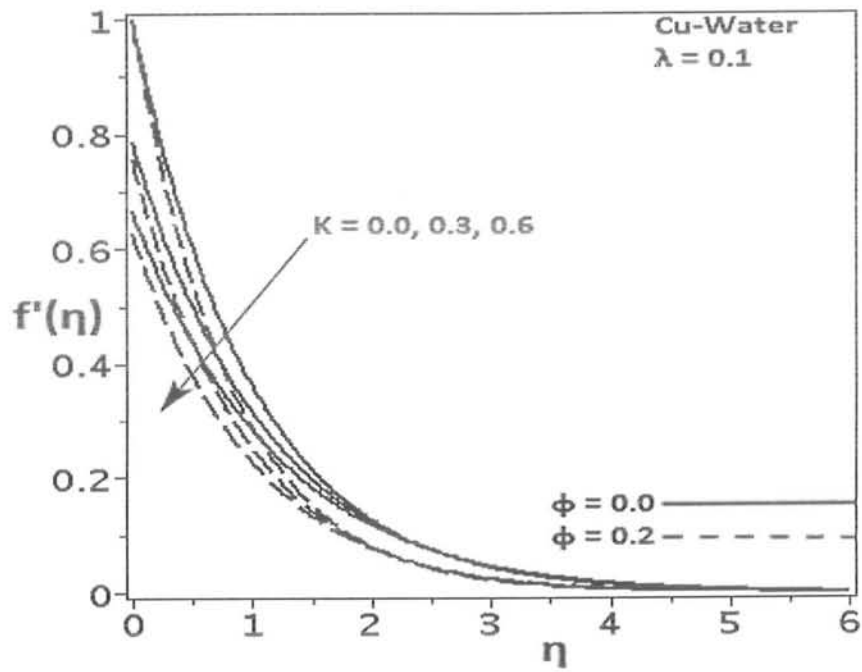


Fig. (3.2): Velocity profile $f'(\eta)$ against slip parameter K for $Cu - water$ nanofluid

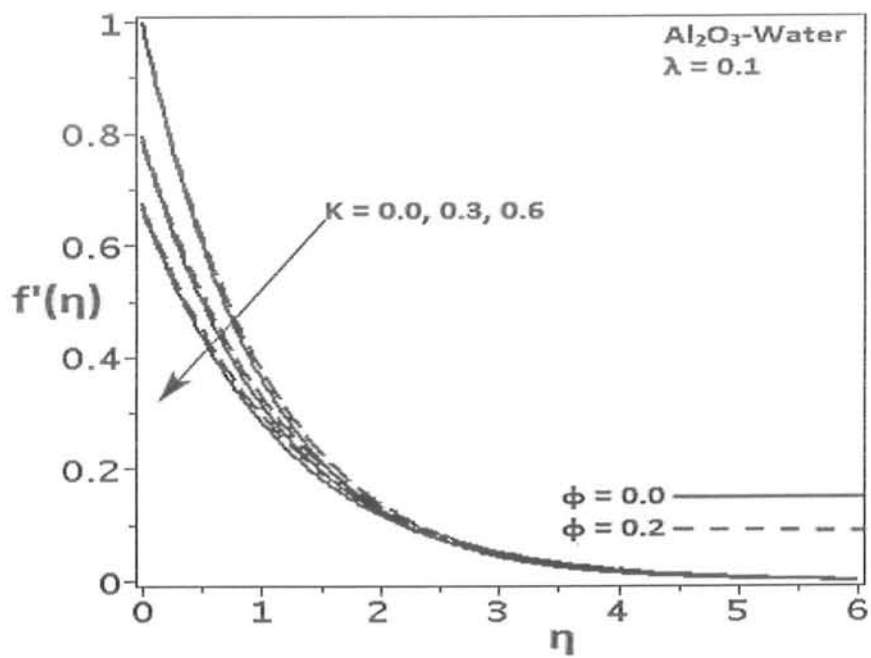


Fig. (3.3): Velocity profile $f'(\eta)$ against slip parameter K for $Al_2 O_3 - water$ nanofluid

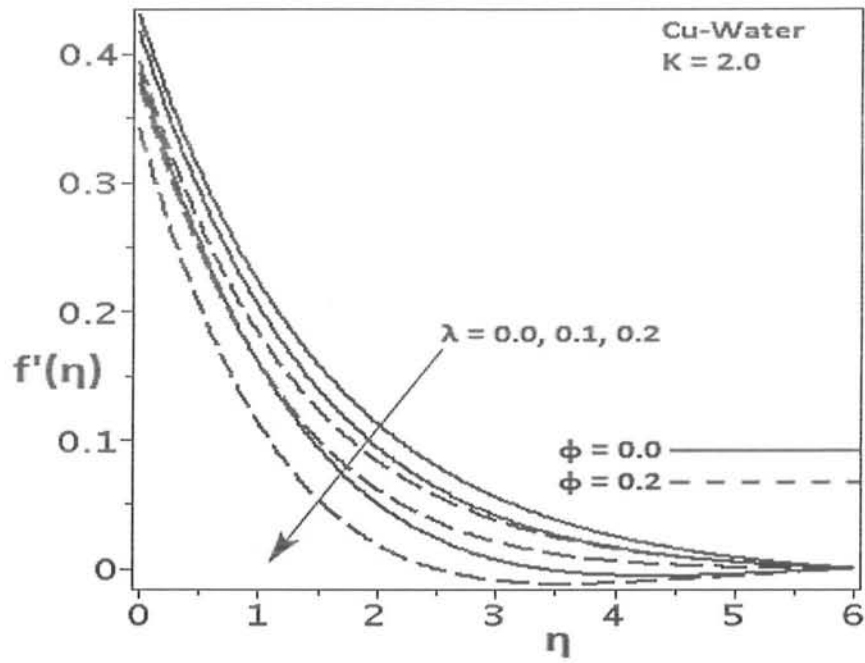


Fig. (3.4): Velocity profile $f'(\eta)$ against rotation parameter λ for $Cu - water$ nanofluid

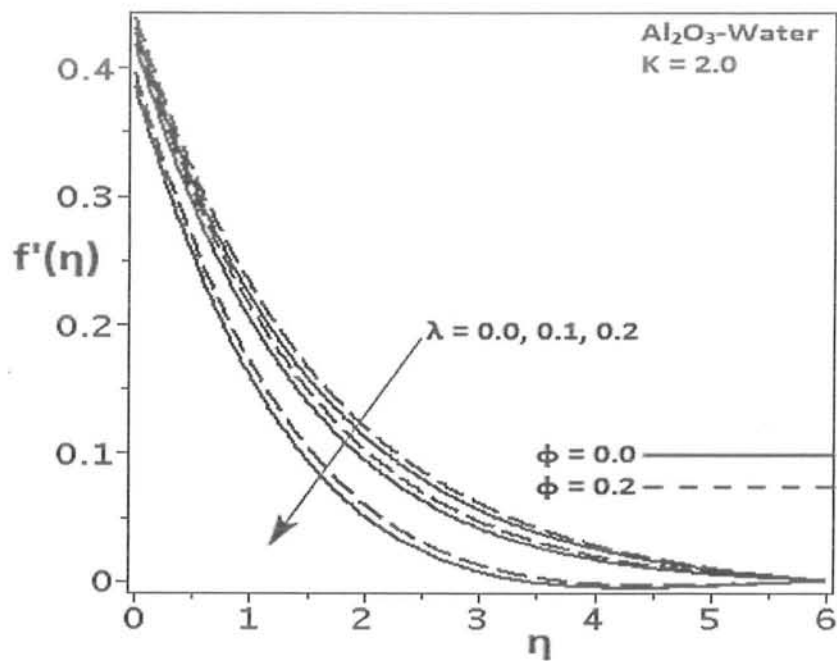


Fig. (3.5): Velocity profile $f'(\eta)$ against rotation parameter λ for $Al_2 O_3 - water$ nanofluid

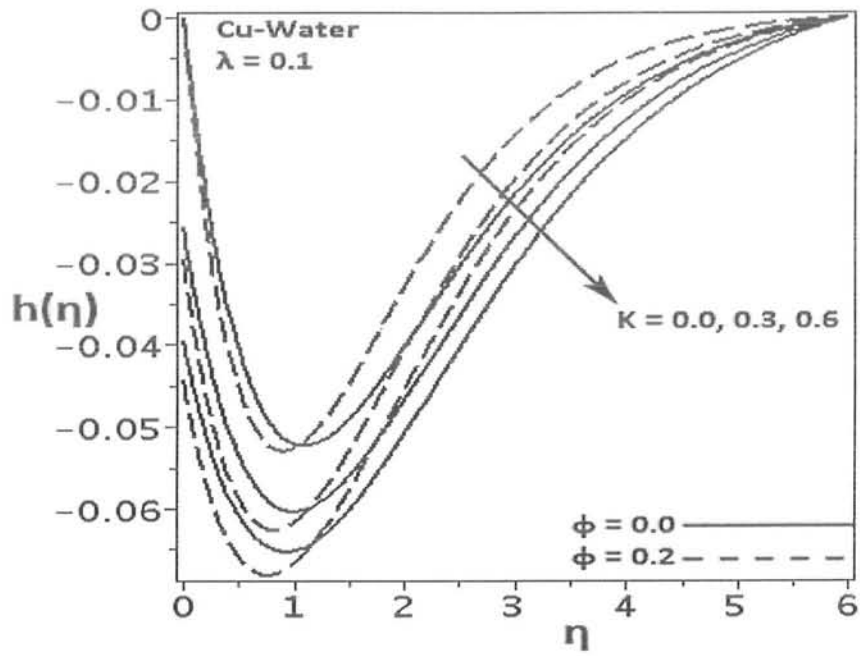


Fig. (3.6): Velocity profile $h(\eta)$ against slip parameter K for $Cu - water$ nanofluid

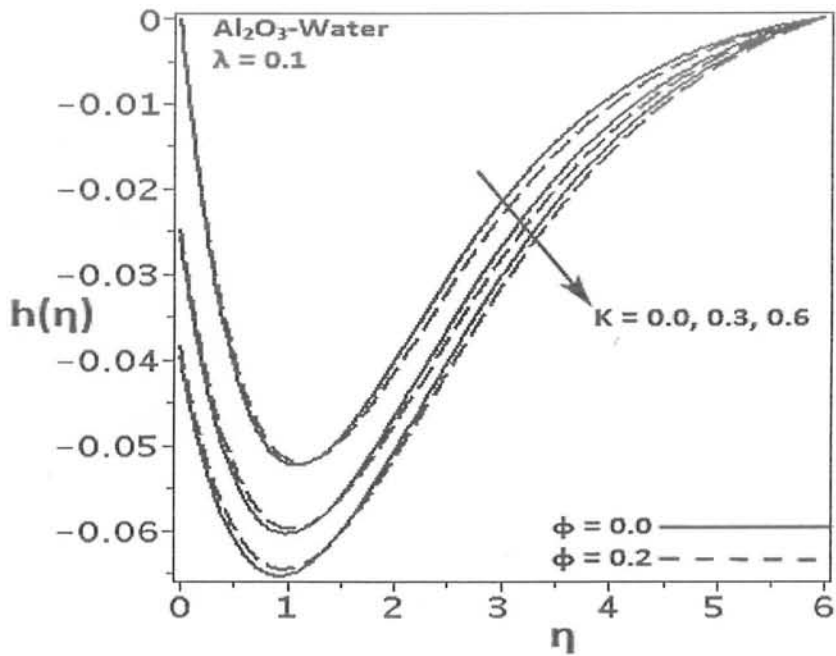


Fig. (3.7): Velocity profile $h(\eta)$ against slip parameter K for $Al_2O_3 - water$ nanofluid

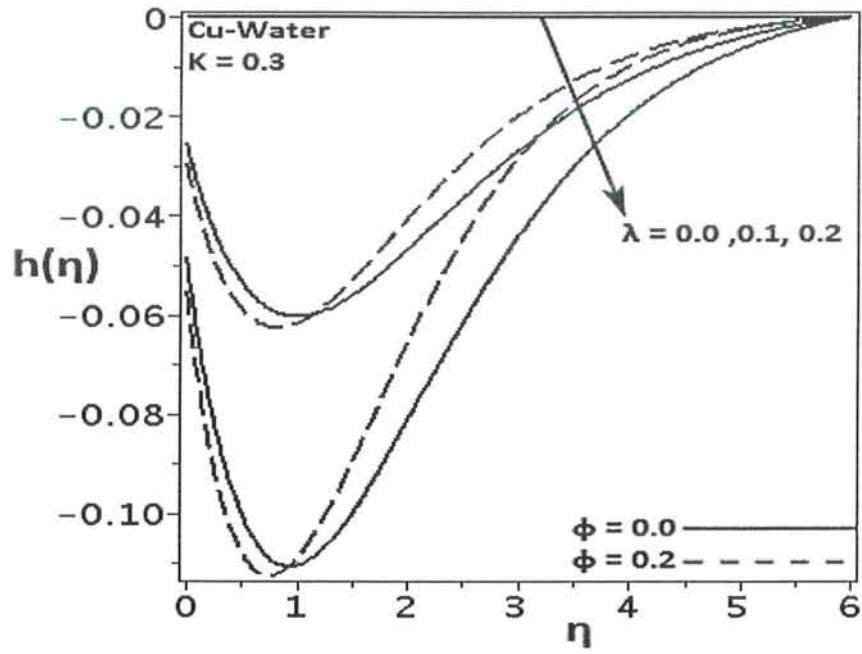


Fig. (3.8): Velocity profile $h(\eta)$ against rotation parameter λ for $Cu - water$ nanofluid

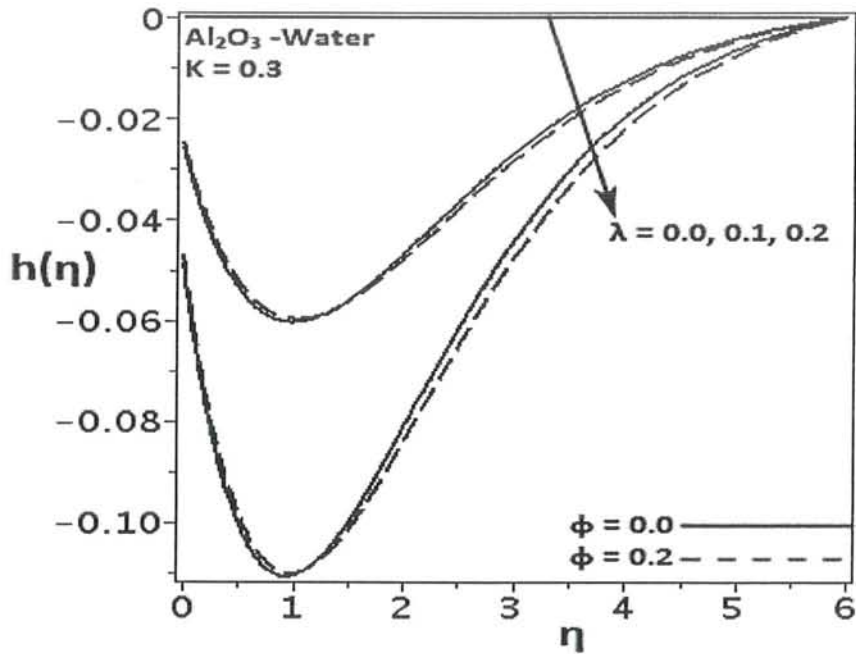


Fig. (3.9): Velocity profile $h(\eta)$ against rotation parameter λ for $Al_2O_3 - water$ nanofluid



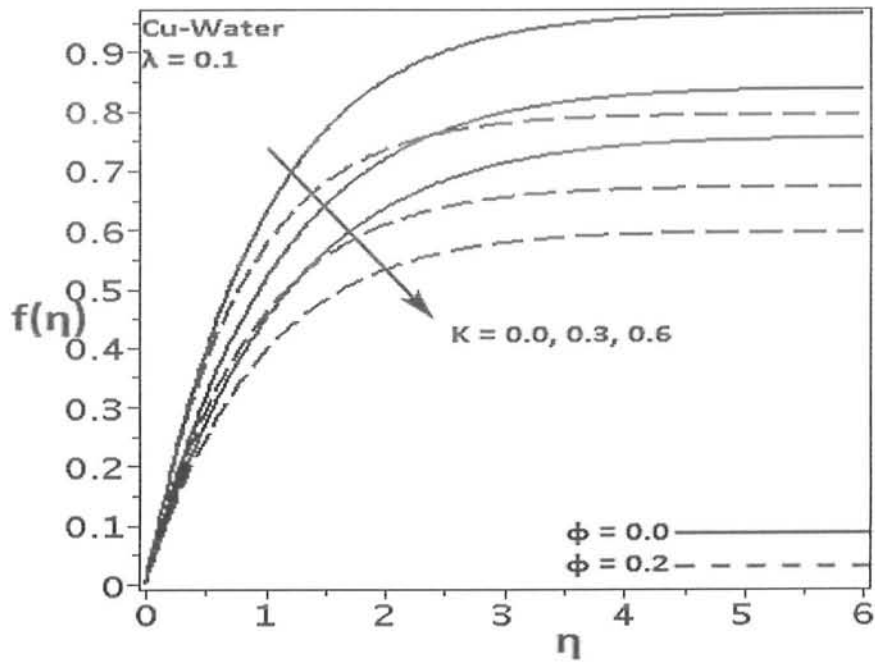


Fig. (3.10): Velocity profile $f(\eta)$ against slip parameter K for $Cu - water$ nanofluid

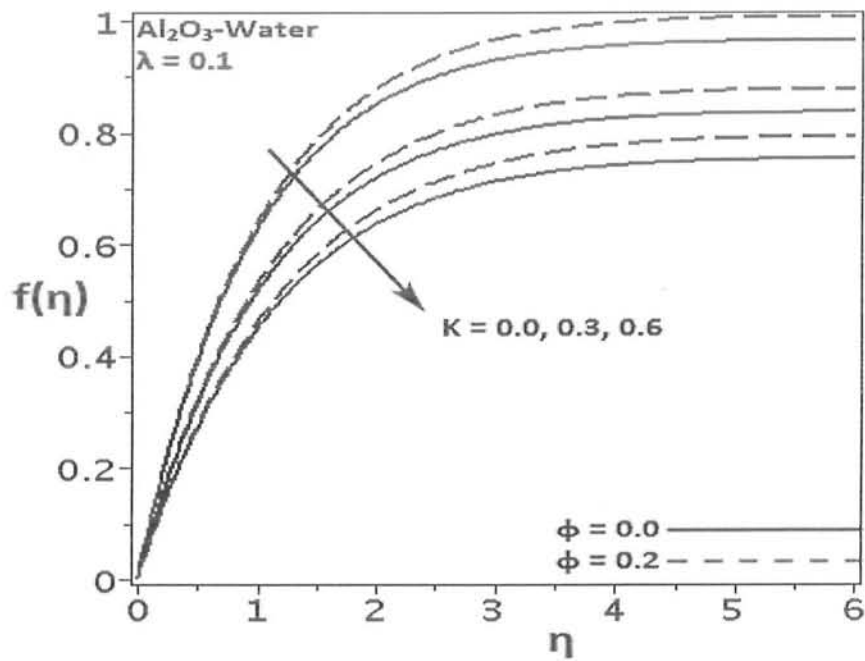


Fig. (3.11): Velocity profile $f(\eta)$ against slip parameter K for $Al_2 O_3 - water$ nanofluid

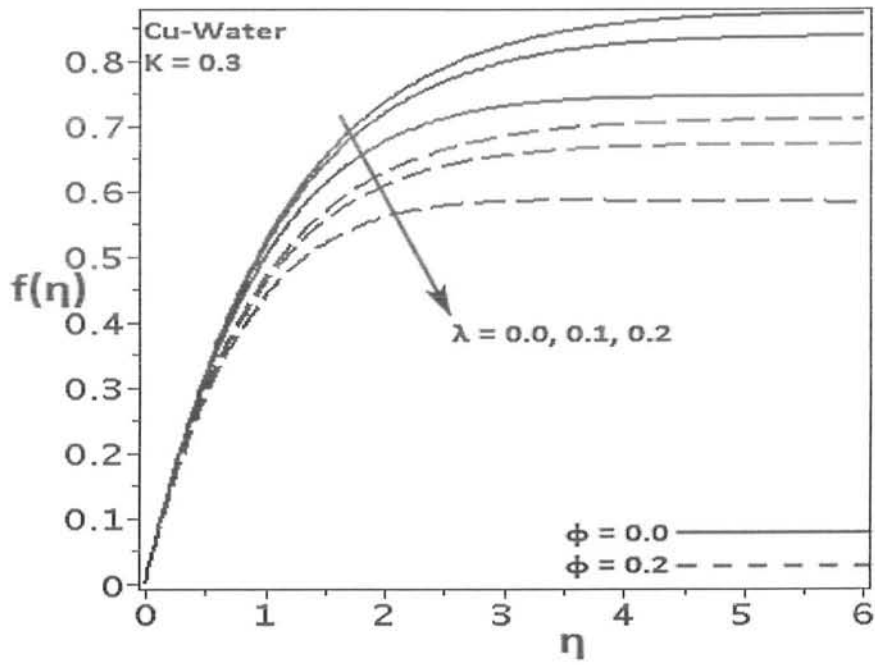


Fig. (3.12): Velocity profile $f(\eta)$ against rotation parameter λ for *Cu – water* nanofluid

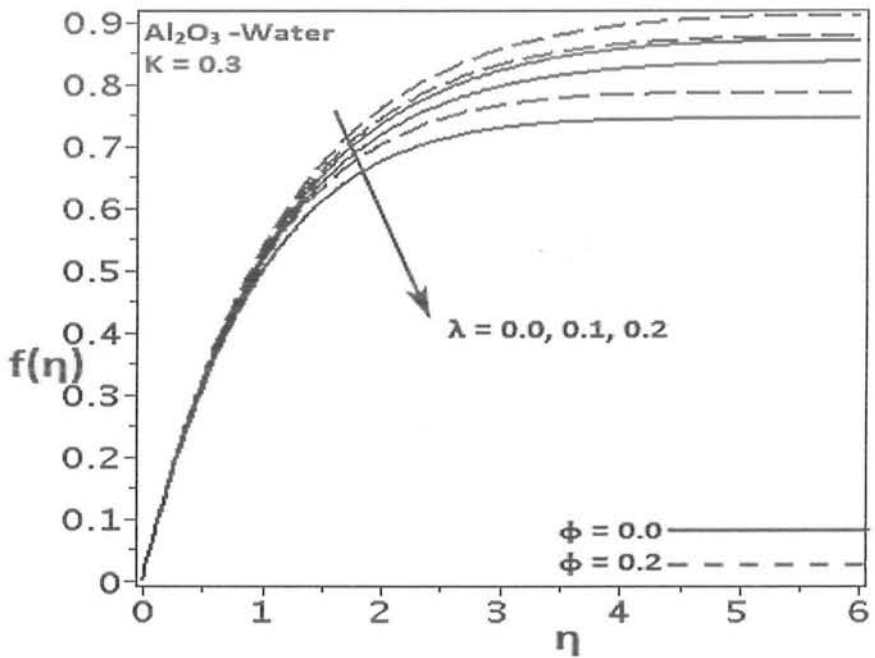


Fig. (3.13): Velocity profile $f(\eta)$ against rotation parameter λ for *Al₂O₃ – water* nanofluid

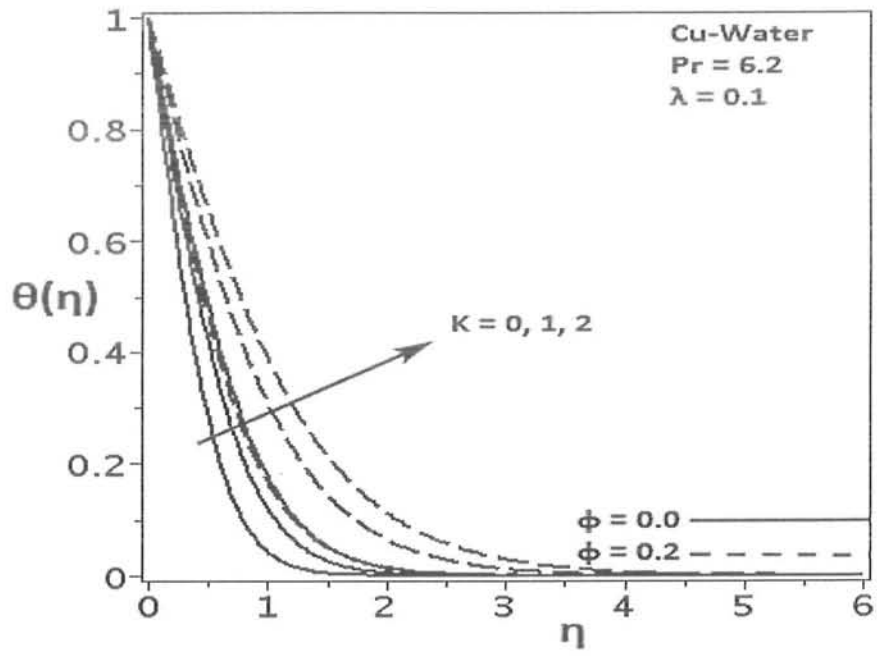


Fig. (3.14): Temperature profile $\theta(\eta)$ against slip parameter K for $Cu - water$ nanofluid

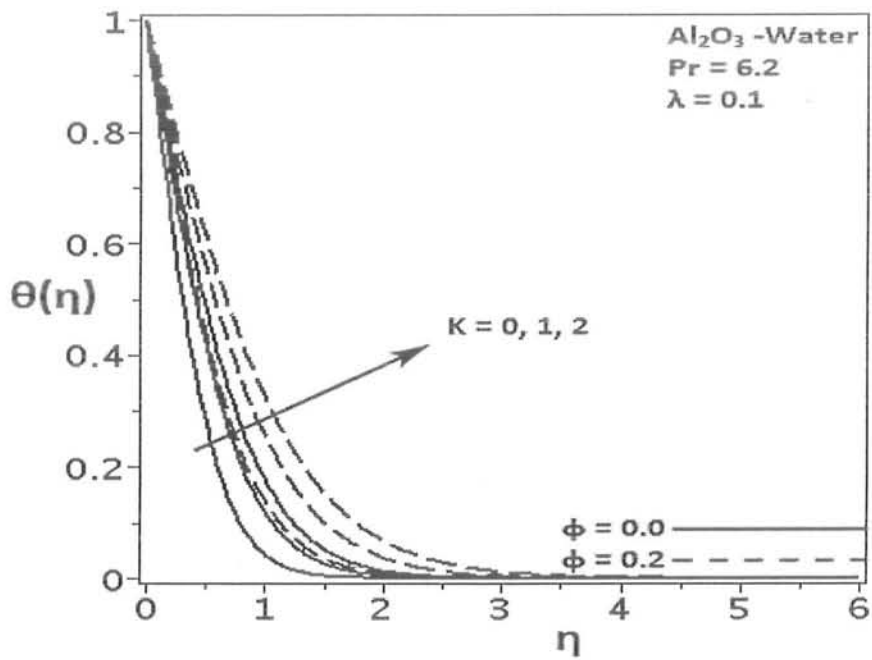


Fig. (3.15): Temperature profile $\theta(\eta)$ against slip parameter K for $Al_2 O_3 - water$ nanofluid

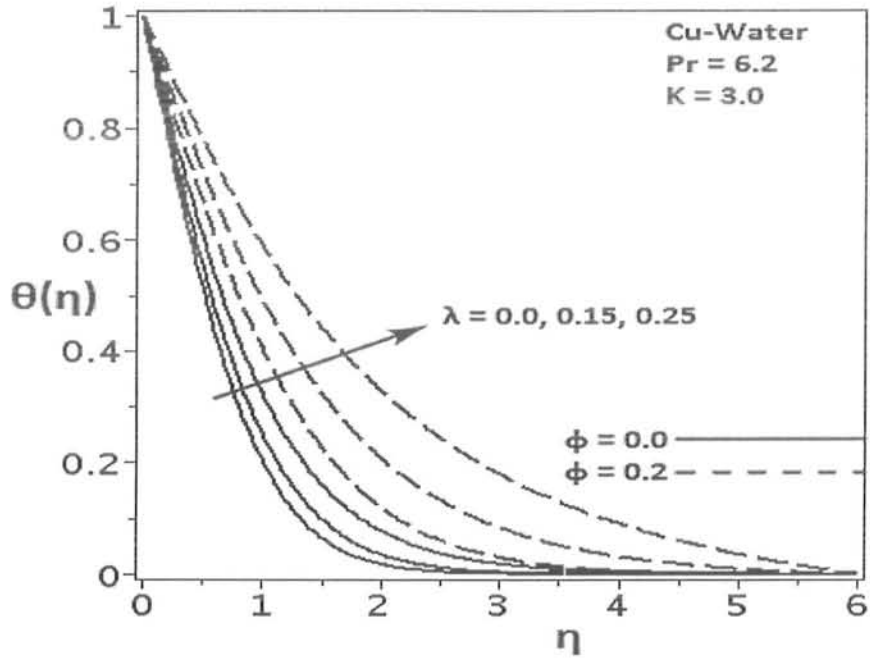


Fig. (3.16): Temperature profile $\theta(\eta)$ against rotation parameter λ for *Cu* – *water* nanofluid

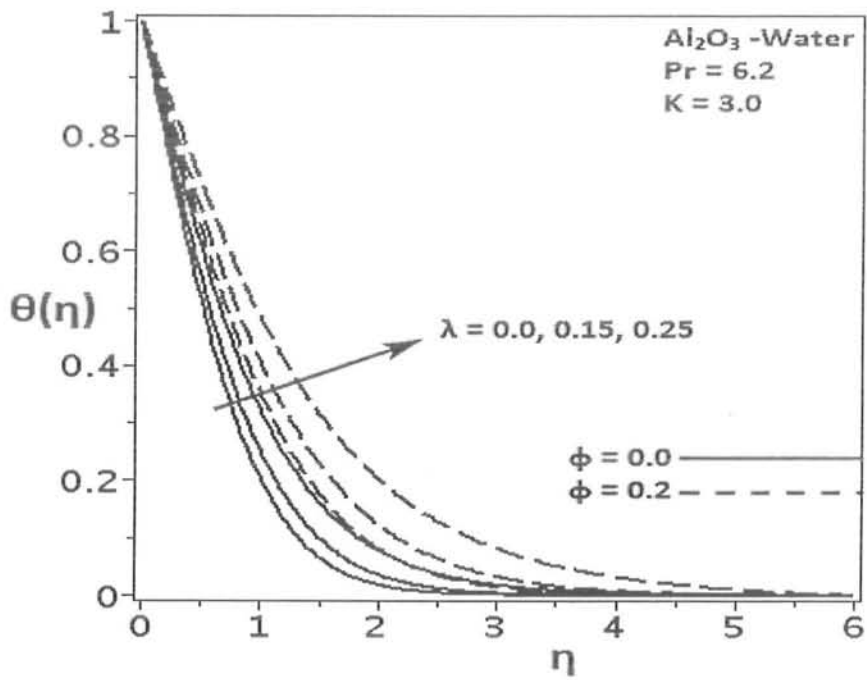


Fig. (3.17): Temperature profile $\theta(\eta)$ against rotation parameter λ for *Al₂O₃* – *water* nanofluid

Table (3.1): Thermo Physical Properties of solute nano particles Cu, Al_2O_3 and the base fluid H_2O [23]

Properties\Constituents	H_2O	Cu	Al_2O_3
Density ρ (Kg/m^3)	997.1	8933	3970
Specific Heat C_p ($J/Kg.K$)	4179	385	765
Thermal Conductivity K ($W/m.K$)	0.613	400	40

Table (3.2): Numerical values of local skin friction and heat flux versus ϕ and K ($\lambda = 0.2, Pr = 6.2$)

ϕ	K	$Cu - water$		$Al_2O_3 - water$	
		$(-1/(1-\phi)^{2.5})f''(0)$	$(-K_{nf}/K_f)\theta'(0)$	$(-1/(1-\phi)^{2.5})f''(0)$	$(-K_{nf}/K_f)\theta'(0)$
0.0	0.0	1.0331048	1.7603159	1.0331048	1.7603159
	0.2	0.8095342	1.6059148	0.8095342	1.6059148
	0.4	0.6733108	1.4940234	0.6733108	1.4940234
	0.6	0.5800166	1.4059447	0.5800166	1.4059447
0.1	0.0	1.5793633	1.9145580	1.3427788	1.9495234
	0.2	1.1943759	1.7186848	1.0524617	1.7772060
	0.4	0.9738939	1.5812177	0.8754891	1.6520225
	0.6	0.8281107	1.4745051	0.7542552	1.5532563
0.2	0.0	2.1982764	2.0890309	1.7252046	2.1526512
	0.2	1.6482606	1.8647765	1.3643963	1.9679136
	0.4	1.3378447	1.7079177	1.1409135	1.8321472
	0.6	1.1342338	1.5860396	0.9863708	1.7242788

Table (3.3): Numerical values of local skin friction and heat flux versus φ and λ
($K = 0.3, Pr = 6.2$)

φ	λ	<i>Cu – water</i>		<i>Al₂O₃ – water</i>	
		$(-1/(1 - \varphi)^{2.5})f''(0)$	$(-K_{nf}/K_f)\theta'(0)$	$(-1/(1 - \varphi)^{2.5})f''(0)$	$(-K_{nf}/K_f)\theta'(0)$
0.0	0.0	0.7015504	1.5735879	0.7015504	1.5735879
	0.1	0.7109125	1.5658203	0.7109125	1.5658203
	0.2	0.7342651	1.5461923	0.7342651	1.5461923
	0.3	0.7644637	1.5202135	0.7644637	1.5202135
0.1	0.0	1.0217856	1.6906300	0.9121606	1.7456913
	0.1	1.0360396	1.6776835	0.9243294	1.7357050
	0.2	1.0713731	1.6449768	0.9546841	1.7104251
	0.3	1.1167411	1.6015137	0.9939394	1.6768502
0.2	0.0	1.4058403	1.8441508	1.1864981	1.9381177
	0.1	1.4256567	1.8261617	1.2021435	1.9261086
	0.2	1.4747051	1.7806638	1.2412386	1.8956299
	0.3	1.5375710	1.7200721	1.2918810	1.8550248

Table (3.4): Comparison of current values of $f''(0)$ and $h'(0)$ with published results
for $\varphi = 0 = K$

λ	<i>Ishak et al[30]</i>		<i>C.Y Wang [31]</i>		<i>Current Results</i>	
	$f''(0)$	$h'(0)$	$f''(0)$	$h'(0)$	$f''(0)$	$h'(0)$
0.0	1.0000	0.0000	1.0000	0.0000	1.000000	0.000000
0.2	1.0331	0.2385	–	–	1.033105	0.238546
0.4	1.1009	0.4310	–	–	1.100906	0.430961
0.5	1.1384	0.5128	1.1384	0.5128	1.138381	0.512760
0.6	1.1764	0.5874	–	–	1.176365	0.587418
0.8	1.2518	0.7204	–	–	1.251775	0.720361
1.0	1.3250	0.8371	1.3250	0.8371	1.325029	0.837098
1.5	–	–	–	–	1.496404	1.082979
2.0	1.6523	1.2873	1.6523	1.2873	1.652352	1.287259
2.5	–	–	–	–	1.795728	1.465217
3.0	1.9289	1.6248	–	–	1.928931	1.624736

Table (3. 5): Comparison of numerical values of $\theta'(0)$ with those
calculated by Wang [31] and Nath [42] for $\varphi = 0 = K$

Pr	$\lambda = 0.0$			$\lambda = 0.5$			$\lambda = 2.0$		
	Present	Wang[31]	Nath[42]	Present	Wang[31]	Nath[42]	Present	Wang[31]	Nath[42]
0.7	0.454048	0.455	0.4550	0.390338	0.390	0.3904	0.254869	0.242	0.2429
2.0	0.911357	0.911	0.9114	0.852436	0.853	0.8525	0.637860	0.638	0.6398
7.0	1.895403	1.894	1.8959	1.851177	1.850	1.8517	1.664364	1.664	1.6648

3.5 Conclusions

Steady flow of rotating nano fluid over stretching surface with partial slip is investigated.

Foremost deductions are as follow:

- 1) Partial slip parameter K and rotation parameter λ both decay velocity boundary and enhance thermal boundary layer of nanofluids.
- 2) Volumetric concentration of nano particles ϕ generally lowers down the velocity in case of $Cu - Water$ nanofluid and enhances the velocity for $Al_2O_3 - water$ nanofluid case.
- 3) Enhancement in temperature due to particle volume fraction ϕ is prominent in $Cu - water$ nanofluid compared to $Al_2O_3 - water$ nanofluid.
- 4) An Increase in velocity slip parameter K results in a decrease in skin friction and heat flux for both types of nanofluids.
- 5) Cu nanoparticles are better heat carriers than Al_2O_3 nanoparticles.
- 6) Higher the rate of angular velocity implies higher skin friction and lower heat flux for both types of nanofluids.



Chapter 4

Heat transfer analysis of a ferromagnetic rotating nanofluid over a stretching surface with viscous dissipation

4.1 Introduction

The flow of a magnetohydrodynamic rotating nano fluid over a stretching plane is investigated in this unit. Viscous dissipation effects are also considered. Water and kerosene are used as traditional base fluids with Barium Ferrite ($BaO.6Fe_2O_3$) nano particles in our analysis. Governing partial differential Eqs. for flow problem are presented and reformed into a set of coupled non-linear ordinary differential Eqs. by means of appropriate similarity transforms. The system of transformed equations is tackled numerically by using RKF45 method [48] with shooting scheme. Effects of relevant flow constraints on velocity/ temperature profiles are offered through graphs. Measures of physical interest as coefficient of local skin friction/ heat flux at the surface are computed and analyzed for both types of base fluid. Analysis revealed that temperature rises with magnetic field and rotation parameter. It is also detected that coefficient of skin friction increases and local heat flux decreases with an upswing in magnetic field and rotation parameter. Inclusion of ferromagnetic nano particles boosts the heat transfer rate at wall.

4.2 Mathematical formulation

Consider an incompressible and electrically conducting nanofluid lying in the region $Z \geq 0$. The fluid moves entirely due to the elastic boundary $z = 0$ which is being linearly stretched by a pair of forces which are equal in magnitude but opposite in directions of x- and x'-axis with the condition that the origin $(0,0,0)$ remains fixed. The fluid is revolving with a fixed angular velocity of magnitude Ω about vertical axis. A magnetic field of fixed strength B_0 is applied

along the direction of vertical axis. Induced magnetic field is supposed to be negligible. All properties related with fluid are assumed to be constant.

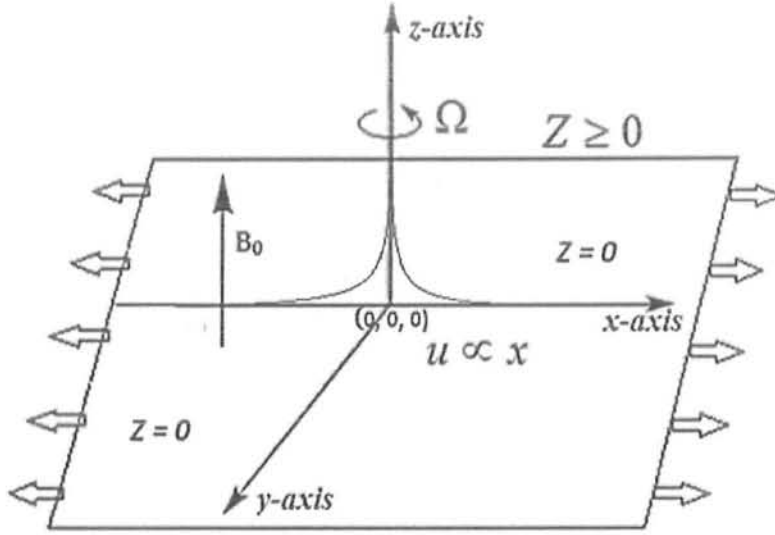


Fig (4.1): Physical flow model

Boundary-layer Eqs. of mass, motion and thermal energy accomplishing *MHD* flow and heat transfer with viscous dissipation effects neglecting pressure gradient are [31, 77]

$$\frac{\partial u}{\partial x} + \frac{\partial v}{\partial y} + \frac{\partial w}{\partial z} = 0, \quad (4.1)$$

$$u \frac{\partial u}{\partial x} + v \frac{\partial u}{\partial y} + w \frac{\partial u}{\partial z} - 2\Omega v = \frac{\mu_{nf}}{\rho_{nf}} \nabla^2 u - \frac{\sigma_{nf} B_0^2}{\rho_{nf}} u, \quad (4.2)$$

$$u \frac{\partial v}{\partial x} + v \frac{\partial v}{\partial y} + w \frac{\partial v}{\partial z} + 2\Omega u = \frac{\mu_{nf}}{\rho_{nf}} \nabla^2 v - \frac{\sigma_{nf} B_0^2}{\rho_{nf}} v, \quad (4.3)$$

$$u \frac{\partial w}{\partial x} + v \frac{\partial w}{\partial y} + w \frac{\partial w}{\partial z} = \frac{\mu_{nf}}{\rho_{nf}} \nabla^2 w, \quad (4.4)$$

$$u \frac{\partial T}{\partial x} + v \frac{\partial T}{\partial y} + w \frac{\partial T}{\partial z} = \alpha_{nf} \frac{\partial^2 T}{\partial z^2} + \frac{\mu_{nf}}{(\rho C_p)_{nf}} \left[\left(\frac{\partial u}{\partial z} \right)^2 + \left(\frac{\partial v}{\partial z} \right)^2 \right]. \quad (4.5)$$

Here σ_{nf} is the electrical conductivity of the nanofluid. Effective physical measures for nanofluid are [23, 37, 47]

$$\left. \begin{aligned} \rho_{nf} &= \rho_f \left[1 - \varphi + \varphi \left(\frac{\rho_s}{\rho_f} \right) \right], \mu_{nf} = \mu_f (1 - \varphi)^{-2.5}, \alpha_{nf} = \frac{K_{nf}}{(\rho C_p)_{nf}}, \\ (\rho C_p)_{nf} &= (\rho C_p)_f \left[1 - \varphi + \varphi \left(\frac{(\rho C_p)_s}{(\rho C_p)_f} \right) \right], \frac{K_{nf}}{K_f} = \frac{K_s + 2K_f - 2\varphi(K_f - K_s)}{K_s + 2K_f + 2\varphi(K_f - K_s)}. \end{aligned} \right\} \quad (4.6a, b)$$

Conforming end point conditions are

$$\left. \begin{aligned} u &= ax, & v &= 0, & w &= 0 & \text{at } z &= 0, \\ u &\rightarrow 0, & v &= 0 & & & \text{as } z &\rightarrow \infty, \\ T &= T_w & & & & & \text{at } z &= 0, \\ T &\rightarrow T_\infty & & & & & \text{as } z &\rightarrow \infty. \end{aligned} \right\} \quad (4.7)$$

Following Wang [31] and Ishak *et al.* [37], similarity transformations can be used as

$$\left. \begin{aligned} u &= axf'(\eta), \quad v = axh(\eta), \quad w = -\sqrt{av} f(\eta), \\ \eta &= z \sqrt{\frac{a}{v}}, \quad \theta(\eta) = \frac{T - T_\infty}{T_w - T_\infty}. \end{aligned} \right\} \quad (4.8)$$

Using Eqs. (4.6) and (4.8), Eq. (4.1) is satisfied identically and Eqs. (4.2) to (4.5) are transformed in to

$$\frac{1}{(1-\varphi)^{2.5}} f'''' + \left(1 - \varphi + \varphi \frac{\rho_s}{\rho_f} \right) (ff'' - f'^2 + 2\lambda h) - M^2 f' = 0, \quad (4.9)$$

$$\frac{1}{(1-\varphi)^{2.5}} h'' + \left(1 - \varphi + \varphi \frac{\rho_s}{\rho_f} \right) (fh' - hf' - 2\lambda f') - M^2 h = 0, \quad (4.10)$$

$$\frac{K_{nf}}{K_f} \theta''(\eta) + Pr \left[\left(1 - \varphi + \varphi \frac{(\rho C_p)_s}{(\rho C_p)_f} \right) (f\theta'(\eta) - 2f'\theta(\eta)) + \frac{1}{(1-\varphi)^{2.5}} [Ec\{f''^2 + h'^2\}] \right] = 0. \quad (4.11)$$

In above Eqs., Ec is the Eckert number and M is the magnetic parameter and are given by

$$Ec = \frac{u^2}{C_p(T_w - T_\infty)}, \quad M = \sqrt{\frac{\sigma_{nf}}{\alpha \rho_f}} B_0. \quad (4.12)$$

Using similarity transformations (4.8), boundary conditions (4.7) take the form

$$\left. \begin{aligned} f(0) &= 0, & f'(0) &= 1, & f'(\infty) &= 0, \\ h(0) &= 0, & h(\infty) &= 0, & \theta(0) &= 1, & \theta(\infty) &= 0. \end{aligned} \right\} \quad (4.13a, b)$$

4.3 Solution method

Solution of the system containing Eqs. (4.9) to (4.11) together with boundary conditions (4.13a,b) is extracted by employing numerical scheme of RKF45 process with shooting procedure. This method was developed by a German mathematician Ervin Fehlberg in his

publication of 1969 [48] and was labeled as RKF45 method i.e., Runge Kutta method of order $O(h^4)$ with an error estimate of order $O(h^5)$. Solution methodology is adopted as under:

$$\text{Let } A_1 = \frac{1}{(1-\varphi)^{2.5}}, A_2 = \left(1 - \varphi + \varphi \frac{\rho_s}{\rho_f}\right), A_3 = \left(1 - \varphi + \varphi \frac{(\rho C_p)_s}{(\rho C_p)_f}\right), \quad (4.14)$$

$$\text{and } f = y_1, f' = y_2, f'' = y_3, f''' = y_3', \quad (4.15)$$

$$h = y_4, h' = y_5, h'' = y_5', \quad (4.16)$$

$$\theta = y_6, \theta' = y_7, \theta'' = y_7'. \quad (4.17)$$

Then the system of Eqs. (4.9) – (4.11) is transformed in to a system of first order ordinary differential Eqs. as

$$\begin{bmatrix} y_2 \\ y_3 \\ y_3' \\ y_5 \\ y_5' \\ y_7 \\ y_7' \end{bmatrix} = \begin{bmatrix} y_1' \\ y_2' \\ \frac{1}{A_1} [A_2(y_2^2 - y_1 y_3 - 2\lambda y_4) + M^2 y_2] \\ y_4' \\ \frac{1}{A_1} [A_2(y_2 y_4 - y_1 y_5 + 2\lambda y_2) + M^2 y_4] \\ y_6' \\ \frac{Pr}{K_{nf}/K_f} [A_3(2y_2 y_6 - y_1 y_7) - A_1 Ec(y_3^2 + y_5^2)] \end{bmatrix}, \quad (4.18)$$

along with initial conditions

$$\begin{bmatrix} y_0(1) \\ y_0(2) \\ y_0(3) \\ y_0(4) \\ y_0(5) \\ y_0(6) \\ y_0(7) \end{bmatrix} = \begin{bmatrix} 0 \\ 1 \\ \alpha_1 \\ 0 \\ \alpha_2 \\ 1 \\ \alpha_3 \end{bmatrix}. \quad (4.19)$$

Here $\alpha_1 = f''(0)$, $\alpha_2 = h'(0)$ and $\alpha_3 = \theta'(0)$ are shooting parameters. These are unknown initial conditions and are guessed to initiate the integration. The unknowns α_1 , α_2 and α_3 are computed iteratively by Newton's method so that solutions satisfy the boundary conditions at infinity in Eq. (4.13 a, b). The convergence standard of 10^{-6} is set in our calculations.

4.4 Physical quantities of interest

We are particularly interested in finding numerically the coefficients of skin frictions and Nusselt

number [37, 77].

$$Cf_x = \frac{\tau_{xz}}{\rho(ax)^2}, \quad Cf_y = \frac{\tau_{yz}}{\rho(ax)^2}, \quad Nu = \frac{xq_w}{K_f(T_w - T_\infty)}, \quad (4.20)$$

where shear stresses τ_{xz} , τ_{yz} and heat flux q_w of the surface are given by

$$\tau_{xz} = \mu_{nf} \left(\frac{\partial u}{\partial z} + \frac{\partial w}{\partial x} \right)_{z=0}, \quad \tau_{yz} = \mu_{nf} \left(\frac{\partial v}{\partial z} + \frac{\partial w}{\partial y} \right)_{z=0}, \quad q_w = -K_{nf} \left(\frac{\partial T}{\partial z} \right)_{z=0}. \quad (4.21)$$

Invoking Eq. (4.21) in Eq. (4.20), we get skin frictions and heat transfer rate in reduced form as

$$\left. \begin{aligned} (Re_x)^{\frac{1}{2}} Cf_x &= \frac{1}{(1-\varphi)^{2.5}} f''(0), \\ (Re_x)^{\frac{1}{2}} Cf_y &= \frac{1}{(1-\varphi)^{2.5}} h'(0), \\ (Re_x)^{-\frac{1}{2}} Nu &= \frac{-K_{nf}}{K_f} \theta'(0). \end{aligned} \right\} \quad (4.22)$$

Local skin friction co-efficient and heat transfer rate have been computed numerically for a number of different values of particle volume fraction φ , rotation parameter λ and magnetic parameter M in *Tables (4.2) and (4.3)*.

4.5 Results and discussion

This section is committed to determine the influence of relevant flow constraints such as volumetric particle fraction φ , magnetic parameter M , rotation parameter λ and Eckert number Ec on velocity and temperature profiles. Two kinds of base fluid namely kerosene and water have been used in our analysis with ferromagnetic nanoparticles ($BaO.6Fe_2O_3$). Figs. (4.2) to (4.21) have been plotted to find out the influence of magnetic field and rotation on velocity and temperature profiles for both water and kerosene based nanofluids. Due to inclusion of ferro particles $BaO.6Fe_2O_3$, both nanofluids are frequently termed as ferrofluids. Figs. (4.2) to (4.5) have been prepared to discover the effects of magnetic parameter M and rotation parameter λ on velocity profile $f'(\eta)$ for water as well as kerosene based ferrofluids. Figs. (4.2) and (4.3) show that a gain in magnetic parameter M results into a loss in non-dimensional velocity $f'(\eta)$ for water as well as kerosene based ferro fluids. This decrease in boundary layer depth is because of the rise in Lorentz force retarding the velocity. It is quite remarkable to note that in the absence

of magnetic field, nanoparticles cause a decrease in velocity profile $f'(\eta)$ while in presence of magnetic field they cause an increase in velocity profile $f'(\eta)$. Similarly Figs. (4.4) and (4.5) depict that an increase in rotation results in a decrease in velocity profile $f'(\eta)$ for both types of fluid. The variations in non-dimensional velocity profile $h(\eta)$ due to magnetic field and rotation are shown through Figs. (4.6) to (4.9). Figs. (4.6) and (4.7) exhibit that an increase in magnetic parameter M leads to a decrease in the velocity profile $h(\eta)$ for both fluids used in practice. Figs. (4.8) and (4.9) reveal that an upsurge in the rotation parameter λ decreases the velocity profile $h(\eta)$ for both base fluids. Influence of magnetic field and rotation on velocity $f(\eta)$ for both types of fluids is presented through Figs. (4.10) to (4.13). Figs. (4.10) and (4.11) show that a proliferation in magnetic parameter M results in a significant reduction in velocity profile $f(\eta)$. Figs. (4.12) and (4.13) are plotted to discover the effects of rotation of fluid on velocity profile $f(\eta)$. As obvious, increasing rotation drops the velocity profile $f(\eta)$ for water as well as kerosene based nanofluids. It is obvious from these Figs. that effect of particle volume fraction φ is prominent for kerosene based fluid in which velocity profile $f(\eta)$ reduces significantly. Figs. (4.14) to (4.17) reveal the influence of magnetic field and rotation on the temperature profile $\theta(\eta)$ for water and kerosene based ferrofluids. In Figs. (4.14) and (4.15) it is quite evident that temperature profile $\theta(\eta)$ increases with an increase in magnetic parameter M . As M amplifies the Lorentz force which causes retardation to flow and this flow delay results in to a rise in temperature profile. From Figs. (4.16) and (4.17), it can be observed that an increase in rotation parameter λ results into an increase in temperature profile $\theta(\eta)$. Figs. (4.18) and (4.19) illustrate the effects of particle volume fraction φ , magnetic parameter M and rotation parameter λ on the skin friction $(-1/(1 - \varphi)^{2.5})f''(0)$. Each of φ , M and λ enhance the skin friction for water based as well as kerosene based ferro fluids. Figs. (4.20) and (4.21) reflect the influence of controlling parameters viz Eckert number Ec , Particle volume fraction φ , magnetic parameter

M and rotation parameter λ on the surface heat flux $(-K_{nf}/K_f) \theta'(0)$. These pictorial solutions indicate that an increase in particle volume fraction φ increases the surface heat flux while other three controlling parameters namely Eckert number (Ec), magnetic field (M) and rotation (λ) cause a decline in the surface heat flux for both ferro fluids. However, due to high Prandtl number, kerosene based ferro fluid defines prominent behaviour as compared with water based ferro fluid.

Tables (4.1 – 4.3) have been computed to discover the behavior of the measures of physical interests such as local skin friction and heat flux against pertinent flow governing parameters. *Table (4.1)* contains the thermo physical properties of components of nanofluids. From *Table (4.2)*, it is evident that for a fixed amount of rotation parameter λ , Prandtl number Pr and Eckert number Ec , an increasing particle volume fraction φ results into a boost in the skin friction $(-(1 - \varphi)^{-2.5})f''(0)$ and heat flux $(-K_{nf}/K_f) \theta'(0)$ for both water and kerosene based nanofluids. It can also be noticed that a growth in magnetic parameter M results into a rise in skin friction $(-1/(1 - \varphi)^{2.5})f''(0)$ but a simultaneous fall in heat flux $(-K_{nf}/K_f) \theta'(0)$. The typical fact is that for any fixed pair (φ, M) with $\varphi \neq 0$, numerical values of local skin friction due to water based nanofluid is always smaller than those due to kerosene based fluid which signifies the type of base fluid to be chosen. In *Table (4.3)*, it can easily be observed that when rotation parameter λ increases, numerical value of local skin friction also increases but corresponding value of heat flux decays for both types of nanofluid. Also for any fixed (φ, λ) with $\varphi \neq 0$, numerical value of heat transfer rate at surface for water based nanofluid is always less than the corresponding values of the fluid based with kerosene. This is because of the fact that Prandtl number of kerosene is higher as compared with that of water. In *Table (4.4)*, comparison of skin friction and heat transfer rate at wall for present study has been observed versus those already published literature for conventional fluid and a good agreement is witnessed. In *Table (4.5)*, some values of local heat flux for conventional fluid are calculated for some values of Prandtl number Pr and rotation parameter λ .



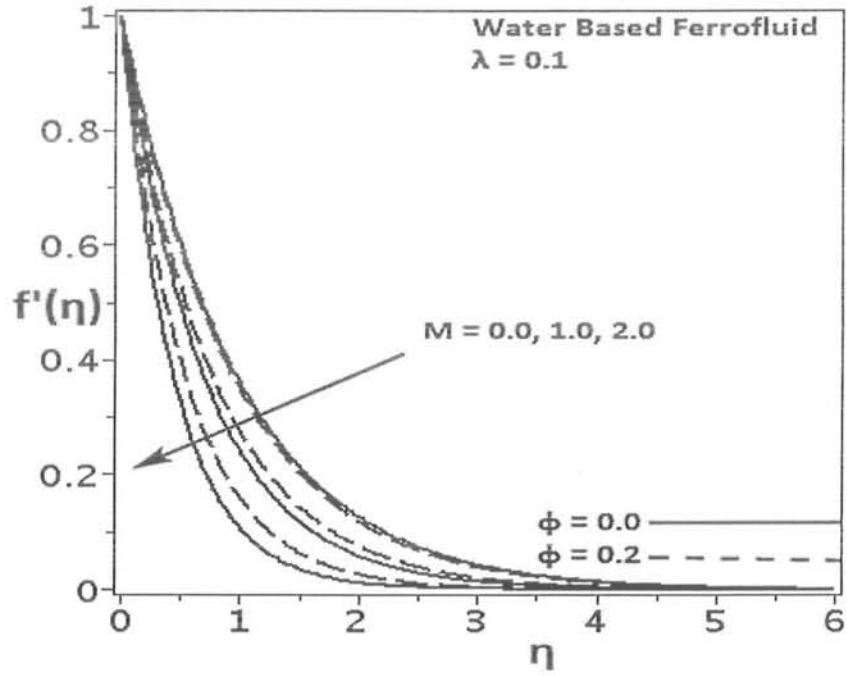


Fig. (4.2): Velocity profile $f'(\eta)$ against magnetic parameter M for water based ferrofluid

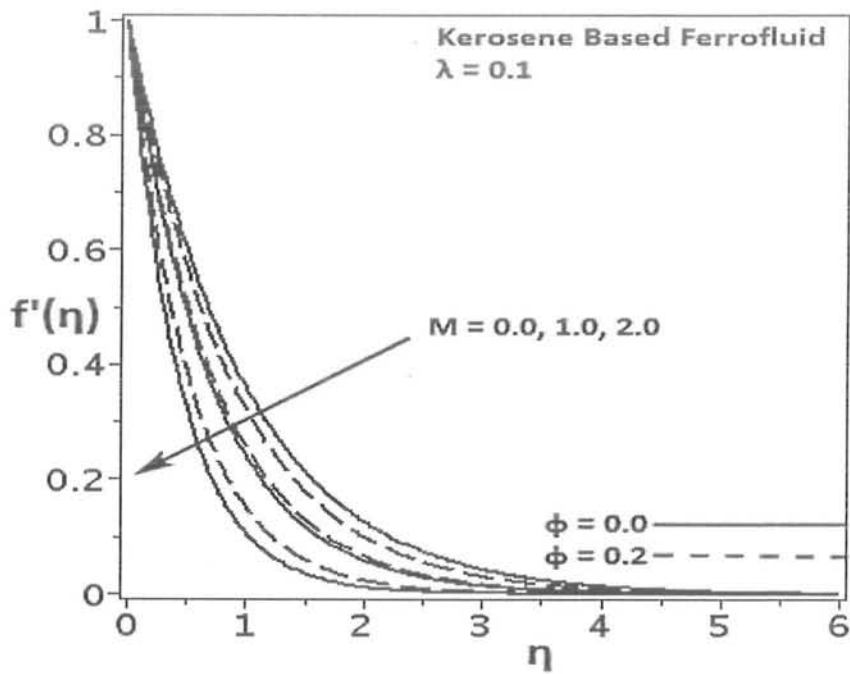


Fig. (4.3): Velocity profile $f'(\eta)$ against magnetic parameter M for kerosene based ferrofluid

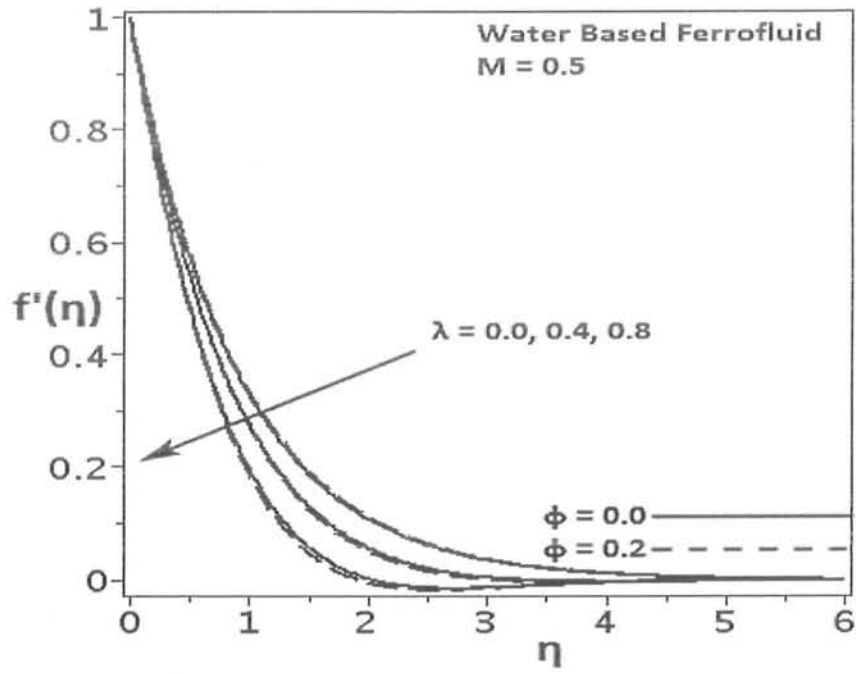


Fig. (4.4): Velocity profile $f'(\eta)$ against rotation parameter λ for water based ferrofluid

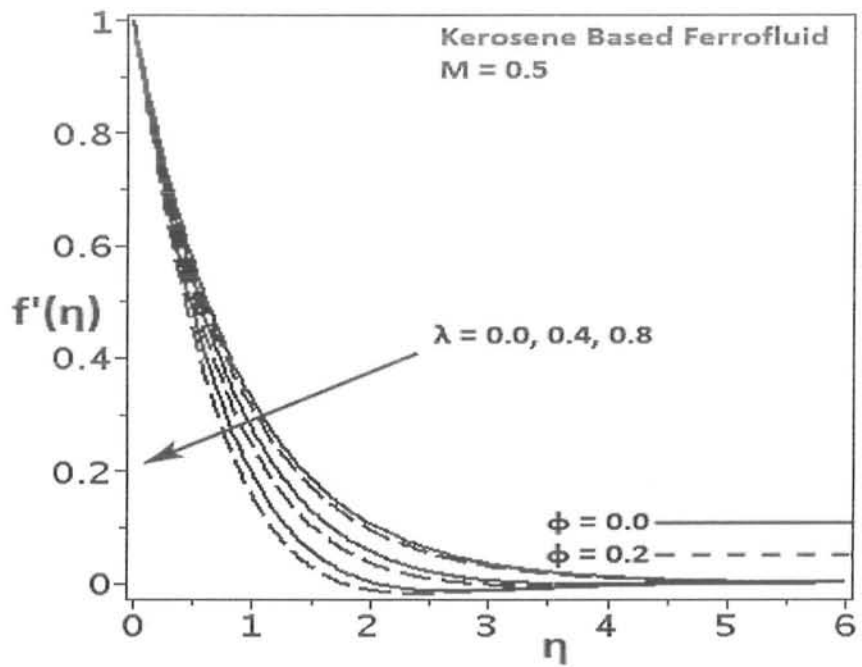


Fig. (4.5): Velocity profile $f'(\eta)$ against rotation parameter λ for kerosene based ferrofluid

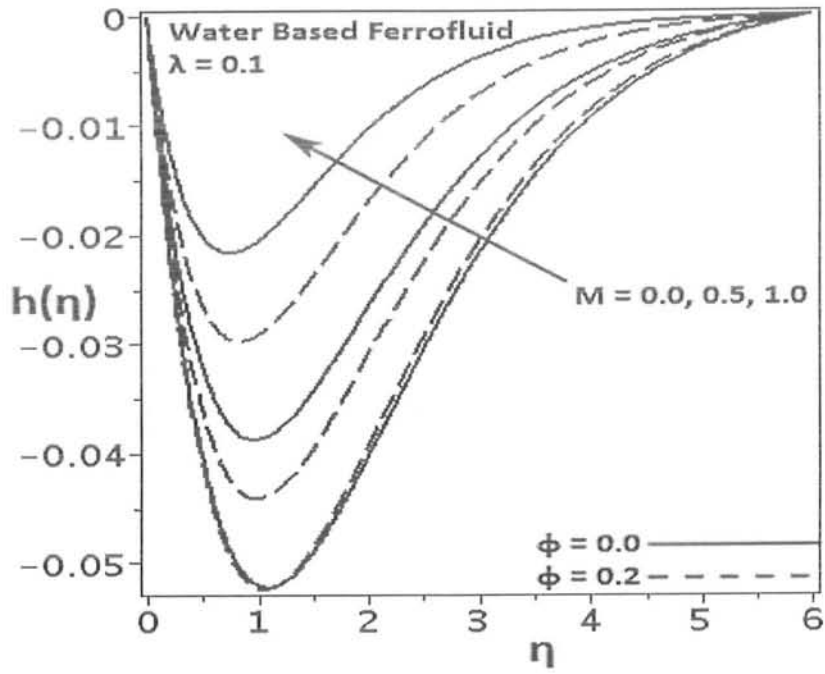


Fig. (4.6): Velocity profile $h(\eta)$ against magnetic parameter M for water based ferrofluid

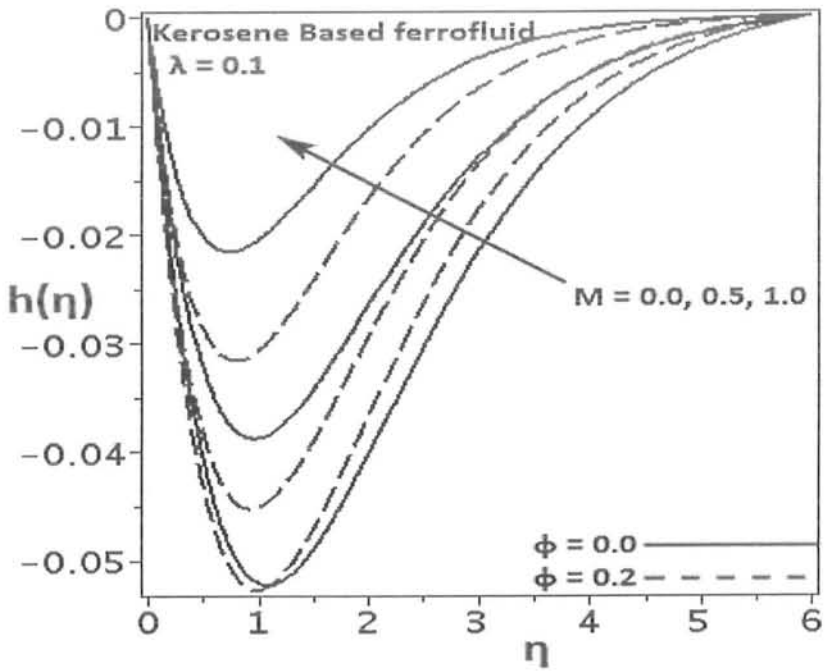


Fig. (4.7): Velocity profile $h(\eta)$ against magnetic parameter M for kerosene based ferrofluid

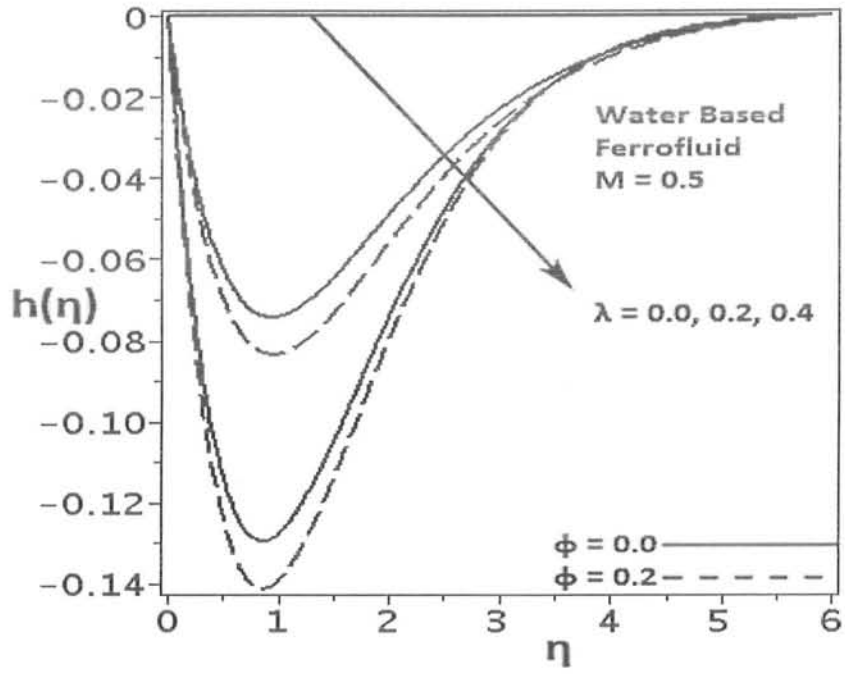


Fig. (4.8): Velocity profile $h(\eta)$ against rotation parameter λ for water based ferrofluid

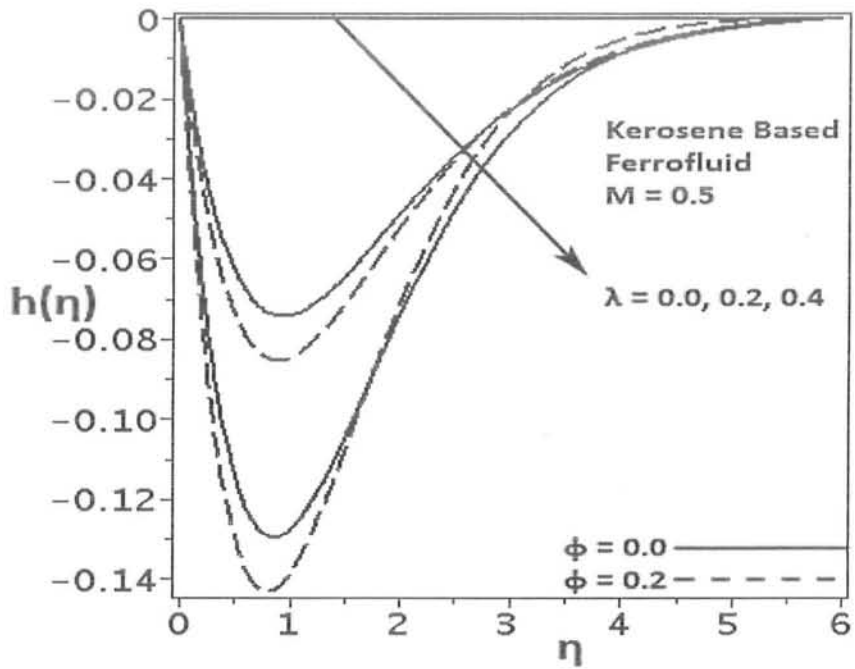


Fig. (4.9): Velocity profile $h(\eta)$ against rotation parameter λ for kerosene based ferrofluid

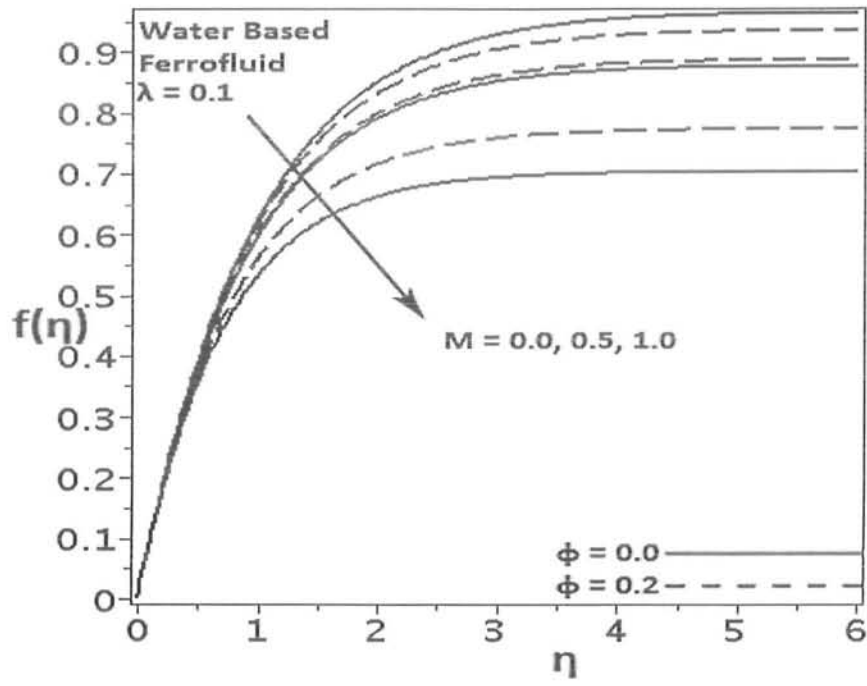


Fig. (4.10): Velocity profile $f(\eta)$ against magnetic parameter M for water based ferrofluid

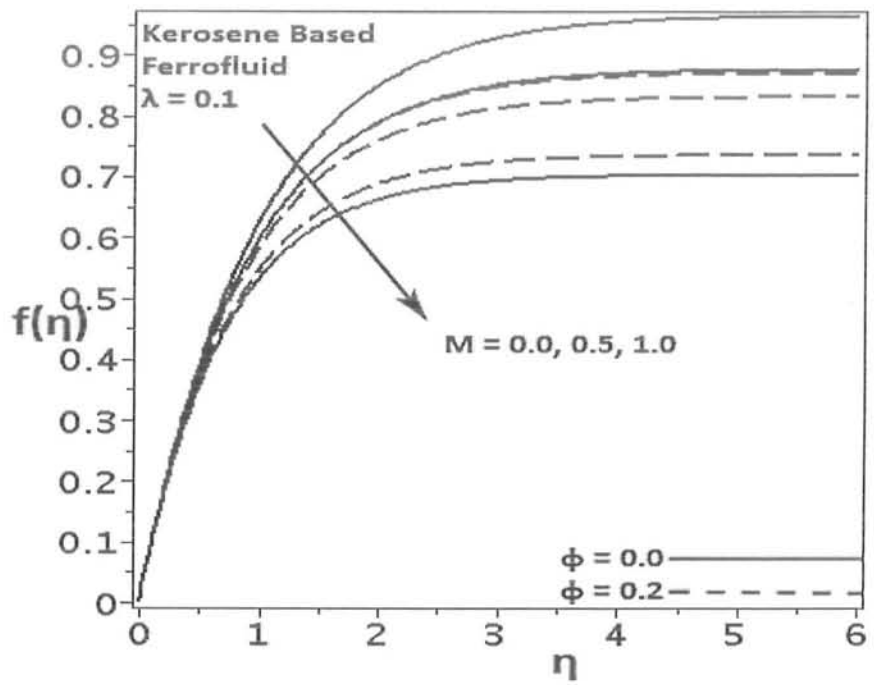


Fig. (4.11): Velocity profile $f(\eta)$ against magnetic parameter M for kerosene based ferrofluid

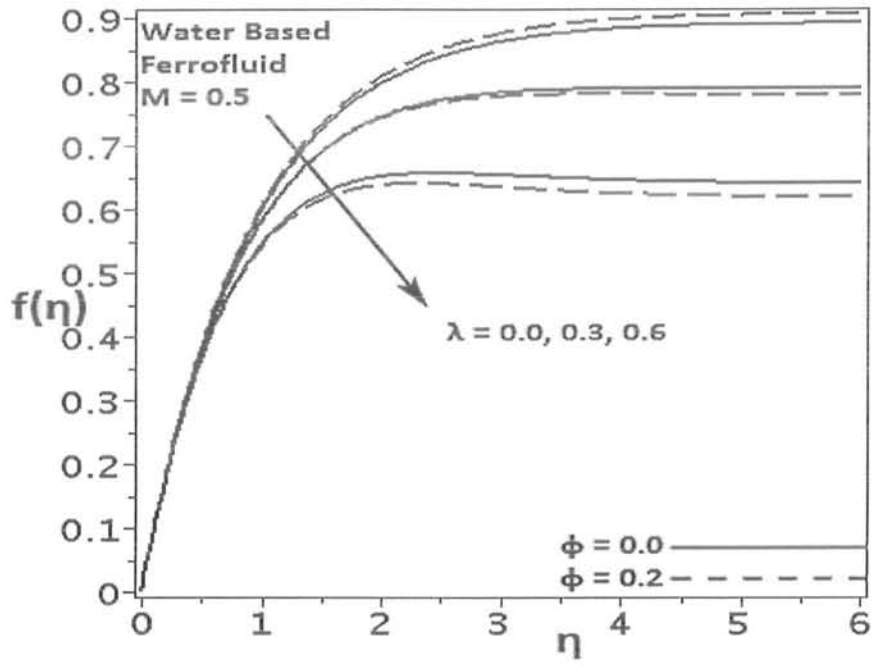


Fig. (4.12): Velocity profile $f(\eta)$ against rotation parameter λ for water based ferrofluid

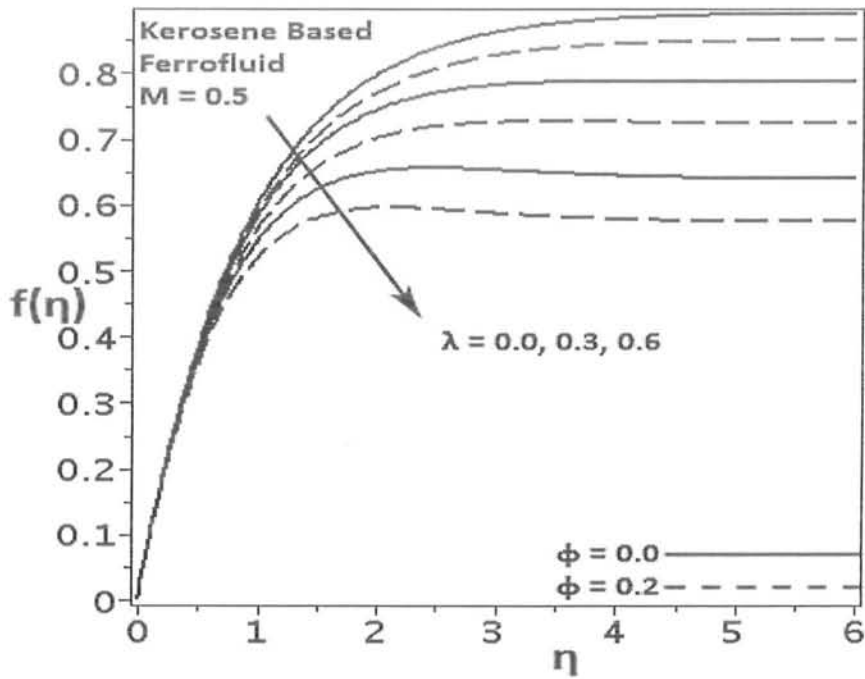


Fig. (4.13): Velocity profile $f(\eta)$ against rotation parameter λ for kerosene based ferrofluid

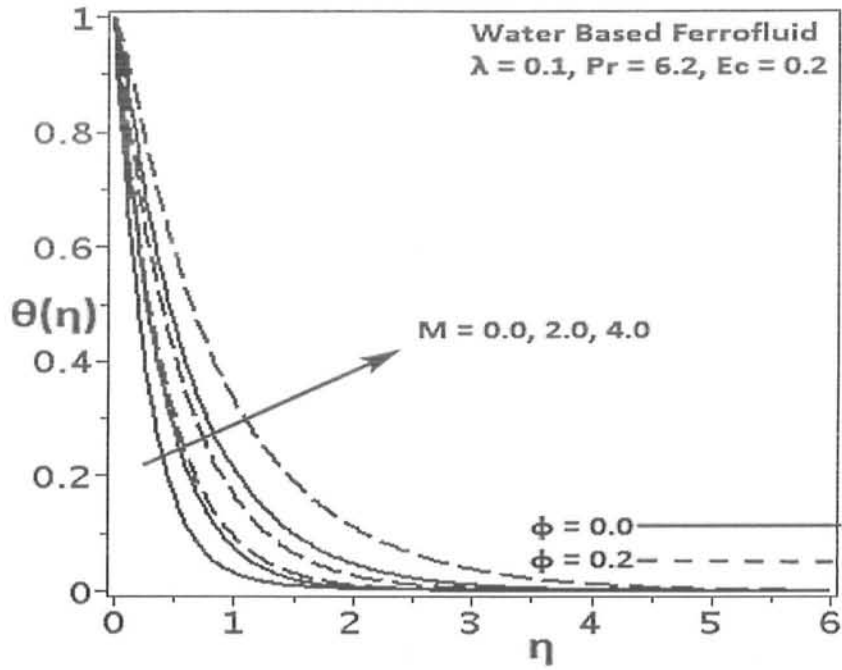


Fig. (4.14): Temperature profile $\theta(\eta)$ against magnetic parameter M for water based ferrofluid

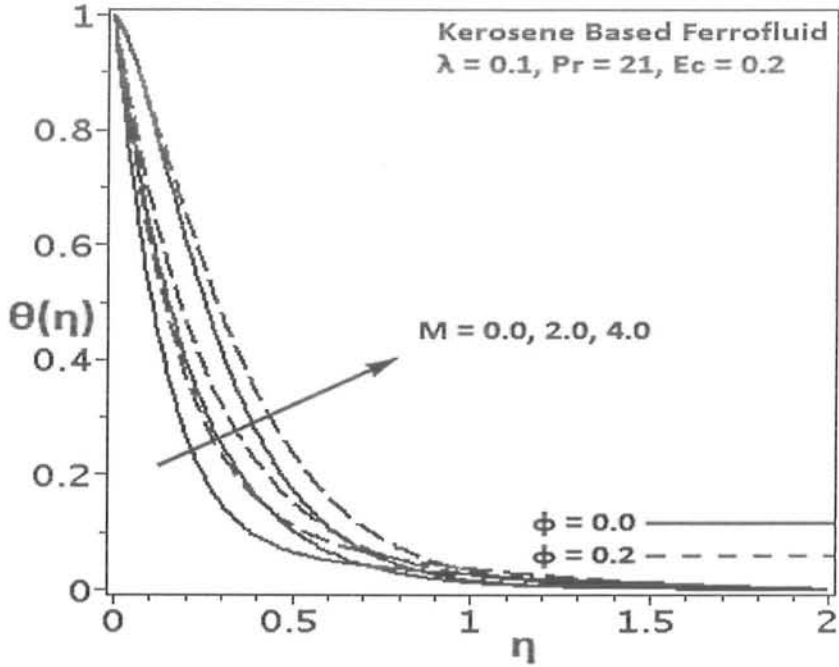


Fig. (4.15): Temperature profile $\theta(\eta)$ against magnetic parameter M for kerosene based ferrofluid

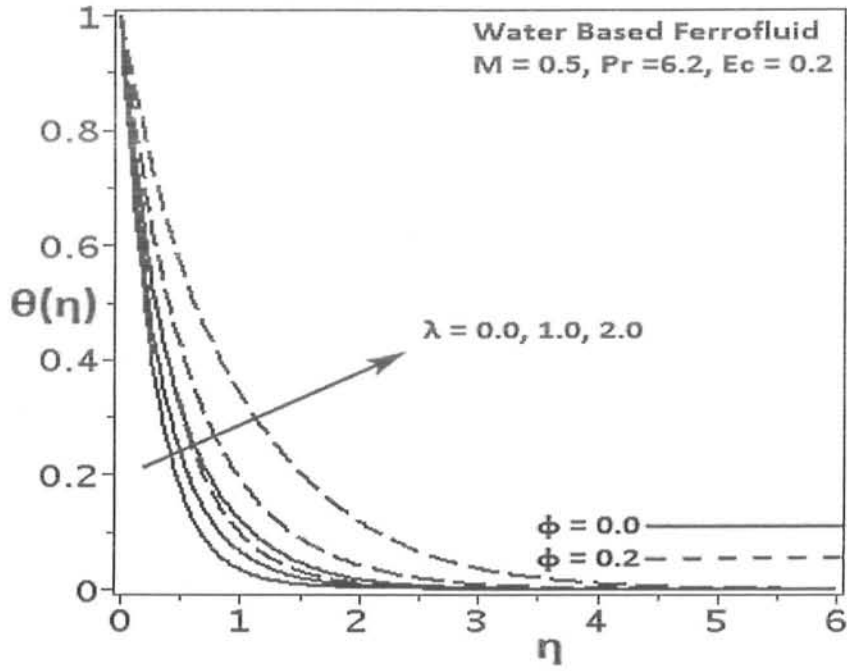


Fig. (4.16): Temperature profile $\theta(\eta)$ against rotation parameter λ for water based ferrofluid

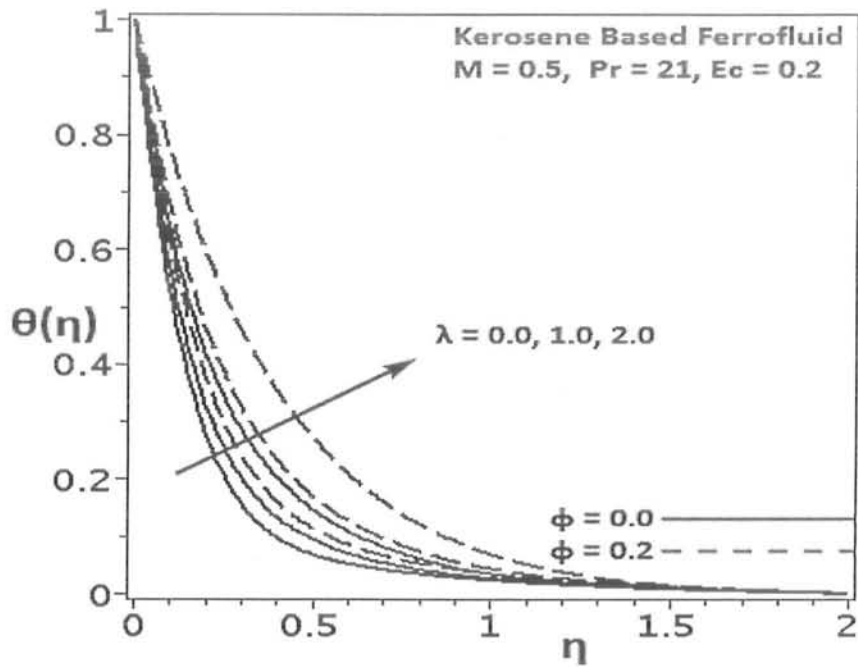


Fig. (4.17): Temperature profile $\theta(\eta)$ against rotation parameter λ for kerosene based ferrofluid

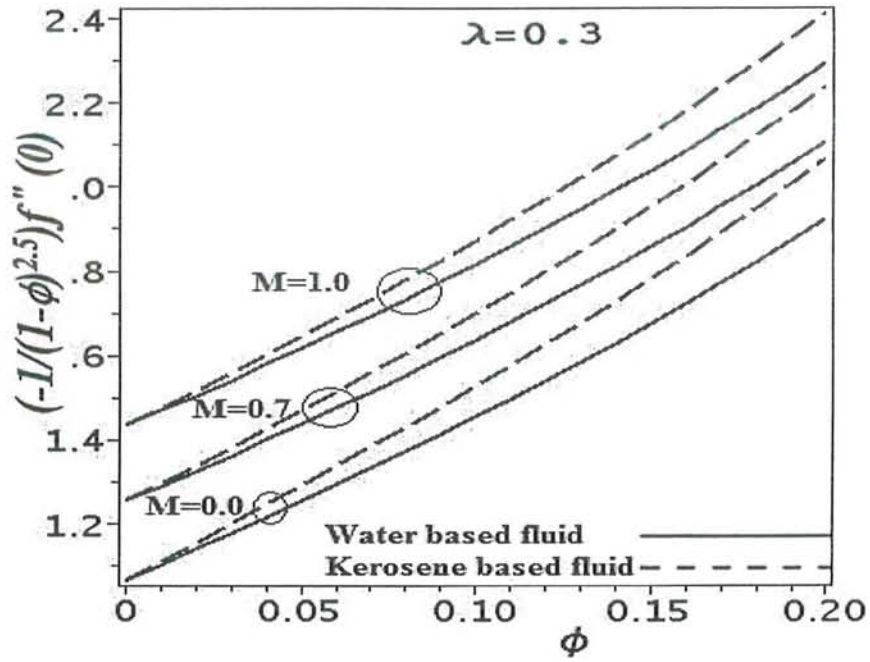


Fig. (4.18): Effects of M and ϕ on skin friction $(-\frac{1}{(1-\phi)^{2.5}})f''(0)$ for both ferrofluids

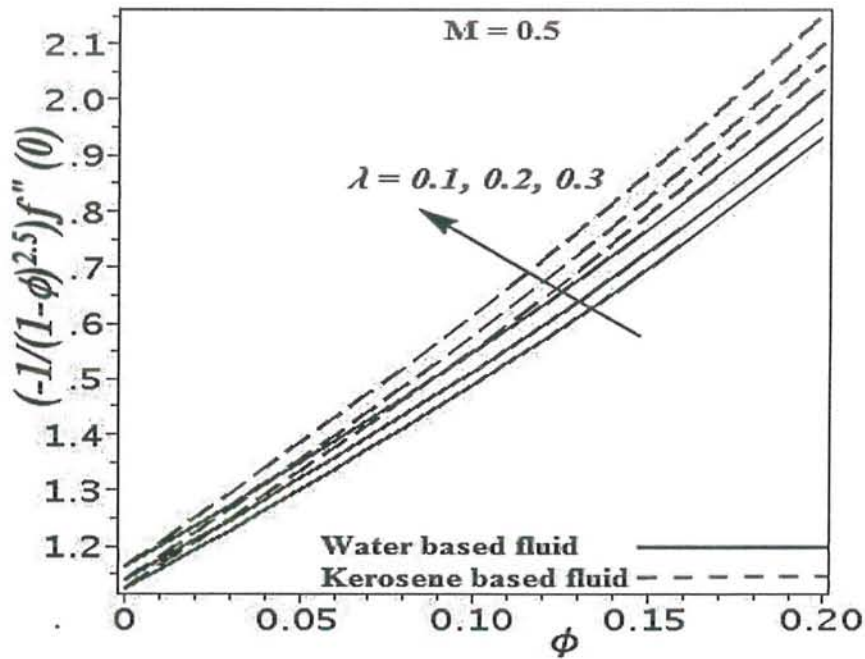
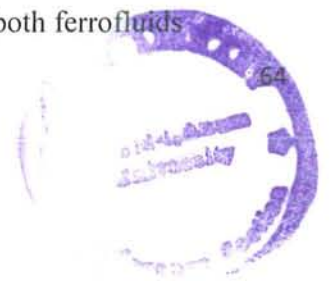


Fig. (4.19): Effects of λ on skin friction $(-\frac{1}{(1-\phi)^{2.5}})f''(0)$ for both ferrofluids



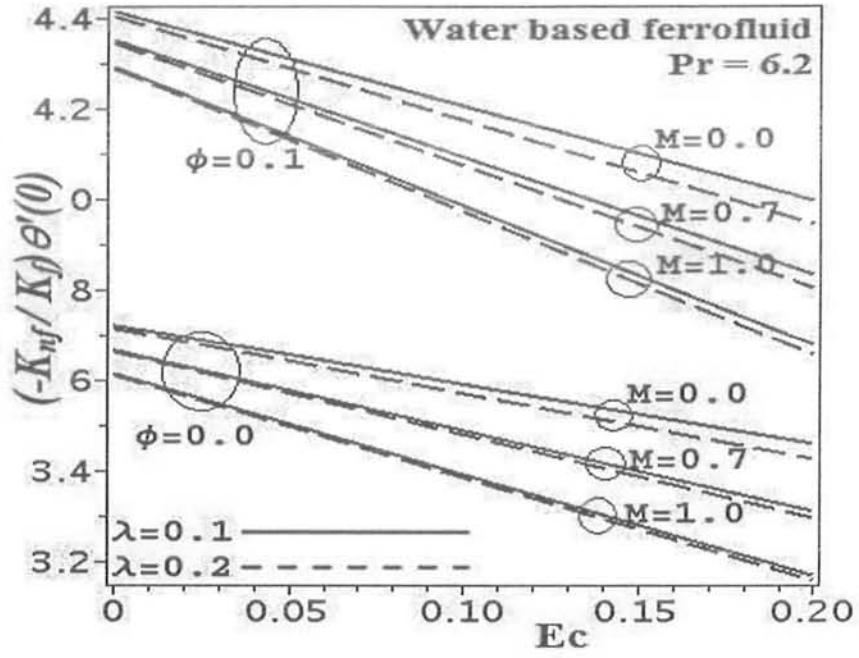


Fig. (4.20): Effects of ϕ, λ, Ec and M on local heat flux $\left(-\frac{K_{nf}}{K_f}\right)\theta'(0)$ for water based ferrofluid

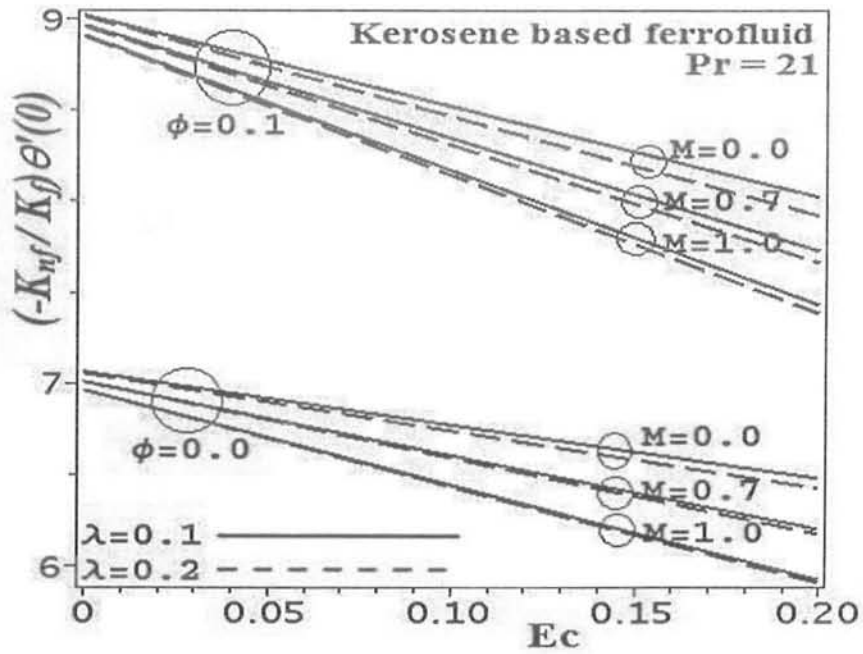


Fig. (4.21): Effects of ϕ, λ, Ec and M on local heat flux $\left(-\frac{K_{nf}}{K_f}\right)\theta'(0)$ for kerosene based ferrofluid

Table (4.1): Thermophysical properties of basefluids and solid nanoparticles [38, 47]

Properties\Constituents	Water	Kerosene Oil	Barium Ferrite ($BaO.6Fe_2O_3$)
Density (ρ) (Kg/m^3)	997.1	783	5280
Specific Heat C_p J/Kg.K	4179	2090	650
Thermal Conductivity (K) W/m.K	0.613	0.15	315
Prandtl Number (Pr)	6.2	21	-

Table (4.2): Effects of φ and M on skin friction and heat flux ($\lambda = 0.2, Ec = 0.2$)

φ	M	Water Based Ferrofluid Pr = 6.2		Kerosene Based Ferrofluid Pr = 21	
		$-(1 - \varphi)^{-2.5} f''(0)$	$\frac{-K_{nf}}{K_f} \theta'(0)$	$-(1 - \varphi)^{-2.5} f''(0)$	$\frac{-K_{nf}}{K_f} \theta'(0)$
0.0	0.0	1.033105	3.425052	1.033105	6.425050
	0.5	1.139403	3.357520	1.139403	6.298543
	1.0	1.423219	3.157379	1.423219	5.912078
	1.5	1.806719	2.861041	1.806719	5.314657
0.1	0.0	1.409090	3.944086	1.478730	7.922196
	0.5	1.511260	3.871845	1.576232	7.790811
	1.0	1.794534	3.652673	1.848817	7.383446
	1.5	2.196177	3.315605	2.240073	6.730525
0.2	0.0	1.861787	4.620825	2.001546	9.989300
	0.5	1.965968	4.539890	2.098602	9.845294
	1.0	2.260911	4.291290	2.375943	9.397217
	1.5	2.692856	3.898601	2.788776	8.663356

Table (4.3): Effects of φ and λ on skin friction and heat flux ($M = 1.0, Ec = 0.2$)

φ	λ	Water Based Ferrofluid $Pr = 6.2$		Kerosene Based Ferrofluid $Pr = 21$	
		$-(1 - \varphi)^{-2.5} f''(0)$	$\frac{-K_{nf}}{K_f} \theta'(0)$	$-(1 - \varphi)^{-2.5} f''(0)$	$\frac{-K_{nf}}{K_f} \theta'(0)$
0.0	0.0	1.414214	3.171291	1.414214	5.939432
	0.1	1.416499	3.167763	1.416499	5.932498
	0.2	1.423219	3.157379	1.423219	5.912078
	0.3	1.433993	3.140679	1.433993	5.879218
0.1	0.0	1.778109	3.681581	1.830328	7.445925
	0.1	1.782312	3.674197	1.835071	7.429930
	0.2	1.794534	3.652673	1.848817	7.383446
	0.3	1.813759	3.618662	1.870312	7.310361
0.2	0.0	2.234858	4.343445	2.345310	9.510975
	0.1	2.241574	4.330034	2.353242	9.481600
	0.2	2.260911	4.291290	2.375943	9.397217
	0.3	2.290830	4.230960	2.410732	9.267064

Table (4.4): Comparison of skin frictions $f''(0)$ and $h'(0)$ for viscous fluid ($\varphi = 0 = M$)

λ	Kumari & Nath[27]		Wang[31]		Present Results	
	$f''(0)$	$h'(0)$	$f''(0)$	$h'(0)$	$f''(0)$	$h'(0)$
0.0	0.9999	0.0000	1.0000	0.0000	1.00000	0.00000
0.5	1.1382	0.5124	1.1384	0.5128	1.13838	0.51276
1.0	1.3251	0.8362	1.3250	0.8371	1.32503	0.83710
2.0	1.6535	1.2851	1.6523	1.2873	1.65235	1.28726

Table (4.5): Some values of $\theta'(0)$ for conventional fluid ($\varphi = 0 = M, Ec = 0.1$)

Pr	$\lambda = 0.0$	$\lambda = 1.0$	$\lambda = 2.0$	$\lambda = 3.0$
0.7	1.04430	0.79926	0.60225	0.48131
2.0	1.94323	1.70376	1.41555	1.17421
6.0	3.53344	3.25129	2.92188	2.60377

4.6 Conclusions

Magnetohydrodynamic steady revolving ferrofluid flow due to stretching surface with viscous dissipation has been investigated. Key points of the study can be stated as:

- 1) Both magnetic field and rotation decay the linear velocity profiles for water and kerosene based fluids.
- 2) Inclusion of ferromagnetic nanoparticles raises the fluid velocity in non-zero magnetic field. This rise is prominent for water based fluid.
- 3) Magnetic field and rotation parameter enhance temperature profile for both types of nano fluids.
- 4) Local skin friction increases with increase in magnetic parameter M , rotation parameter λ and particle volume fraction of nano particles φ . Higher skin friction is recorded for kerosene based fluid compare to water based nanofluid.
- 5) Heat transfer rate at wall increases with increase in solid particle volume fraction φ but it drops with increasing magnetic field , rotation, and Eckert number. Relatively high values of local heat flux have been observed for kerosene based ferrofluid.
- 6) Category of base fluid selected for heat transfer purpose is of vital importance. To achieve the optimal results, water is preferred as base fluid.

Chapter 5

Effects of single and multi-walled carbon nanotubes on water and engine oil based rotating fluid with internal heating

5.1 Introduction

Three dimensional (3D) flow of a rotating nano fluid is analyzed in this unit. Single walled carbon nano tubes (SWCNTs) and multiwalled carbon nanotubes (MWCNTs) are suspended in traditional water and engine oil base fluids. Mathematical formulation is presented with internal heating. Solution of consequential equations is extracted numerically by using a combination of Quasi-linearization and Chebyshev pseudo-spectral methods [63-66]. Effects of relevant parameters on the flow quantities are examined.

5.2 Mathematical formulation

Let us consider steady 3D incompressible nanofluid in thermal equilibrium with itself is considered here at lying in the region $Z \geq 0$. The elastic boundary $Z = 0$ is being stretched along $x - axis$ in the opposite directions keeping the origin (0,0,0) fixed. A constant angular velocity Ω is associated with the fluid rotating about the $Z-axis$. Boundary layer balances of mass, motion and thermal energy accomplishing the flow and heat transfer with heat source / sink neglecting pressure gradient and viscous dissipation are [31, 77]

$$\frac{\partial u}{\partial x} + \frac{\partial v}{\partial y} + \frac{\partial w}{\partial z} = 0, \quad (5.1)$$

$$u \frac{\partial u}{\partial x} + v \frac{\partial u}{\partial y} + w \frac{\partial u}{\partial z} - 2\Omega v = \frac{\mu_{nf}}{\rho_{nf}} \nabla^2 u, \quad (5.2)$$

$$u \frac{\partial v}{\partial x} + v \frac{\partial v}{\partial y} + w \frac{\partial v}{\partial z} + 2\Omega u = \frac{\mu_{nf}}{\rho_{nf}} \nabla^2 v, \quad (5.3)$$

$$u \frac{\partial w}{\partial x} + v \frac{\partial w}{\partial y} + w \frac{\partial w}{\partial z} = \frac{\mu_{nf}}{\rho_{nf}} \nabla^2 w, \quad (5.4)$$

$$u \frac{\partial T}{\partial x} + v \frac{\partial T}{\partial y} + w \frac{\partial T}{\partial z} = \alpha_{nf} \frac{\partial^2 T}{\partial z^2} + \frac{Q_0}{(\rho C_p)_{nf}} (T - T_\infty), \quad (5.5)$$

where Q_0 is the dimensional heat absorption / generation coefficient. Relations of particle volume fraction φ are given by [22, 23, 24, 55].

$$\left. \begin{aligned} \rho_{nf} &= \rho_f \left[1 - \varphi + \varphi \left(\frac{\rho_{CNT}}{\rho_f} \right) \right], \mu_{nf} = \frac{\mu_f}{(1-\varphi)^{2.5}}, \alpha_{nf} = \frac{K_{nf}}{(\rho C_p)_{nf}}, \\ v_{nf} &= \frac{\mu_{nf}}{\rho_{nf}}, \quad (\rho C_p)_{nf} = (\rho C_p)_f \left[1 - \varphi + \varphi \left(\frac{(\rho C_p)_{CNT}}{(\rho C_p)_f} \right) \right], \\ \frac{K_{nf}}{K_f} &= \frac{(1-\varphi) + 2\varphi \left(\frac{K_{CNT}}{K_{CNT} - K_f} \right) \ln \frac{K_{CNT} + K_f}{2K_f}}{(1-\varphi) + 2\varphi \left(\frac{K_f}{K_{CNT} - K_f} \right) \ln \frac{K_{CNT} + K_f}{2K_f}}, \end{aligned} \right\} \quad (5.6a, b, c)$$

where ρ_{CNT} is density of carbon nanotubes, K_{CNT} represents the thermal conductance of carbon nanotubes and $(\rho C_p)_{CNT}$ is the volumetric heat capacity of carbon nanotubes.

Corresponding boundary conditions are defined as [31]

$$\begin{aligned} u &= ax, v = 0, w = 0 \quad \text{at } z = 0, \\ u &\rightarrow 0, v = 0 \quad \text{as } z \rightarrow \infty, \\ T &= T_w \quad \text{at } z = 0, \\ T &\rightarrow T_\infty \quad \text{as } z \rightarrow \infty. \end{aligned} \quad (5.7a, b, c, d)$$

Following the similarity transformations [31]

$$\left. \begin{aligned} u &= axf'(\eta), v = axh(\eta), w = -\sqrt{av} f(\eta), \\ \eta &= z \sqrt{\frac{a}{v}}, \quad \theta(\eta) = \frac{T - T_\infty}{T_w - T_\infty}. \end{aligned} \right\} \quad (5.8a, b)$$

Using relations (5.6a – c) and similarity transformations (5.8a, b), we observe that Eq. (5.1) is identically satisfied while Eqs. (5.2) – (5.5) take the form as

$$\frac{1}{(1-\varphi)^{2.5}} f'''' + \left(1 - \varphi + \varphi \frac{\rho_{CNT}}{\rho_f} \right) (ff'' - f'^2 + 2\lambda h) = 0, \quad (5.9)$$

$$\frac{1}{(1-\varphi)^{2.5}} h'' + \left(1 - \varphi + \varphi \frac{\rho_{CNT}}{\rho_f} \right) (fh' - hf' - 2\lambda f') = 0, \quad (5.10)$$

$$\frac{K_{nf}}{K_f} \theta'' + Pr \left(1 - \varphi + \varphi \frac{(\rho C_p)_{CNT}}{(\rho C_p)_f} \right) f\theta' + Pr\delta \theta = 0. \quad (5.11)$$

Here δ is the heat source (for $\delta > 0$) or heat sink (for $\delta < 0$) parameter and is defined as

$$\delta = \frac{Q_0}{a(\rho C_p)_f}. \quad (5.12)$$

Employment of Eqs. (5.6a, b, c) and (5.8a, b) in to (5.7a, b, c, d) provides us an adimensional set of boundary conditions as

$$\left. \begin{aligned} f(0) = 0, \quad f'(0) = 1, \quad f'(\infty) = 0, \\ h(0) = 0, h(\infty) = 0, \theta(0) = 1, \theta(\infty) = 0. \end{aligned} \right\} \quad (5.13a - b)$$

5.3 Solution method

Governing system of coupled non-linear differential Eqs. (5.9) – (5.11) with boundary conditions (5.13a, b) have been solved numerically by the *Chebyshev pseudo – spectral* method [63 – 66] after linearizing using the quasi-linearization method. The quasi-linearization method is a one term Taylor series expansion approach based on the assumption that the difference between values of approximate functions at successive iterations is small. We denote the difference between the approximate solution at current ($r + 1$) and previous (r) iterations by $f_{r+1} - f_r$. Application of the quasi-linearization technique on Eqs. (5.9) – (5.11) and on boundary conditions (5.13a – b) gives

$$\frac{1}{(1-\varphi)^{2.5}} f_{r+1}'''' + a_{1,r} f_{r+1}'' + a_{2,r} f_{r+1}' + a_{3,r} f_{r+1} + a_{4,r} h_{r+1} = R_{1,r}, \quad (5.14)$$

$$\frac{1}{(1-\varphi)^{2.5}} h_{r+1}'' + b_{1,r} h_{r+1}' + b_{2,r} h_{r+1} + b_{3,r} f_{r+1}' + b_{4,r} f_{r+1} = R_{2,r}, \quad (5.15)$$

$$\frac{K_{nf}}{K_f} \theta_{r+1}'' + Pr \left(1 - \varphi + \varphi \frac{(\rho C_p)_{CNT}}{(\rho C_p)_f} \right) f_{r+1} \theta_{r+1}' + Pr \delta \theta_{r+1} = 0, \quad (5.16)$$

where the coefficients in (5.14) – (5.15) are defined as

$$a_{1,r} = \left(1 - \varphi + \varphi \frac{\rho_{CNT}}{\rho_f} \right) f_r, \quad a_{2,r} = -2 \left(1 - \varphi + \varphi \frac{\rho_{CNT}}{\rho_f} \right) f_r',$$



$$\begin{aligned}
a_{3,r} &= \left(1 - \varphi + \varphi \frac{\rho_{CNT}}{\rho_f}\right) f_r'', & a_{4,r} &= 2\lambda \left(1 - \varphi + \varphi \frac{\rho_{CNT}}{\rho_f}\right), \\
R_{1,r} &= \left(1 - \varphi + \varphi \frac{\rho_{CNT}}{\rho_f}\right) (f_r f_r'' - f_r'^2), \\
b_{1,r} &= \left(1 - \varphi + \varphi \frac{\rho_{CNT}}{\rho_f}\right) f_r, & b_{2,r} &= -\left(1 - \varphi + \varphi \frac{\rho_{CNT}}{\rho_f}\right) f_r', \\
b_{3,r} &= \left(1 - \varphi + \varphi \frac{\rho_{CNT}}{\rho_f}\right) (-h_r - 2\lambda), & b_{4,r} &= \left(1 - \varphi + \varphi \frac{\rho_{CNT}}{\rho_f}\right) h_r', \\
R_{2,r} &= \left(1 - \varphi + \varphi \frac{\rho_{CNT}}{\rho_f}\right) (f_r h_r' - h_r f_r').
\end{aligned}$$

The boundary conditions at the current iteration take the form of (5.13a, b). Differential Eqs. (5.14) – (5.16) are not but linear ordinary in nature with variable coefficients and can be solved numerically. In this work, we engage the *Chebyshev pseudo – spectral* method to solve the system of Eqs. (5.14) – (5.16). For brevity, we omit details of the numerical procedure and refer interested readers to Nadeem *et al.* [39] for details.

To ensure the accuracy of our applied numerical algorithm residual errors are plotted through Figs. (5.1a – c) and a remarkable accuracy in the results is observed. The residual error is defined as the error obtained when the approximate numerical solutions are substituted in the governing Eqs. (5.9) – (5.11).

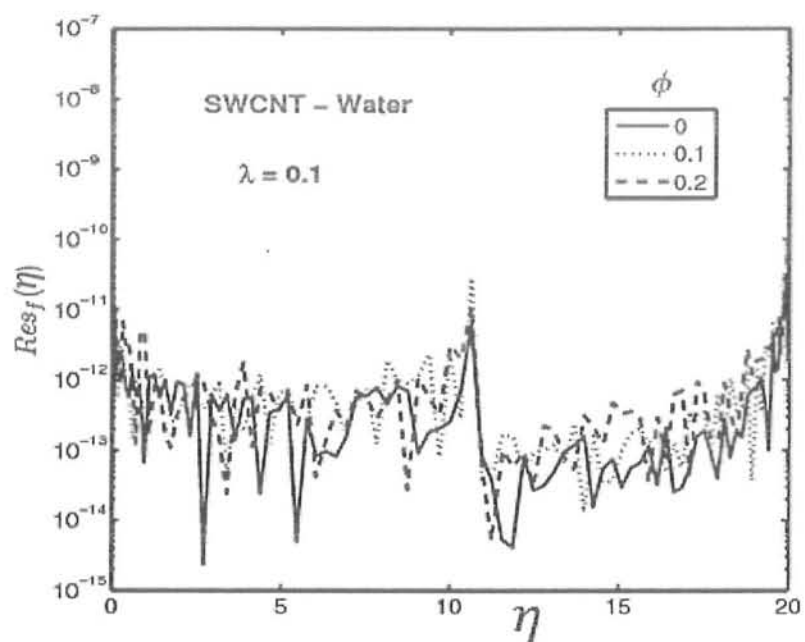


Fig. (5.1 a)

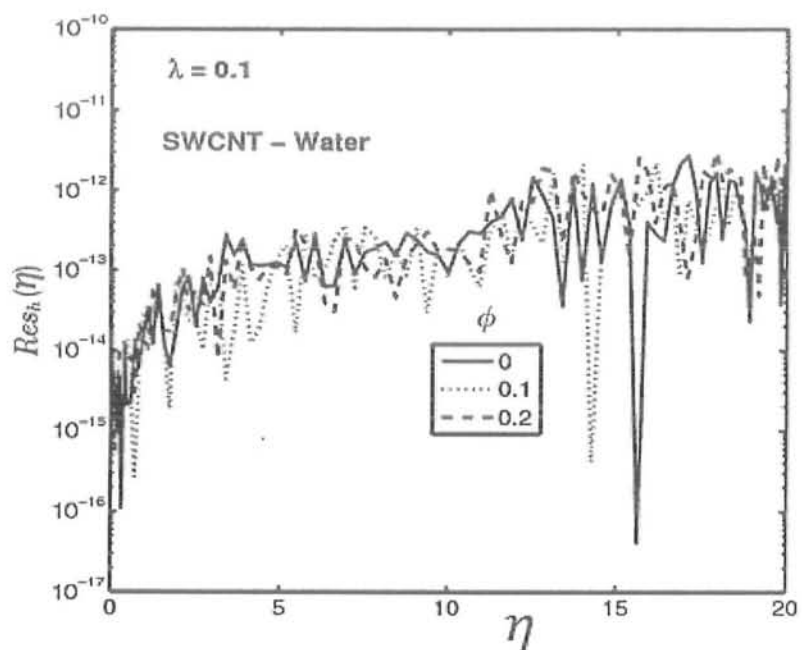


Fig. (5.1 b)

Figs. (5.1a, b): Residual errors against velocity profile

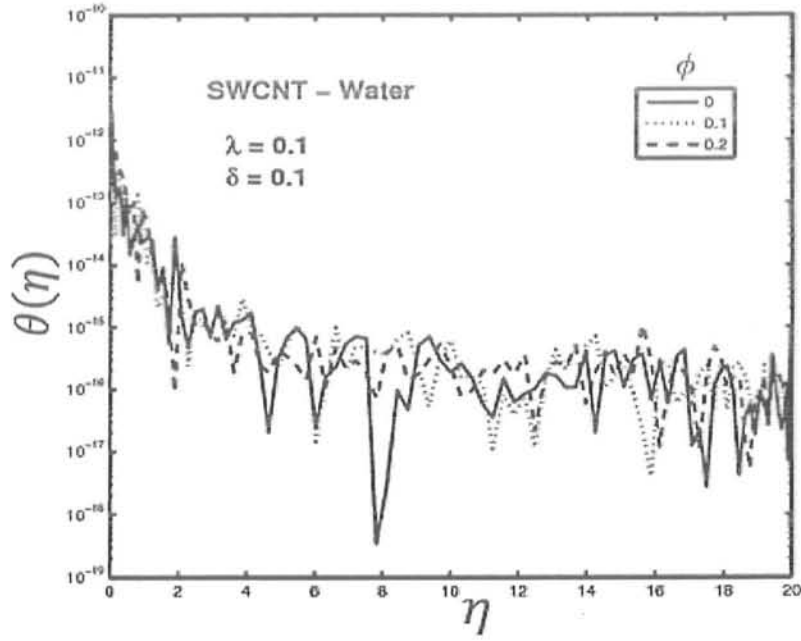


Fig. (5.1 c): Residual errors against temperature profile

5.4 Physical quantities of interest

Skin friction coefficient along x-axis (Cf_x) and along y-axis (Cf_y) are defined as [26]

$$Cf_x = \frac{\tau_{xz}}{\rho(ax)^2}, \quad Cf_y = \frac{\tau_{yz}}{\rho(ax)^2}, \quad (5.17)$$

τ_{xz}, τ_{yz} being shear stresses of the surface and are defined as

$$\tau_{xz} = \mu_{nf} \left(\frac{\partial u}{\partial z} \right)_{z=0}, \quad \tau_{yz} = \mu_{nf} \left(\frac{\partial v}{\partial z} \right)_{z=0}, \quad (5.18)$$

substituting values from Eqs. (5.8a,b) and Eq. (5.18) in Eq. (5.17), we take as

$$(Re_x)^{\frac{1}{2}} Cf_x = \frac{1}{(1-\phi)^{2.5}} f''(0), \quad (Re_x)^{\frac{1}{2}} Cf_y = \frac{1}{(1-\phi)^{2.5}} h'(0). \quad (5.19)$$

Where Re_x is the local Reynolds number defined as

$$Re_x = \frac{Ux}{\nu_f}. \quad (5.20)$$

In Eq. (5.19), $(Re_x)^{\frac{1}{2}} Cf_x$ and $(Re_x)^{\frac{1}{2}} Cf_y$ are non-dimensional skin frictions along x - axis and y - axis respectively.

The confined Nusselt number Nu may be determined as [23, 24]

$$Nu = \frac{xq_w}{K_f(T_w - T_\infty)}, \quad (5.21)$$

Where q_w is the local heat flux defined as

$$q_w = -K_{nf} \left(\frac{\partial T}{\partial z} \right)_{z=0}. \quad (5.22)$$

Using Eqs. (5.8a, b) and (5.22) in Eq. (5.21), we get

$$(Re_x)^{\frac{-1}{2}} Nu = \frac{-K_{nf}}{K_f} \theta'(0). \quad (5.23)$$

These physical quantities have been computed numerically against four types of nanofluids naming *SWCNT – water*, *MWCNT – water*, *SWCNT – engine Oil* and *MWCNT – engine Oil* for various values of particle volume fraction φ , rotation parameter λ and heat source/sink parameter δ in *Tables (5.2), (5.3) and (5.4)*.

5.5 Results and discussion

This subdivision examines the impact of individually suspended single and multiwalled carbon nanotubes in the traditional water based fluid on velocities, temperature and local heat flux rate. Figs. (5.2) – (5.9) have been plotted to meet the purpose. The influence of nano particle volume fraction φ on dimensionless horizontal velocity $f'(\eta)$ is presented through Figs. (5.2a) and (5.2b) for single and multiwalled carbon nanotubes with water based fluid. It can be perceived from both these Figs. that velocity $f'(\eta)$ rises with rise in volumetric nano particle fraction φ . Moreover this increasing trend is found to be more significant for the event of *MWCNTs*. This is due to the fact that *MWCNTs* retain lower density compare to *SWCNTs*. Figs. (5.3a) and (5.3b) shows that increasing nano particle volumetric fraction φ leads to an increasing dimensionless z-component of velocity $f(\eta)$ for single as well as multiwalled carbon nanotubes with water based fluid. From Figs. (5.4a) and (5.4b) we can notice that with a growth in volumetric nano particle fraction φ , dimensionless y-component of velocity $h(\eta)$ decreases for the case of single as well as multiwall carbon nanotubes. Figs. (5.5a) and (5.5b) depicts that an increasing nano particle volume fraction φ leads to a growth in temperature $\theta(\eta)$ as well as the corresponding thermal boundary layer depth for both single and multiwalled carbon nanotubes.

Where q_w is the local heat flux defined as

$$q_w = -K_{nf} \left(\frac{\partial T}{\partial z} \right)_{z=0}. \quad (5.22)$$

Using Eqs. (5.8a, b) and (5.22) in Eq. (5.21), we get

$$(Re_x)^{\frac{-1}{2}} Nu = \frac{-K_{nf}}{K_f} \theta'(0). \quad (5.23)$$

These physical quantities have been computed numerically against four types of nanofluids naming *SWCNT – water*, *MWCNT – water*, *SWCNT – engine Oil* and *MWCNT – engine Oil* for various values of particle volume fraction φ , rotation parameter λ and heat source/sink parameter δ in *Tables (5.2), (5.3) and (5.4)*.

5.5 Results and discussion

This subdivision examines the impact of individually suspended single and multiwalled carbon nanotubes in the traditional water based fluid on velocities, temperature and local heat flux rate. Figs. (5.2) – (5.9) have been plotted to meet the purpose. The influence of nano particle volume fraction φ on dimensionless horizontal velocity $f'(\eta)$ is presented through Figs. (5.2a) and (5.2b) for single and multiwalled carbon nanotubes with water based fluid. It can be perceived from both these Figs. that velocity $f'(\eta)$ rises with rise in volumetric nano particle fraction φ . Moreover this increasing trend is found to be more significant for the event of *MWCNTs*. This is due to the fact that *MWCNTs* retain lower density compare to *SWCNTs*. Figs. (5.3a) and (5.3b) shows that increasing nano particle volumetric fraction φ leads to an increasing dimensionless z-component of velocity $f(\eta)$ for single as well as multiwalled carbon nanotubes with water based fluid. From Figs. (5.4a) and (5.4b) we can notice that with a growth in volumetric nano particle fraction φ , dimensionless y-component of velocity $h(\eta)$ decreases for the case of single as well as multiwall carbon nanotubes. Figs. (5.5a) and (5.5b) depicts that an increasing nano particle volume fraction φ leads to a growth in temperature $\theta(\eta)$ as well as the corresponding thermal boundary layer depth for both single and multiwalled carbon nanotubes.

The physical reason behind it is that carbon nano tubes having higher thermal conductivities and lower specific heat as compared to their base fluid water and consequently heat up the fluid. Figs. (5.6a, b) depict that temperature $\theta(\eta)$ rises with rise in heat generation parameter $\delta > 0$ for *SWCNTs – water* as well as *MWCNTs – water* based fluid. On the other hand it can be perceived from Figs. (5.7a) and (5.7b) that when heat absorption parameter is increased the temperature $\theta(\eta)$ decreases near the wall for *SWCNTs – water* as well as *MWCNTs – water* based fluid. Physical quantities of our attention such as skin friction along x-axis i.e., $\frac{-1}{(1-\varphi)^{2.5}} f''(0)$, skin friction along y-axis i.e., $\frac{-1}{(1-\varphi)^{2.5}} h'(0)$ are shown in Figs. (5.8a) and (5.8b) respectively. It can be noticed from these Figs. that increasing the nano particle volume fraction φ lead to an increase in both types of skin friction coefficients for single as well as multi walled carbon nano tubes. Moreover it is also noticed that *SWCNTs* offered higher skin friction compared to *MWCNTs*. This is due to the fact that *SWCNTs* are higher in density compare to *MWCNTs*. We have also observed that an increase in rotation parameter λ consequently increases the local skin frictions. Influence of rotation parameter λ , heat generation parameter $\delta > 0$ and nano particle volume fraction φ on surface heat flux $\frac{-K_{nf}}{K_f} \theta'(0)$ has been presented through Figs. (5.9a) and (5.9b) for single and multiwalled carbon nanotubes. We can notice from Fig. (5.9a) that local heat flux $\frac{-K_{nf}}{K_f} \theta'(0)$ increases significantly with an increase in particle volumetric fraction φ for *SWCNTs* as well as *MWCNTs – water* based fluid. It is worth stating here that when $0 < \varphi < 0.1$, *SWCNTs* has offered higher heat transfer rate while for $0.1 < \varphi < 0.2$, *MWCNTs* proved to be more rapid heat transfer agent at the surface. Similarly from Fig. (5.9b) it can be perceived that local heat flux $\frac{-K_{nf}}{K_f} \theta'(0)$ reduces with a growth in heat generation parameter $\delta > 0$. Table (5.1) gives the thermo physical properties of base fluids and carbon nano tubes. Tables (5.2 – 5.6) are prepared to discover the effects of

pertinent physical parameters on tangential stresses and heat transfer rate at wall for *SWCNTs* as well as *MWCNTs* using water and engine oil based fluids. From *Table (5.2)* we can deduce that local skin friction $\frac{-1}{(1-\varphi)^{2.5}} f''(0)$ rises with a rise in volumetric fraction φ of nano particles and rotation parameter λ . This increasing behavior is found to be similar for *SWCNTs* as well as *MWCNTs* using water and engine oil based fluids. Moreover higher values of $\frac{-1}{(1-\varphi)^{2.5}} f''(0)$ are observed when engine oil is used as base fluid compared to water base fluid. Similar kind of observations can be found in *Table (5.3)*, where we notice that there is direct influence of nano particle volume fraction φ and rotation parameter λ on skin friction $\frac{-1}{(1-\varphi)^{2.5}} h'(0)$. It is noticed that for water as well as engine oil based fluid, *MWCNTs* offered less resistance compared to *SWCNTs* in term of skin friction $\frac{-1}{(1-\varphi)^{2.5}} h'(0)$. *Table (5.4)* gives the numerical values of local heat flux i.e., $\frac{-K_{nf}}{K_f} \theta'(0)$ against nano particle volume fraction φ and heat generation parameter $\delta > 0$. Local heat flux rate $\frac{-K_{nf}}{K_f} \theta'(0)$ significantly proliferates with a rise in nano particle volume fraction φ for *SWCNTs* and *MWCNTs* for water as well as engine oil based fluids. On the other hand local heat flux rate $\frac{-K_{nf}}{K_f} \theta'(0)$ declines with a growth in heat generation parameter $\delta > 0$ for both types of base fluids and carbon nano tubes. Finally *Table (5.5)* and *(5.6)* are prepared to validate our present results. We can easily detect from these two tables that our obtained consequences are in outstanding agreement with those of already published literature in absence of nano particles/ internal heating.

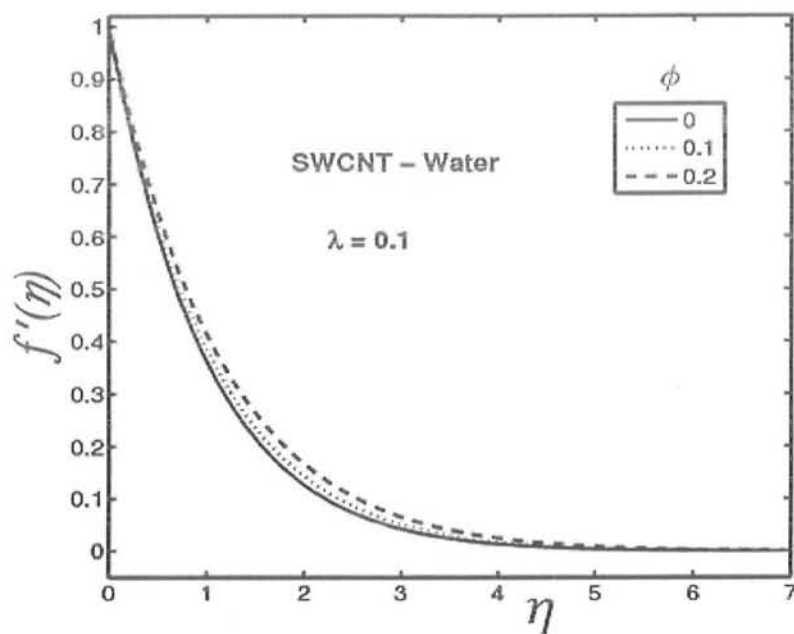


Fig. (5.2 a)

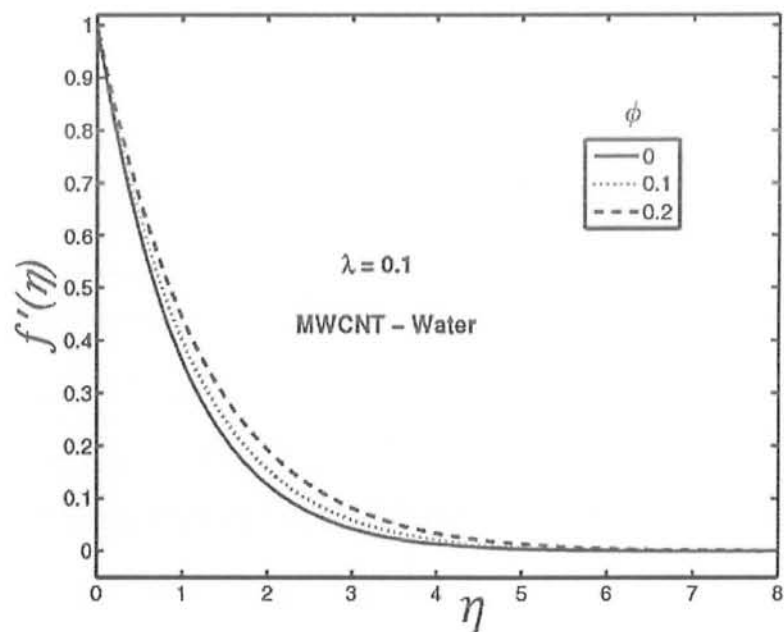


Fig. (5.2 b)

Figs. (5.2 a, b): Influence of volumetric particle fraction ϕ on velocity $f'(\eta)$ for *SWCNT – water* and *MWCNT – water* nanofluids

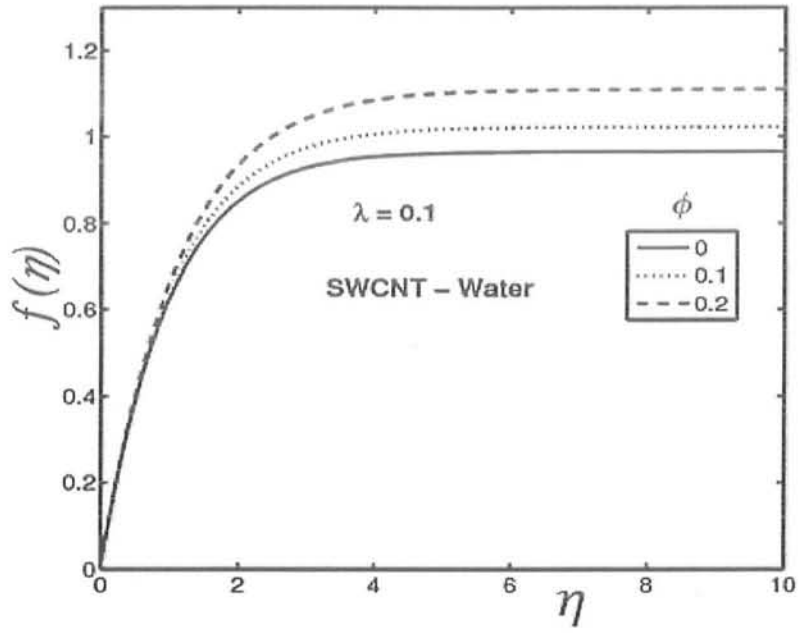


Fig. (5.3 a)

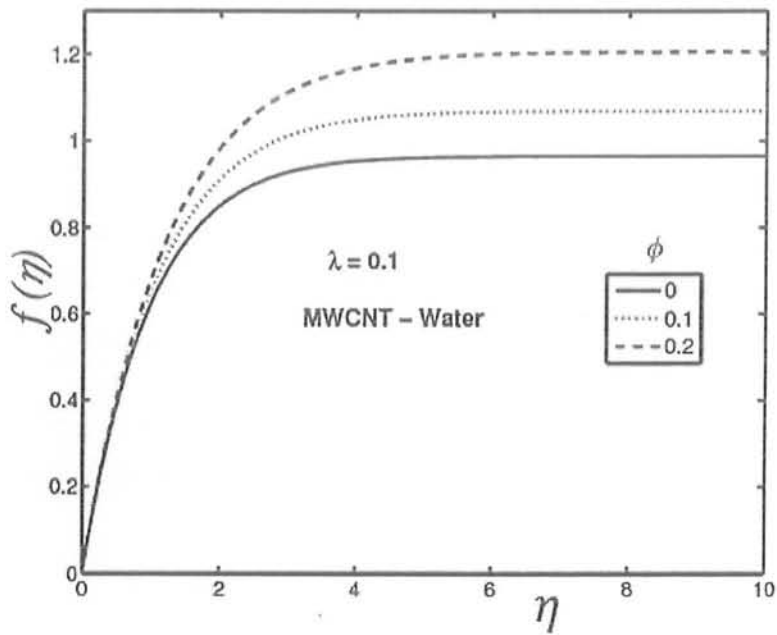


Fig. (5.3 b)

Figs. (5.3 a, b): Influence of volumetric particle fraction ϕ on velocity $f(\eta)$ for SWCNT and MWCNT - water nanofluids

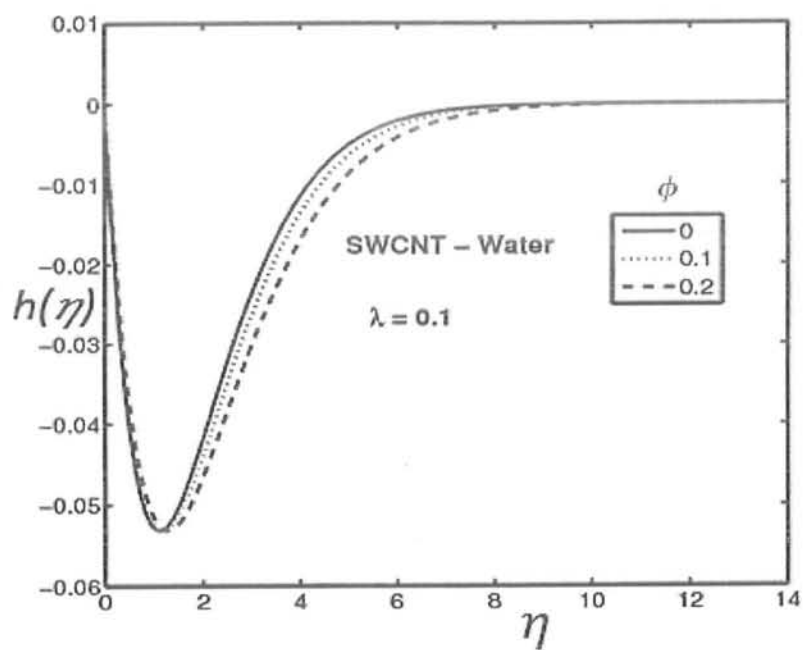


Fig. (5.4 a)

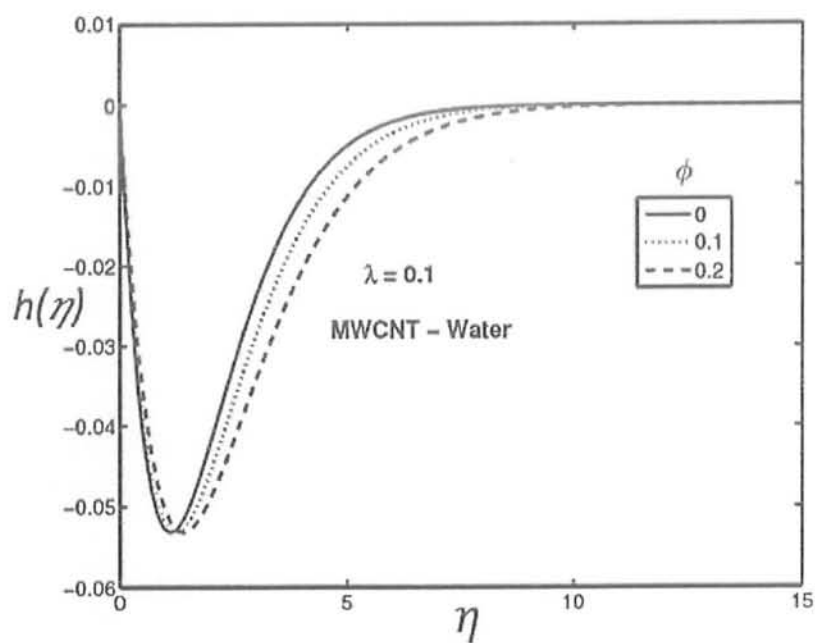


Fig. (5.4 b)

Figs. (5.4 a, b): Influence of volumetric particle fraction ϕ on velocity $h(\eta)$ for SWCNT and MWCNT - water nanofluids

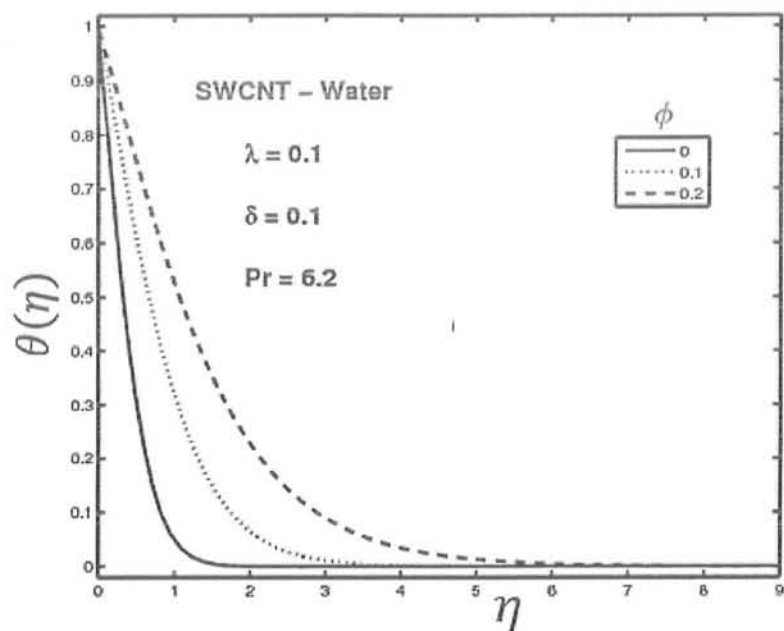


Fig. (5.5 a)

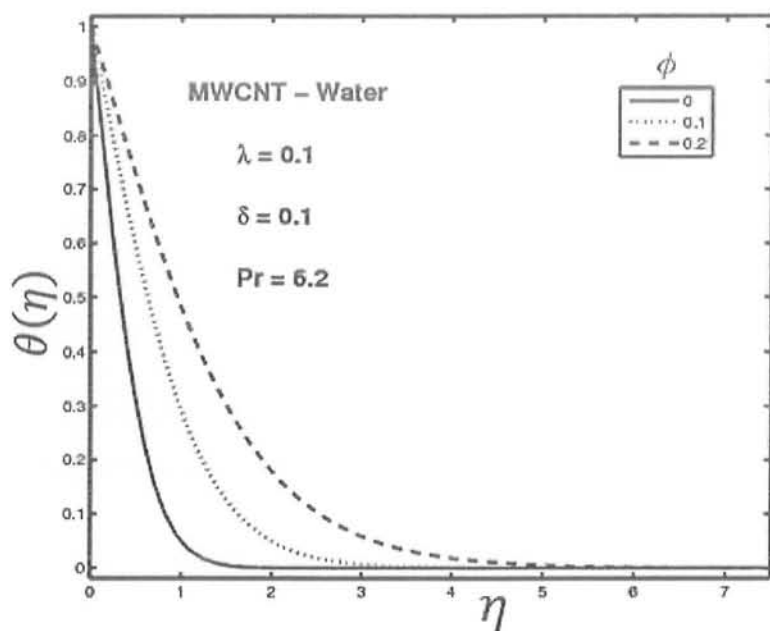


Fig. (5.5 b)

Figs. (5.5 a, b): Impact of volumetric particle fraction ϕ on $\theta(\eta)$ for SWCNT and MWCNT – water nanofluids

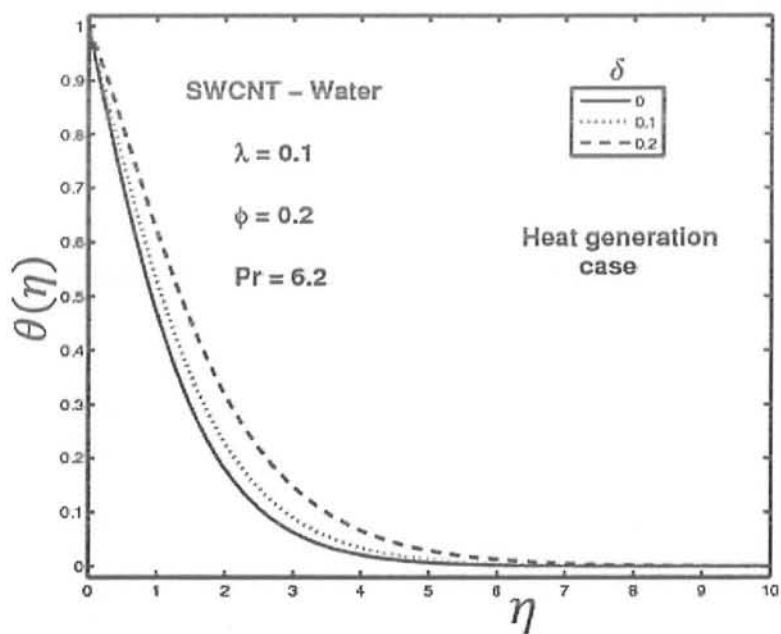


Fig. (5.6 a)

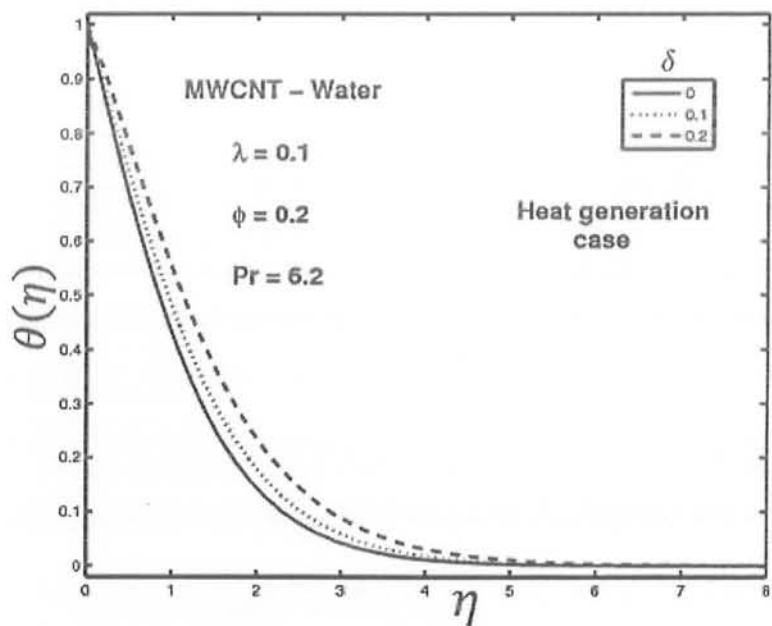


Fig. (5.6 b)

Figs. (5.6 a, b): Influence of heat generation parameter $\delta > 0$ on $\theta(\eta)$ for *SWCNT* and *MWCNT* – water nanofluids

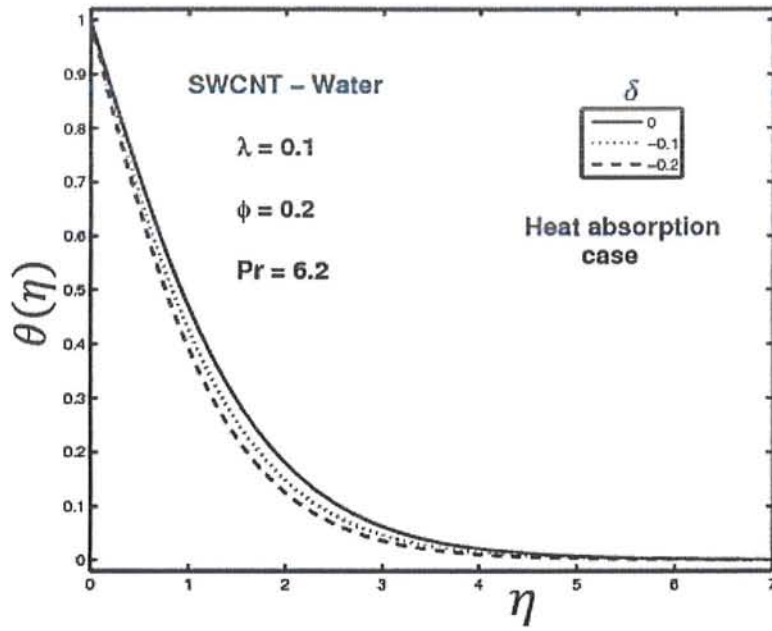


Fig. (5.7 a)

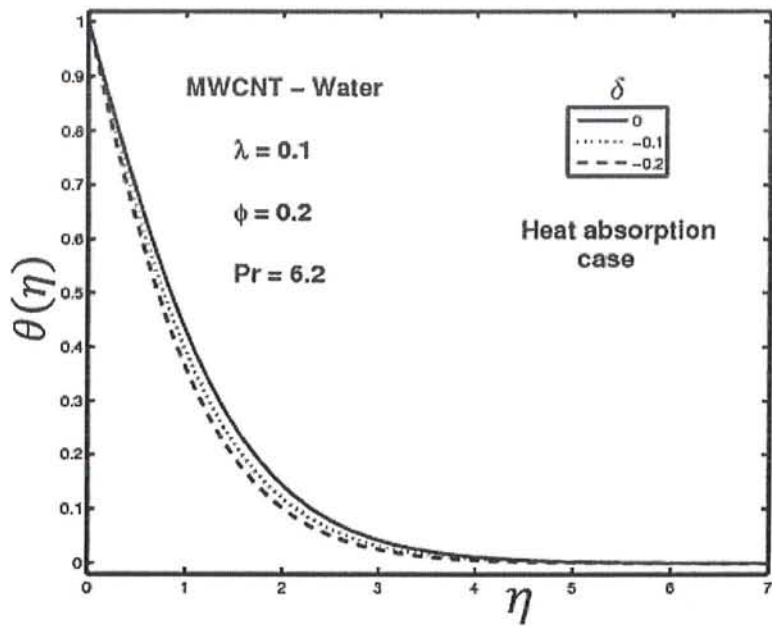
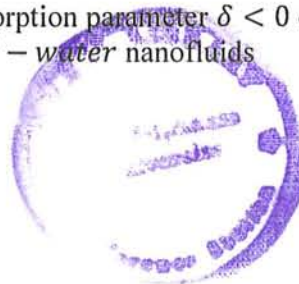


Fig. (5.7 b)

Figs. (5.7 a, b): Influence of heat absorption parameter $\delta < 0$ on $\theta(\eta)$ for SWCNT and MWCNT – water nanofluids



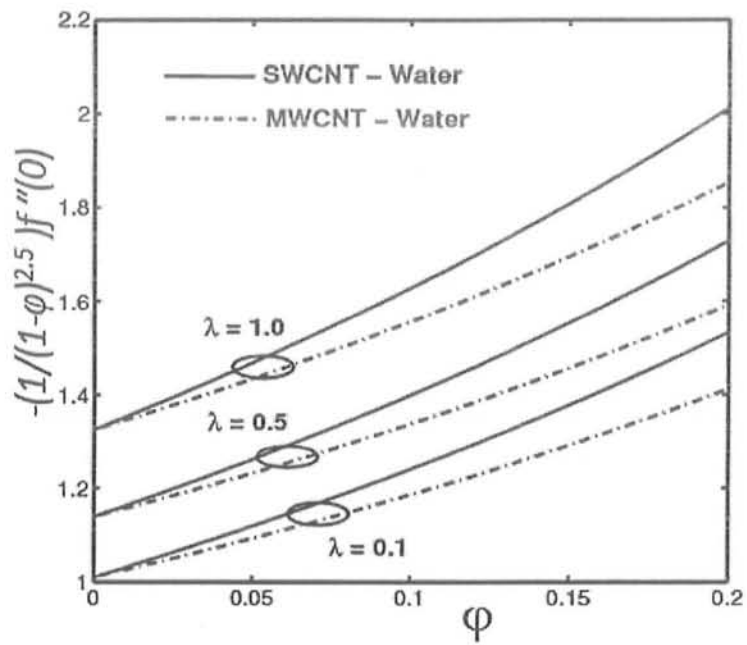


Fig. (5.8 a)

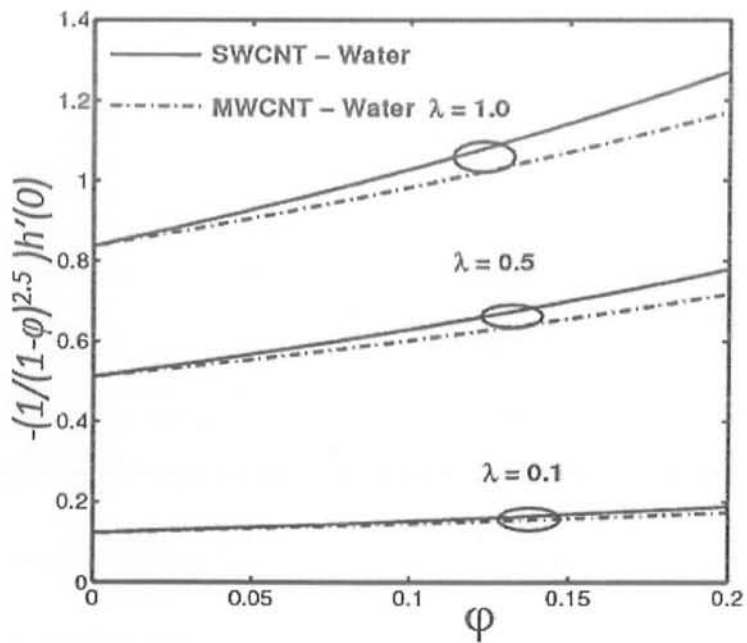


Fig. (5.8 b)

Figs. (5.8 a, b): Influence of particle volume fraction ϕ and rotation parameter λ on skin frictions $(1 - \phi)^{-2.5} f''(0)$ and $(1 - \phi)^{-2.5} h'(0)$

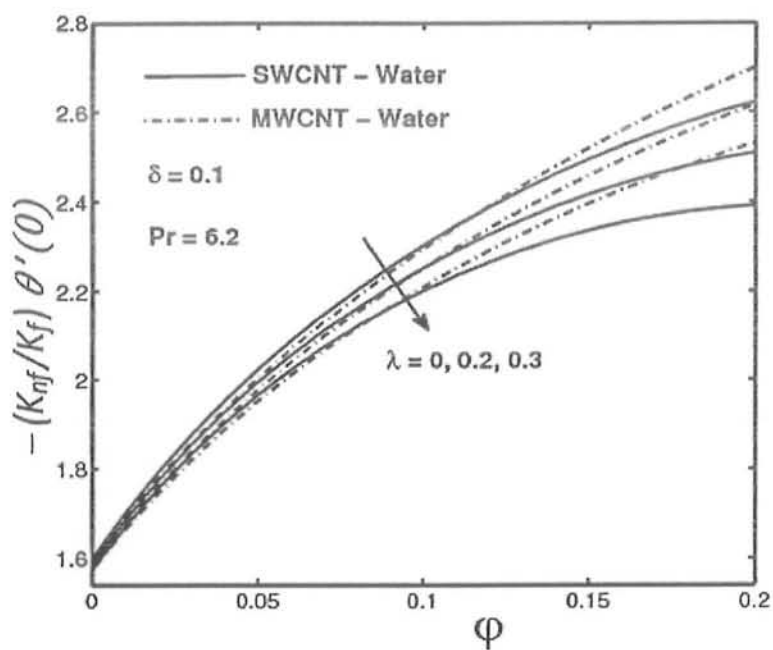


Fig. (5.9 a)

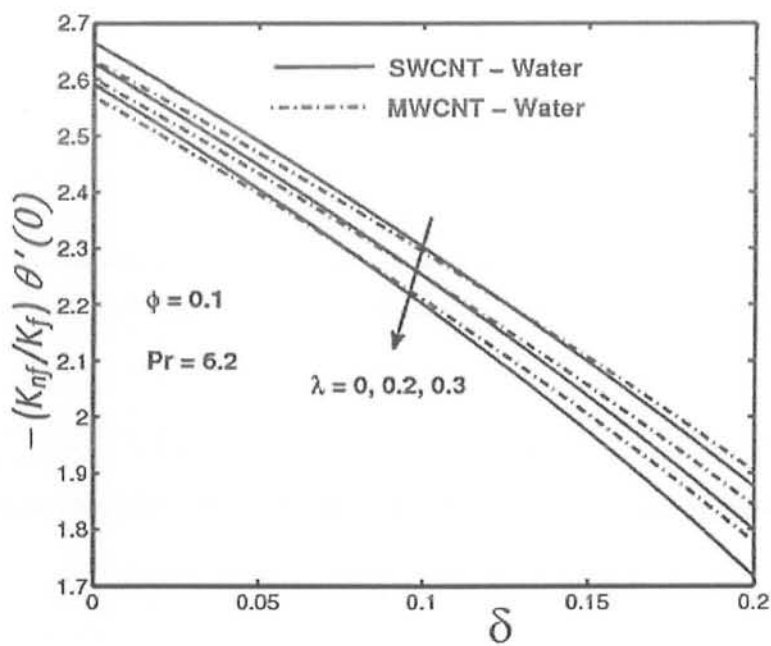


Fig. (5.9 b)

Figs. (5.9 a, b): Influence of particle volume fraction ϕ and heat generation parameter δ on surface heat flux $\frac{-K_{nf}}{K_f} \theta'(0)$

Table (5.1): Thermophysical properties of constituents

Properties\Constituents	Water	Engine Oil	SWCNT	MWCNT
Density (ρ) Kg/m ³	997	884	2600	1600
Specific Heat (Cp) J/Kg.k	4179	1910	425	796
Thermal Conductivity (K) W/m.K	0.613	0.144	6600	3000
Prandtl Number (Pr)	6.2	6450	-	-

Table (5.2): Numerical values of local skin friction $\frac{-1}{(1-\varphi)^{2.5}} f''(0)$

φ	$\lambda = 0.00$	$\lambda = 0.10$	$\lambda = 0.20$	$\lambda = 0.30$	$\lambda = 0.00$	$\lambda = 0.10$	$\lambda = 0.20$	$\lambda = 0.30$
<i>SWCNT – Water Nanofluid</i>					<i>SWCNT – Engine Oil Nanofluid</i>			
0.00	1.00000	1.00925	1.03310	1.06507	1.00000	1.00925	1.03310	1.06507
0.05	1.10825	1.11850	1.14493	1.18036	1.11677	1.12710	1.15373	1.18943
0.10	1.22906	1.24043	1.26975	1.30904	1.24658	1.25812	1.28785	1.32770
0.20	1.51944	1.53349	1.56973	1.61831	1.55729	1.57170	1.60885	1.65862
<i>MWCNT – Water Nanofluid</i>					<i>MWCNT – Engine Oil Nanofluid</i>			
0.00	1.00000	1.00925	1.03310	1.06507	1.00000	1.00925	1.03310	1.06507
0.05	1.08222	1.09223	1.11805	1.15264	1.08759	1.099766	1.12360	1.15837
0.10	1.17476	1.18563	1.21365	1.25120	1.18607	1.19704	1.22533	1.26325
0.20	1.39937	1.41232	1.44570	1.49043	1.42475	1.43794	1.47192	1.51746

Table (5.3): Various values of skin friction $\frac{-1}{(1-\varphi)^{2.5}} h'(0)$

φ	$\lambda = 0.00$	$\lambda = 0.10$	$\lambda = 0.20$	$\lambda = 0.30$	$\lambda = 0.00$	$\lambda = 0.10$	$\lambda = 0.20$	$\lambda = 0.30$
	<i>SWCNT – Water Nanofluid</i>				<i>SWCNT – Engine Oil Nanofluid</i>			
0.00	0.00000	0.12429	0.23855	0.34026	0.00000	0.12429	0.23855	0.34026
0.05	0.00000	0.13774	0.26437	0.37709	0.00000	0.13880	0.26640	0.37999
0.10	0.00000	0.15276	0.29319	0.41820	0.00000	0.15494	0.29737	0.42416
0.20	0.00000	0.18885	0.36246	0.51700	0.00000	0.19355	0.37148	0.52988
	<i>MWCNT – Water Nanofluid</i>				<i>MWCNT – Engine Oil Nanofluid</i>			
0.00	0.00000	0.12429	0.23855	0.34026	0.00000	0.12429	0.23855	0.34026
0.05	0.00000	0.13451	0.25816	0.36824	0.00000	0.13518	0.25944	0.37006
0.10	0.00000	0.14601	0.28023	0.39972	0.00000	0.14741	0.28293	0.40357
0.20	0.00000	0.17392	0.33382	0.47615	0.00000	0.17708	0.33987	0.48478

Table (5.4): Various values of local heat transfer rate $\frac{-K_{nf}}{K_f} \theta'(0)$

φ	δ	$\lambda = 0.00$	$\lambda = 0.10$	$\lambda = 0.20$	$\lambda = 0.30$	$\lambda = 0.00$	$\lambda = 0.10$	$\lambda = 0.20$	$\lambda = 0.30$
		<i>SWCNT – Waterbased (Pr = 6.2)</i>				<i>SWCNT – Engine Oilbased (Pr = 6450)</i>			
0.00		1.59898	1.59543	1.58620	1.57364	45.61891	45.11030	43.76874	41.89943
0.05	0.10	2.02369	2.01570	1.99481	1.96610	81.93448	81.91913	81.87828	81.82023
0.10		2.30222	2.28831	2.25173	2.20091	106.40627	106.50056	106.75251	107.11276
0.20		2.62337	2.59233	2.50939	2.39022	139.78445	139.77371	139.74376	139.69779
	0.00	2.79310	2.78106	2.74986	2.70757	120.86245	120.85055	120.82072	120.78221
0.12	0.05	2.59805	2.58401	2.54739	2.49718	116.88710	116.88177	116.86737	116.84655
	0.10	2.38752	2.37079	2.32669	2.26510	113.91324	113.98369	114.16923	114.42769
	0.15	2.15740	2.13685	2.08185	2.00263	115.05383	115.62943	117.26042	119.83267
		<i>MWCNT – Waterbased (Pr = 6.2)</i>				<i>MWCNT – Engine Oilbased (Pr = 6450)</i>			
0.00		1.59898	1.59543	1.58620	1.57364	45.61891	45.11030	43.76874	41.89943
0.05	0.10	2.00415	1.99692	1.97804	1.95215	79.77626	79.73530	79.62530	79.46661
0.10		2.29434	2.28263	2.25189	2.20940	103.77472	103.85842	104.08230	104.40303
0.20		2.70079	2.67774	2.61670	2.53062	137.28047	137.27704	137.26657	137.24841
	0.00	2.76483	2.75462	2.72813	2.69219	117.97727	117.96657	117.93975	117.90511
0.12	0.05	2.58403	2.57229	2.54168	2.49975	114.17360	114.17055	114.16226	114.15006
	0.10	2.39053	2.37679	2.34072	2.29065	111.31683	111.38641	111.57054	111.82954
	0.15	2.18145	2.16503	2.12144	2.05969	112.10042	112.60895	114.04409	116.29362

Table (5.5): Match of local skin frictions $f''(0)$ and $h'(0)$ with previously published results
($\varphi = 0$)

λ	Nazar et al. [26]		Wang[31]		Takhar et al. [42]		Present Results	
	$f''(0)$	$h'(0)$	$f''(0)$	$h'(0)$	$f''(0)$	$h'(0)$	$f''(0)$	$h'(0)$
0.0	1.0000	0.0000	1.0000	0.0000	1.0000	0.0000	1.00000	0.00000
0.5	1.1384	0.5128	1.1384	0.5128	1.1383	0.5127	1.13838	0.51276
1.0	1.3250	0.8371	1.3250	0.8371	1.3250	0.8370	1.32503	0.83710
2.0	1.6523	1.2873	1.6523	1.2873	1.6524	1.2870	1.65235	1.28726

Table (5.6): Comparison of absolute values of $\theta'(0)$ for $\varphi = 0 = \delta$

	$\lambda = 0.0$			$\lambda = 0.5$			$\lambda = 1.0$			$\lambda = 2$		
	Pr = 0.7	Pr = 2.0	Pr = 7.0	Pr = 0.7	Pr = 2.0	Pr = 7.0	Pr = 0.7	Pr = 2.0	Pr = 7.0	Pr = 0.7	Pr = 2.0	Pr = 7.0
	Wang [31]	0.455	0.911	1.894	0.390	0.853	1.850	0.321	0.770	1.788	0.242	0.638
Present outcomes	0.45391	0.91136	1.89540	0.38907	0.85243	1.85117	0.32083	0.77030	1.78763	0.24397	0.63774	1.66436

5.6 Conclusions

Flow/ heat transfer features of a 3D rotating fluid using single and multi-walled carbon nanotubes are analyzed. The governing physical task has been modeled and tackled numerically by a combination of *Quasi – linearization* and *Chebyshev pseudo – spectral* methods. Results for pertinent flow parameters are sketched and discussed.

Some of the main findings of this study are as under

- 1) A rise in volumetric nano particle fraction φ significantly enhances the corresponding fluid velocities for both types of carbon nanotubes.
- 2) Temperature $\theta(\eta)$ and thermal boundary layer depth increase with a rise in φ for single and multi-walled carbon nano tubes.
- 3) Influence of heat generation parameter on temperature is found to be positive whereas the

thermal boundary declines with an increase in heat absorption parameter for both categories of carbon nanotubes.

- 4) Skin frictions as well as local heat flux are increasing functions of nano particle volume fraction φ for *SWCNTs* and *MWCNTs* based fluids.
- 5) Engine oil base fluid depicted higher heat transfer rate as well as local skin friction as compared to water based fluid for both type of carbon nano tubes.
- 6) Local heat flux is a decreasing function of heat generation parameter δ for *SWCNTs* and *MWCNTs* nano fluids.

Chapter 6

Entropy analysis of radioactive rotating nanofluid with thermal slip

6.1 Introduction

This unit discourses the effects of thermal slip and thermal radiations on flow/ heat transfer and entropy generation of rotating nano fluid. The nano fluid is lying on a horizontal plane surface which is being stretched in opposite but mutually perpendicular directions in such a way that the origin remains fix. The fluid rotation is being executed about the vertical axis with a constant angular velocity Ω . Three types of nano particles naming copper oxide (CuO), silver (Ag) and gold (Au) are involved for investigation in the present study. Water is taken as base fluid. Corresponding Navier Stokes Eqs. of mass, motion and energy are presented. By using suitable similarity transforms these partial differential equations are converted in to a set of ordinary differential Eqs. which are highly non-linear in nature. The system is solved by a commonly known numerical RK-Fehlberg scheme [48] along with shooting procedure. Effects of pertinent parameters such as stretching ratio α , thermal radiation parameter R , thermal slip parameter γ on the flow are presented through graphs. Validation of the numerical scheme is confirmed through comparison with some previously published literature. An appropriate settlement is observed authenticating our current numerical structure.

6.2 Mathematical formulation

Consider 3D Cartesian coordinate system in which x – and y – axis are lying in horizontal plane. Steady state water based nanofluid with CuO , Ag and Au as nano particles is lying in the region $Z \geq 0$. Due to two equal and opposite forces, the plane $Z = 0$ is being continuously and linearly stretched in both X – and X' – directions along the plane $Z = 0$. Other two forces equal in magnitude

(which may not be equal in magnitude to first two forces) and opposite in directions are also linearly stretching the same plane in $Y -$ and $Y' -$ directions. As the point of action of all these four forces is $(0, 0, 0)$, so the same point being an origin remains fix in its unique position. The stretching velocity of the plane in the direction of x -axis is $u = u_w$ and in the direction of y -axis is $v = v_w$ with $u_w = ax$ and $v_w = by$. Where 'a' and 'b' are constants of proportionalities and termed as stretching rates along $x -$ and $y -$ directions respectively.

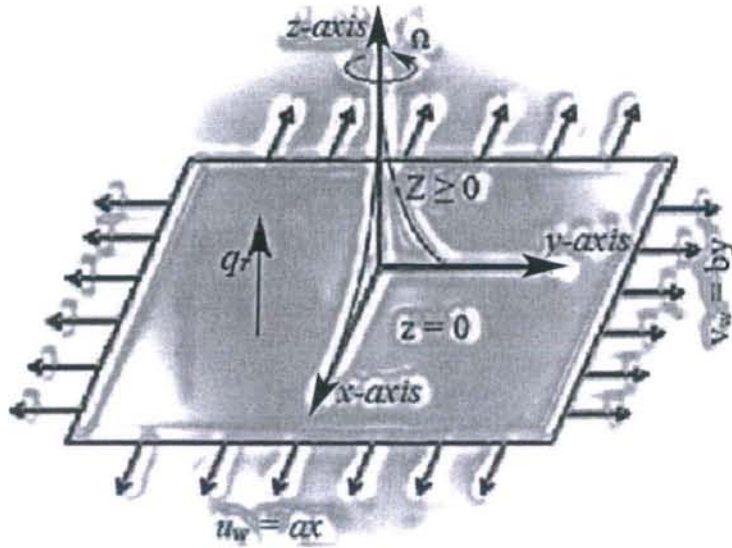


Fig. (6.1): Physical view of problem

Surface temperature is subjected to partial slip and so is $T_w + D \frac{\partial T}{\partial z}$ where D is the slip factor.

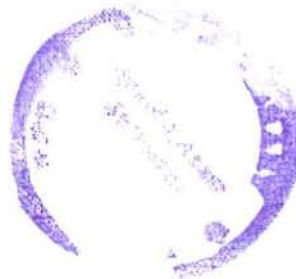
The mathematics of the problem representing the physical flow consists of the continuity Eq., momentum Eq. and energy Eq. as [75,76,77]

$$\frac{\partial u}{\partial x} + \frac{\partial v}{\partial y} + \frac{\partial w}{\partial z} = 0, \quad (6.1)$$

$$u \frac{\partial u}{\partial x} + v \frac{\partial u}{\partial y} + w \frac{\partial u}{\partial z} - 2\Omega v = \nu_{nf} \frac{\partial^2 u}{\partial z^2}, \quad (6.2)$$

$$u \frac{\partial v}{\partial x} + v \frac{\partial v}{\partial y} + w \frac{\partial v}{\partial z} + 2\Omega u = \nu_{nf} \frac{\partial^2 v}{\partial z^2}, \quad (6.3)$$

$$u \frac{\partial w}{\partial x} + v \frac{\partial w}{\partial y} + w \frac{\partial w}{\partial z} = \nu_{nf} \frac{\partial^2 w}{\partial z^2}, \quad (6.4)$$



$$u \frac{\partial T}{\partial x} + v \frac{\partial T}{\partial y} + w \frac{\partial T}{\partial z} = \alpha_{nf} \frac{\partial^2 T}{\partial z^2} + \frac{\mu_{nf}}{(\rho C_p)_{nf}} \left[\left(\frac{\partial u}{\partial z} \right)^2 + \left(\frac{\partial v}{\partial z} \right)^2 \right] - \frac{\partial q_r}{\partial z}. \quad (6.5)$$

Here q_r is the radiation flux and is considered according to Roseland approximation as [69,70,75]

$$q_r = - \frac{4\sigma_e}{3\beta_R} \frac{\partial T^4}{\partial z} \quad (6.6)$$

where σ_e is the constant related with Stefan-Boltzman and β_R is mean absorption co-efficient.

Temperature differences for fluid phase are taken small such that T^4 by expanding through Tailor series about T_∞ may be approximated as a direct function of T as

$$T^4 \approx 4 T_\infty^3 T - 3 T_\infty^4. \quad (6.7)$$

The corresponding boundary conditions of Eqs. (6.1) to (6.5) are [6, 72]

$$\left. \begin{aligned} u = ax, \quad v = by, \quad w = 0, \quad T = T_w + D \frac{\partial T}{\partial z} \quad \text{when } z = 0, \\ u \rightarrow 0, \quad v \rightarrow 0 \quad \quad \quad T \rightarrow T_\infty \quad \quad \quad \text{when } z \rightarrow \infty, \end{aligned} \right\} \quad (6.8 a, b)$$

In order to shift the system of Eqs. (6.1) to (6.5) from its partial status to ordinary status, the set of similarity transformations is [4, 6, 77]

$$\left. \begin{aligned} u = axf'(\eta), \quad v = ayg'(\eta), \quad w = -\sqrt{av} (f(\eta) + g(\eta)), \\ \eta = z \sqrt{\frac{a}{v}}, \quad \theta(\eta) = \frac{T - T_\infty}{T_w - T_\infty}. \end{aligned} \right\} \quad (6.9 a, b)$$

Various factors characterizing and relating the physical properties of base fluid water with those the solid particles are described as [37, 75]

$$\left. \begin{aligned} \rho_{nf} = \rho_f \left[1 - \varphi + \varphi \left(\frac{\rho_s}{\rho_f} \right) \right], \quad \mu_{nf} = \frac{\mu_f}{(1-\varphi)^{2.5}}, \quad \alpha_{nf} = \frac{K_{nf}}{(\rho C_p)_{nf}}, \\ (\rho C_p)_{nf} = (\rho C_p)_f \left[1 - \varphi + \varphi \left(\frac{(\rho C_p)_s}{(\rho C_p)_f} \right) \right], \quad \frac{K_{nf}}{K_f} = \frac{K_s + 2K_f - 2\varphi(K_f - K_s)}{K_s + 2K_f + 2\varphi(K_f - K_s)}. \end{aligned} \right\} \quad (6.10 a, b)$$

Invoking Eqs. (6.9 a, b) and (6.10 a, b) in Eqs. (6.1) to(6.5) and in (6.8 a, b), we obtain a nonlinear system of differential Eqs. which are ordinary in nature as

$$f''''(\eta) + (1 - \varphi)^{2.5} \left(1 - \varphi + \varphi \frac{\rho_s}{\rho_f} \right) \left((f(\eta) + g(\eta))f''(\eta) - (f'(\eta))^2 + 2\lambda\xi g'(\eta) \right) = 0, \quad (6.11)$$

$$g'''(\eta) + (1 - \varphi)^{2.5} \left(1 - \varphi + \varphi \frac{\rho_s}{\rho_f} \right) \left((f(\eta) + g(\eta))g''(\eta) - (g'(\eta))^2 - (2\lambda/\xi)f'(\eta) \right) = 0, \quad (6.12)$$

$$\left(\frac{K_{nf}}{K_f} + \frac{4}{3}R \right) \theta''(\eta) + Pr \left(1 - \varphi + \varphi \frac{(\rho C_p)_s}{(\rho C_p)_f} \right) \cdot (f(\eta) + g(\eta))\theta'(\eta) + \frac{1}{(1-\varphi)^{2.5}} \cdot Pr \cdot Ec [(f''(\eta))^2 + \xi^2 (g''(\eta))^2] = 0. \quad (6.13)$$

Here ξ is the ratio y/x and the thermal radiation parameter R is given by

$$R = \frac{4\sigma_e T_\infty^3}{\beta_R K_f} \quad (6.14)$$

Here notations used are usual and can be seen in nomenclature.

Corresponding boundary conditions for system of new ordinary non-linear Eqs. are

$$\left. \begin{aligned} f(0) = 0, & \quad f'(0) = 1, & \quad f'(\infty) = 0, \\ g(0) = 0, & \quad g'(0) = \alpha, & \quad g'(\infty) = 0, \\ \theta(0) = 1 + \gamma \theta'(0), & & \quad \theta(\infty) = 0. \end{aligned} \right\} \quad (6.15a, b, c)$$

Where $\alpha = b/a$ represents ratio between stretching rate in y direction to stretching rate in x direction. For special case when stretching rates in both x and y directions are equal i.e., when $a = b$ we have $\alpha = 1$ and thus $f(\eta)$ is identical with $g(\eta)$ and then the flow is axisymmetric.

When $\alpha = 0$ stretching is unidirectional [1 – 3].

γ is the thermal slip parameter and is described as

$$\gamma = D \sqrt{\frac{a}{\nu}},$$

with D as slip factor.

When we put $\lambda = 0$, $\varphi = 0$ and $R = 0$, flow Eqs. (6.11) and (6.12) represents three dimensional flow identical with that of Ariel [6] and Ullah *et al.* [7]. Further if we consider $\lambda = 0 = \gamma = \varphi = R$, we get a nonlinear system of Eqs. representing three dimensional flow identical with those of Butt *et al.* [77] provided the magnetic parameter $M = 0$. Further, when we put $\alpha = \frac{b}{a} = 0 = \gamma$ our problem reduces to Wang [31].

6.3 Solution method

Solution of the coupled non-linear system containing Eqs. (6.11) to (6.13) together with boundary conditions (6.15a, b, c) is taken out by launching fourth-fifth order Runge-Kutta-Fehlberg numerical process with shooting procedure.

Solution technique is implemented as underneath:

$$\text{Let } A_1 = \frac{1}{(1-\varphi)^{2.5}}, A_2 = \left(1 - \varphi + \varphi \frac{\rho_s}{\rho_f}\right), A_3 = \left(1 - \varphi + \varphi \frac{(\rho C_p)_s}{(\rho C_p)_f}\right), \quad (6.16)$$

and

$$f = y_1, f' = y_2, f'' = y_3, f''' = y_3', \quad (6.17)$$

$$g = y_4, g' = y_5, g'' = y_6, g''' = y_6', \quad (6.18)$$

$$\theta = y_7, \theta' = y_8, \theta'' = y_8'. \quad (6.19)$$

Then we have

$$\begin{bmatrix} y_2 \\ y_3 \\ y_3' \\ y_5 \\ y_6 \\ y_6' \\ y_8 \\ y_8' \end{bmatrix} = \begin{bmatrix} y_1' \\ y_2' \\ \frac{A_2}{A_1} [y_2^2 - (y_1 + y_4)y_3 - 2\lambda\xi y_5] \\ y_4' \\ y_5' \\ \frac{A_2}{A_1} [y_5^2 - (y_1 + y_4)y_6 + \left(\frac{2\lambda}{\xi}\right)y_2] \\ y_7' \\ \frac{-Pr}{\left(\frac{Knf}{K_f} + \frac{4}{3}R\right)} [A_3(y_1 + y_4)y_8 + A_1Ec(y_3^2 + \xi^2 y_6^2)] \end{bmatrix}, \quad (6.20)$$

together with initial conditions

$$\begin{bmatrix} y_0(1) \\ y_0(2) \\ y_0(3) \\ y_0(4) \\ y_0(5) \\ y_0(6) \\ y_0(7) \\ y_0(8) \end{bmatrix} = \begin{bmatrix} 0 \\ 1 \\ \beta_1 \\ 0 \\ \alpha = b/a \\ \beta_2 \\ 1 + \gamma y_0(8) \\ \beta_3 \end{bmatrix}. \quad (6.21)$$

Where β_1 , β_2 and β_3 are shooting parameters and are dealt as in unit 4. γ is thermal slip parameter. In our computation a convergence criterion of 10^{-6} is fixed to extract the results.

6.4 Physical quantities of interest

6.4.1 Skin friction and local heat transfer rate

Physical quantities of our interest are skin friction along x -axis Cf_x , along y -axis Cf_y and Nusselt number Nu . These are given by [26,77]

$$Cf_x = \frac{\tau_{xz}}{\rho(ax)^2}, Cf_y = \frac{\tau_{yz}}{\rho(ax)^2}, Nu = \frac{xq_w}{K_f(T_w - T_\infty)}, \quad (6.22)$$

where

$$\left. \begin{aligned} \tau_{xz} &= \mu_{nf} \left(\frac{\partial u}{\partial z} + \frac{\partial w}{\partial x} \right)_{z=0}, \\ \tau_{yz} &= \mu_{nf} \left(\frac{\partial v}{\partial z} + \frac{\partial w}{\partial y} \right)_{z=0}, \\ q_w &= -K_{nf} \left(\frac{\partial T}{\partial z} \right)_{z=0}. \end{aligned} \right\} \quad (6.23)$$

Invoking Eqs. (6.9a, b) in (6.23) and then using the resulting values of τ_{xz} , τ_{yz} and q_w in Eq. (6.22), we get reduced skin frictions and rate of heat transfer for the current problem as

$$\left. \begin{aligned} (Re_x)^{\frac{1}{2}} Cf_x &= (1 - \varphi)^{-2.5} f''(0), \\ \xi^{-1} (Re_x)^{\frac{1}{2}} Cf_y &= (1 - \varphi)^{-2.5} g''(0), \\ (Re_x)^{-\frac{1}{2}} Nu &= \frac{-K_{nf}}{K_f} \theta'(0). \end{aligned} \right\} \quad (6.24)$$

$Re_x = \frac{u_\infty x}{\nu_f}$ is the local Reynolds number.

Here $(Re_x)^{\frac{1}{2}} Cf_x$ is the non-dimensional skin friction along x -axis, $\xi^{-1} (Re_x)^{\frac{1}{2}} Cf_y$ is non-dimensional skin friction along y -axis and $(Re_x)^{-\frac{1}{2}} Nu$ is the non-dimensional surface heat flux. All these are calculated in Tables (6.2), (6.3) and (6.4) for nanofluids used in practice for various numerical values of thermal slip parameter γ , rotation parameter λ , particle volume fraction φ and radiation parameter R .

6.4.2 Entropy generation and Bejan number

The dimensional local entropy rate $S_{g,t}$ per unit volume is [73],

$$S_{g,t} = \frac{K_{nf}}{T_{\infty}^2} [(\nabla T)^2 + \frac{16\sigma_e T_{\infty}^3}{3\beta_R K_f} (\nabla T)^2] + \frac{\mu_{nf}}{T_{\infty}} \Phi$$

or

$$S_{g,t} = \frac{K_{nf}}{T_{\infty}^2} \left[\left(1 + \frac{16\sigma_e T_{\infty}^3}{3\beta_R K_f}\right) (\nabla T)^2 \right] + \frac{\mu_{nf}}{T_{\infty}} \Phi, \quad (6.25)$$

where $\nabla T = \frac{\partial T}{\partial x} + \frac{\partial T}{\partial y} + \frac{\partial T}{\partial z}$ and Φ is related with viscous dissipation.

For our case

$$S_{g,t} = \frac{K_{nf}}{T_{\infty}^2} \left[\left(1 + \frac{16\sigma_e T_{\infty}^3}{3\beta_R K_f}\right) \left(\frac{\partial T}{\partial z}\right)^2 \right] + \frac{\mu_{nf}}{T_{\infty}} \left[\left(\frac{\partial u}{\partial z}\right)^2 + \left(\frac{\partial v}{\partial z}\right)^2 \right], \quad (6.26)$$

$$S_{g,t} = S_h + S_R + S_f. \quad (6.27)$$

Obviously Eq. (6.27) infers that in our case there are three sub generators of entropy. First one is S_h the dimensional entropy generator because of heat transfer, the second is S_R the dimensional entropy generator because of thermal radiations and the third one is S_f which is due to inter frictions of fluid layers.

We define the characteristic entropy generation rate $S_{g,c}$ as

$$S_{g,c} = \frac{K_{nf}(\Delta T)^2}{T_w^2 L^2}. \quad (6.28)$$

Now we are able to define the non-dimensional entropy generation ' N_s ' as

$$N_s = \frac{S_{g,t}}{S_{g,c}}. \quad (6.29)$$

In order to evaluate non-dimensional entropy generation N_s , we use Eqs. (6.26) and (6.28)

together with (6.9a, b) in Eq. (6.29) to get

$$N_s = Re_L \left(1 + \frac{4}{3} R\right) (\theta'(\eta))^2 + Re_L \frac{Br}{\omega} \left[(f''(\eta))^2 + \xi^2 (g''(\eta))^2 \right] / \left[(1 - \varphi)^{2.5} A \right]. \quad (6.30)$$

Here ' A ' is the ratio $\frac{K_{nf}}{K_f}$ designated in Eq. (6.10 b), Re_L , Br are Reynolds number and Brinkman number respectively and ω is the non-dimensional temperature defined by

$$\omega = \frac{(T_w - T_\infty)}{T_\infty}. \quad (6.31)$$

Again Eq. (6.30) can be written as

$$Ns = N_h + N_R + N_f, \quad (6.32)$$

where N_h , N_R and N_f are non-dimensional entropy generators because of heat transfer, thermal radiations and inter friction of fluid layers respectively.

Various features of non-dimensional entropy generation are highlighted via Figs. (6.8a-d).

According to the definition of non-dimensional Bejan number Be ,

$$Be = \frac{N_h}{N_h + N_R + N_f}, \quad (6.33)$$

$$Be = Re_L (\theta'(\eta))^2 / \left[Re_L \left(1 + \frac{4}{3}R\right) (\theta'(\eta))^2 + Re_L Gp \left\{ (f''(\eta))^2 + \xi^2 (g''(\eta))^2 \right\} / \left\{ (1 - \varphi)^{2.5} A \right\} \right], \quad (6.34)$$

with $Gp = \frac{Br}{\omega}$ and may be termed as group parameter.

From Eq. (6.33) it is evident that 'Be' is confined to unit interval [0,1]. Different behaviors of Bejan number are analyzed in Figs. (6.9a - d).

6.5 Results and discussion

As usual this segment is dedicated to analyze the graphical/data outcomes of the problem. Figs. (6.2) to (6.9) and *Table* (6.1) to *Table* (6.6) have been computed for this purpose. In Figs. (6.2a, b) the deviations of dimensionless velocity $f'(\eta)$ with η for different values of rotation parameter λ and stretching ratio α is described for pure water with particle volume fraction of nano particle $\varphi = 0$ together with three types of nano fluids viz *CuO - water*, *Ag - water* and *Au - water* with $\varphi = 0.1$. One can ultimately observe that velocity $f'(\eta)$ decreases monotonically while φ , λ and the stretching ratio α all decrease velocity boundary. In Fig. (6.3), the shear stress $f''(\eta)$ with η is found to increase monotonically. Obviously here

CuO – *water* nano fluid has the least and *Au* – *water* nano fluid has the most numerical value near the surface but this status of both these nano fluids is reversed at a height of about 0.8 from the surface. In Figs. (6.4*a, b*) deviation of velocity $g'(\eta)$ with η for various values of φ, λ and stretching parameter α is shown. A bird eye view reveals that again φ and λ decrease the velocity boundary of velocity $g'(\eta)$ but α produces a sudden positive contribution to the magnitude of velocity near the surface and the least contribution beyond the surface. From Fig. (6.5) we conclude that stretching parameter α and particle volume fraction φ both promote the absolute tangential shear stress $g''(\eta)$ near the surface and the effects of both these are void beyond the surface. In Figs. (6.6*a – d*), the variation of non-dimensional temperature profile $\theta(\eta)$ with η is designated for differing $\varphi, \alpha, Ec, \gamma$ and R . The particle volume fraction φ , the Eckert number Ec and the radiation parameter R all three boost the thermal boundary. As thermal conductance of solid nano particles is greater than that of water, so their inclusion in water results in to a rise in temperature. Eckert number (Ec) results in to a rise in friction forces within fluid and hence causes a rise in temperature of fluid. Radiation parameter R having direct relation with free stream temperature upswings the temperature. On the other hand thermal slip parameter γ and stretching ratio parameter α result in to a collapse in the thermal boundary. In Fig. (6.7), a clarification of temperature gradient $\theta'(\eta)$ with η for various values of thermal slip parameter γ is clarified. It can be observed that particle volume fraction φ and thermal slip parameter γ both result in to a decline in numerical value of temperature gradient $\theta'(\eta)$ near the surface.

Figs. (6.8*a – d*) describe the effects of stretching ratio α , rotation parameter λ , radiation parameter R , particle volume fraction φ and thermal slip parameter γ on non-dimensional entropy Ns . Fig. (6.8*a*) reveals that stretching ratio α and particle volume fraction φ both enhance the entropy generation Ns for the nano fluids used in practice. From Fig. (6.8*b*), an

enhancement in Ns with rotation parameter λ is depicted. From Figs. (6.8c) and (6.8d) it is observed that near the surface non-dimensional entropy generation Ns is a decreasing function of radiation parameter R and thermal slip parameter γ for $Au - water$ nanofluid.

From Fig. (6.9a) we observe that very near the surface, particle volume fraction φ makes tend the Bejan number Be from values greater than 0.5 to the values less than 0.5 which implies that this parameter has the authority to replace the dominance of entropy sub generator N_h with the collective dominance of entropy sub generators N_R and N_f . These results are important to employ a balanced contribution of particle volume fraction φ . As due to rotation massive particles cause greater friction with the surface and so entropy due to fluid friction (N_f) increases and thus Bejan number decreases. This sensation is apparent from Fig. (6.9b). From Fig. (6.9c) and Fig. (6.9d) we infer that away from surface Bejan number Be is a decreasing function of both thermal slip parameter γ and radiation parameter R for $Ag - water$ fluid. For both these parameters, Be monotonically increases up to a specific height and then monotonically decreases beyond that height. Thus a general result from Figs. (6.9a - d) may be extracted that very near the surface entropy creation because of heat transfer is dominant and beyond the surface entropy creation because of other factors is dominant.

In Table (6.1) thermo physical possessions of components of nanofluid are arranged. Table (6.2) presents numerical values of skin friction $\frac{-1}{(1-\varphi)^{2.5}} f''(0)$ along the surface. It can be observed that the stretching ratio α , particle volume fraction φ and rotation parameter λ all boost the shear stress along $x - axis$ for all nano fluids used in practice. Au-water fluid is more frictive than other two nano fluids. It is because due to greater density of gold nano particles than other two types of particles, their collision with the surface is more effective to create the friction. In Table (6.3), some numerical values of skin friction $\frac{-1}{(1-\varphi)^{2.5}} g''(0)$ have been calculated for various values of α , φ and λ . We observe

that these parameters again augment the skin friction $\frac{-1}{(1-\varphi)^{2.5}}g''(0)$ along y-axis. From *Table (6.4)*, it can merrily be detected that stretching ratio α and particle volume fraction φ enhance the heat transfer while rotation, radiation, thermal slip and Eckert number slow down the same for all nano fluids used here at. *CuO – water* nano fluid is the supper heat transfer agent because *Cuo* nano particles have least density but the highest thermal conductivity as compared with other two types of particles. To validate our present numerical structure, comparisons of fluid frictions $f''(0)$ and $g''(0)$ with previous published literature for $\varphi = 0 = \lambda$ is made in *Tables (6.5)* and *(6.6)*. A satisfactory settlement is declared to corroborate the numerical scheme.

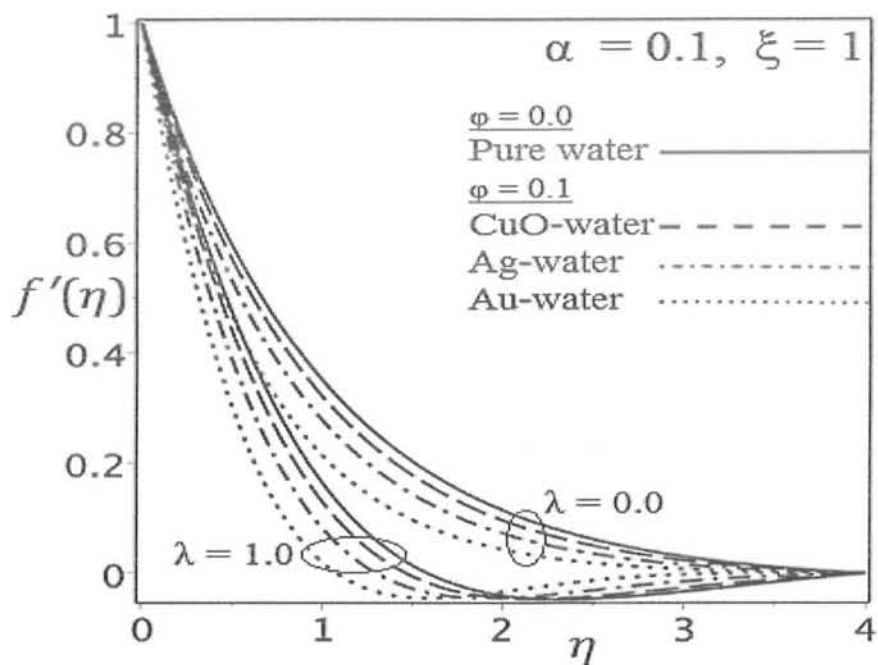


Fig. (6.2a)

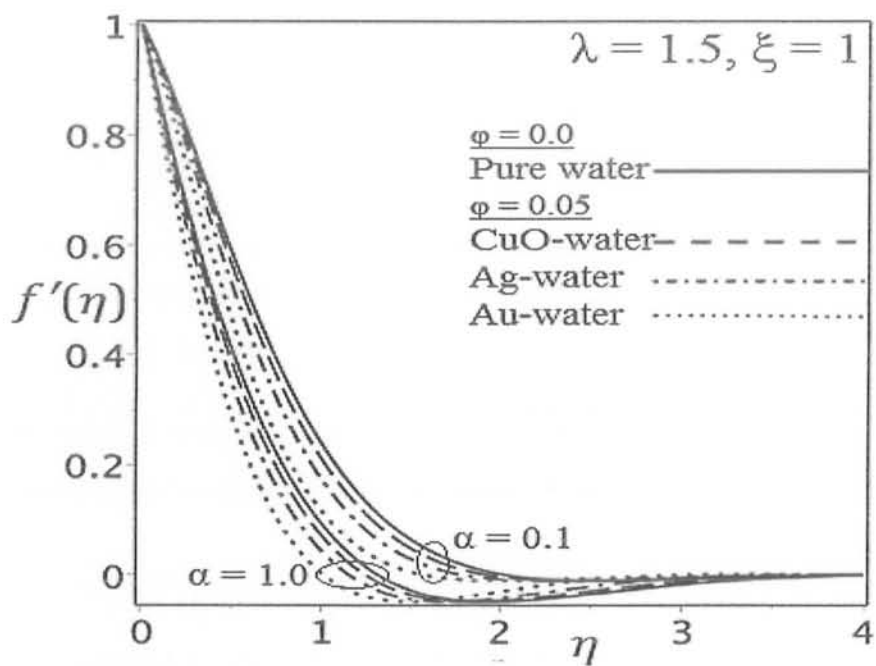


Fig. (6.2b)

Figs. (6.2a, b): Variation of velocity $f'(\eta)$ of nanofluids with η for different values of rotation parameter λ and stretching ratio α

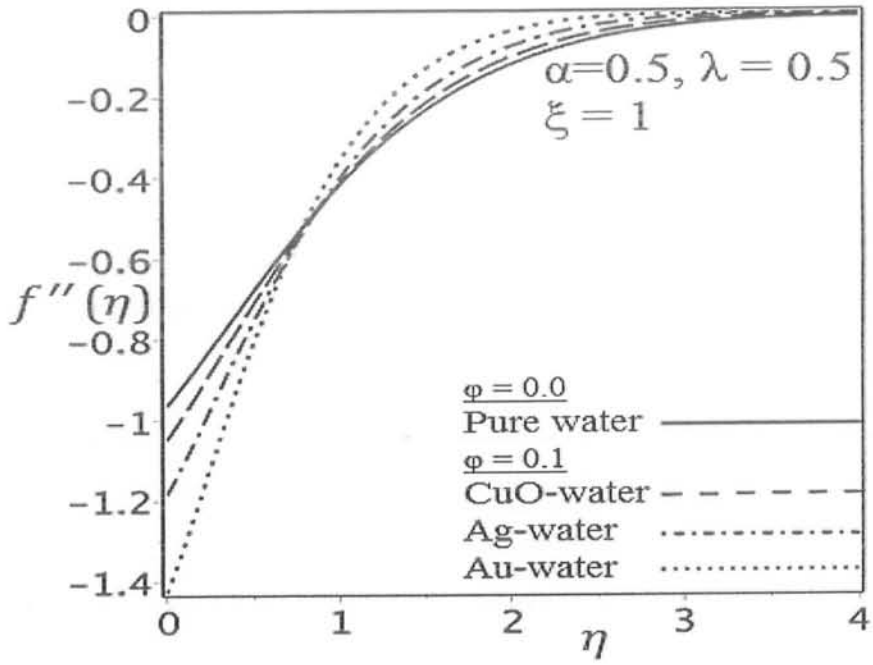


Fig. (6.3): Variation of shear stress $f'''(\eta)$ with η

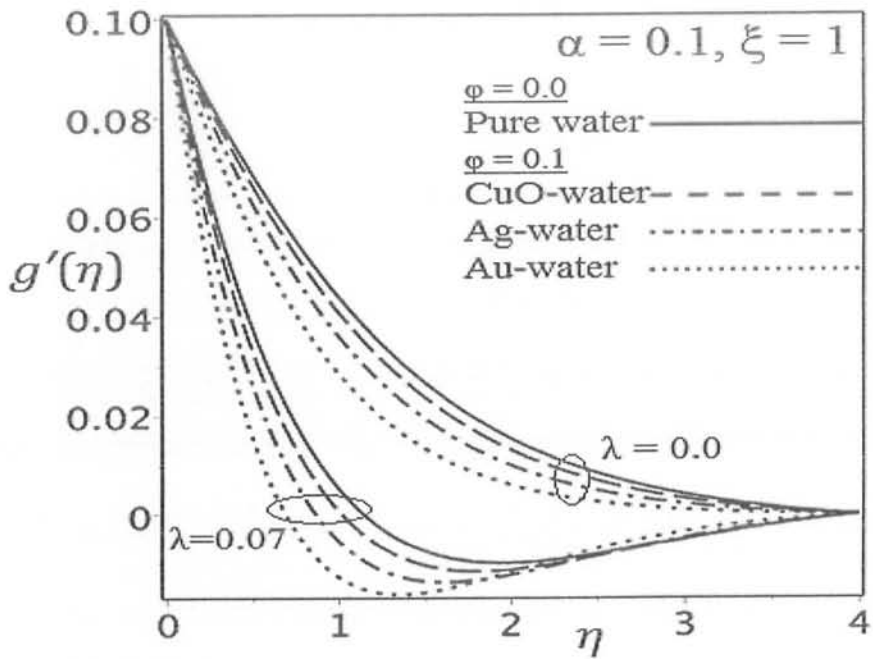


Fig. (6.4a)

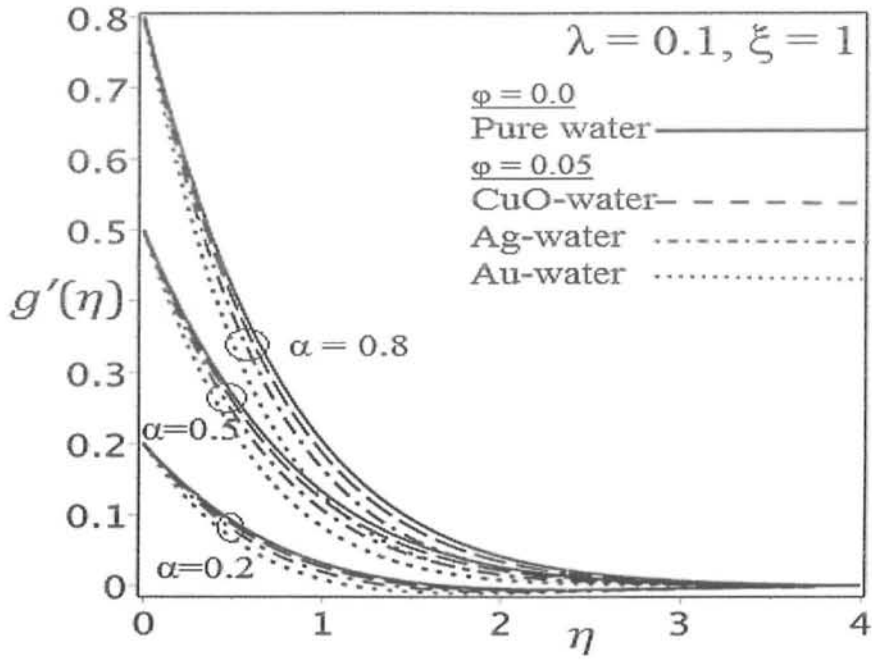


Fig. (6.4b)

Figs. (6.4a, b): Deviation of velocity $g'(\eta)$ versus η for various values of α and λ

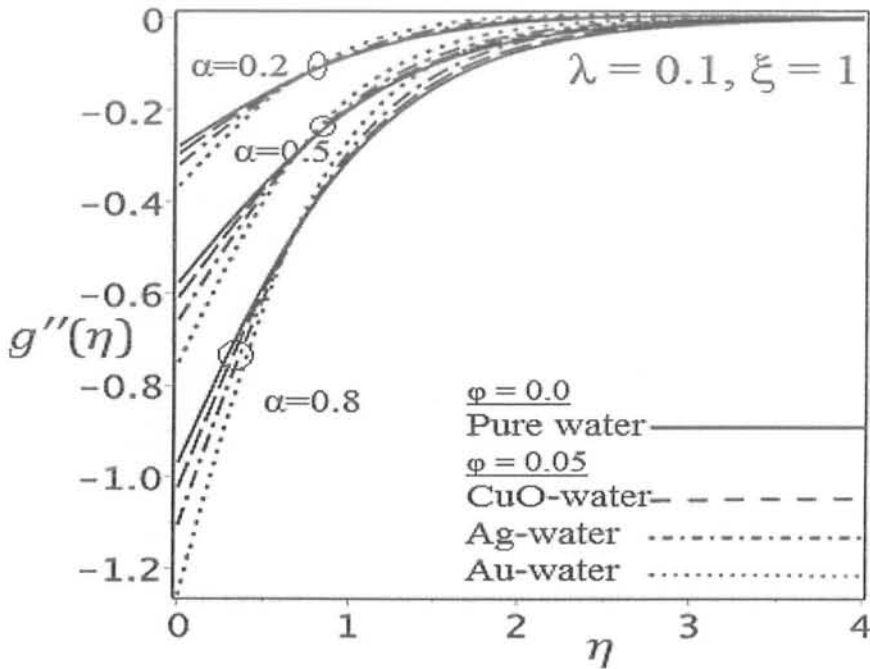


Fig. (6.5): Deviation of shear stress $g''(\eta)$ versus η for various estimates of stretching parameter α

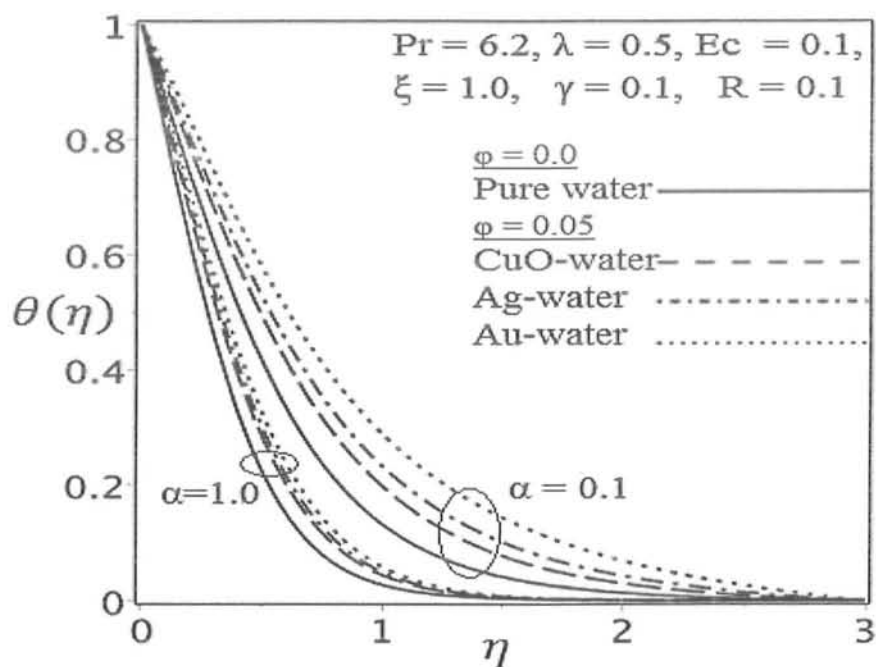


Fig. (6.6a)

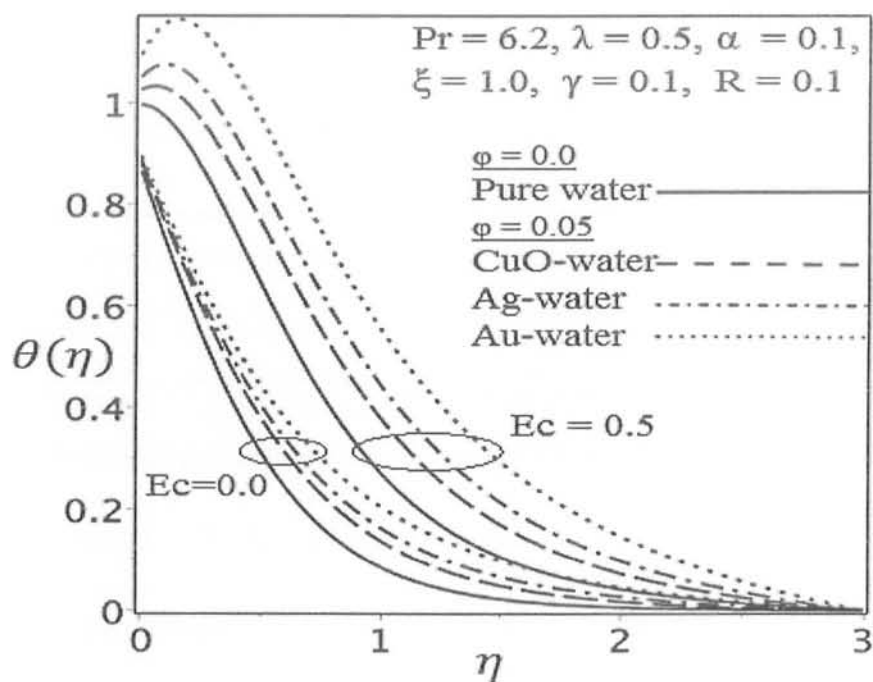


Fig. (6.6b)

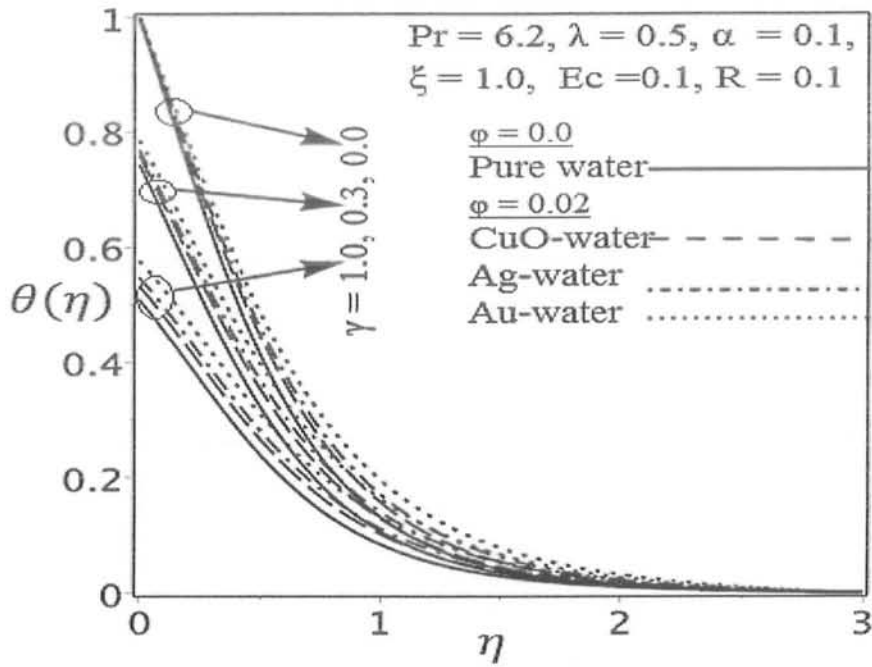


Fig. (6.6c)

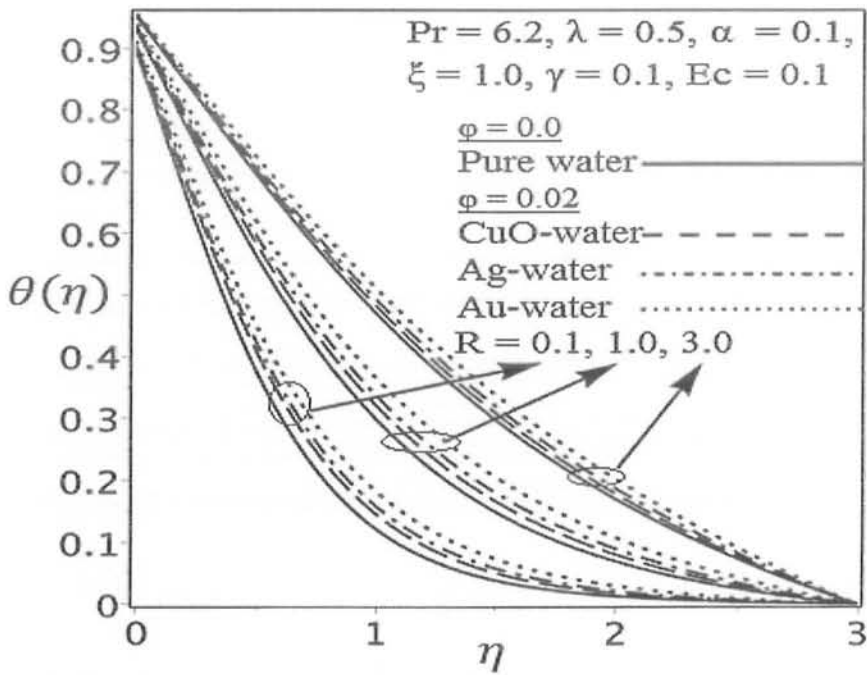


Fig. (6.6d)

Figs. (6.6a – d): Variation of non-dimensional temperature profile $\theta(\eta)$ versus η for various estimates of α, Ec, γ and R

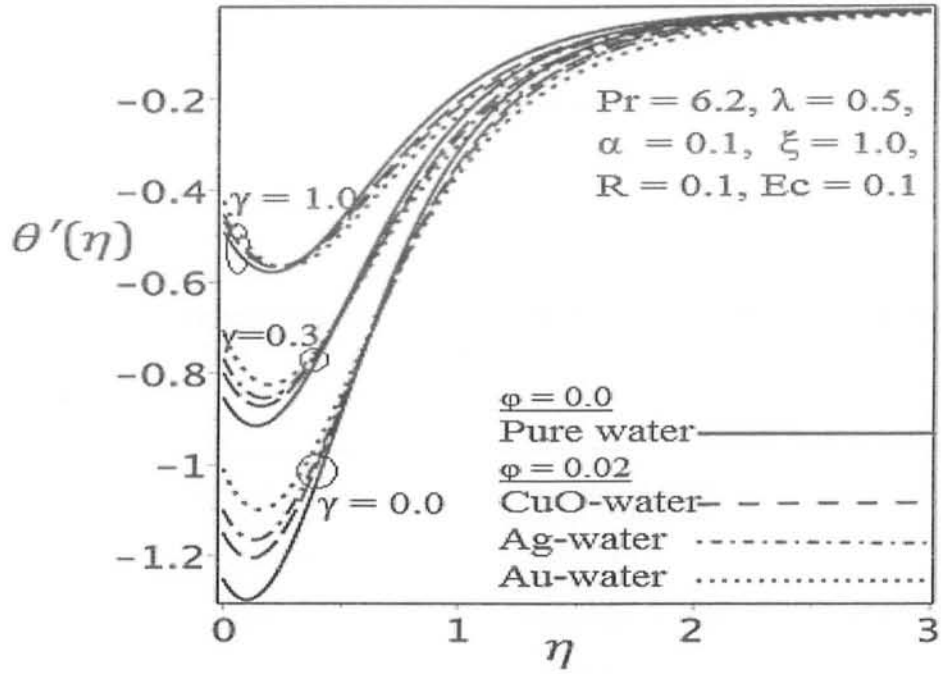


Fig. (6.7): Variation of temperature gradient $\theta'(\eta)$ versus η for various estimates of thermal slip constraint γ

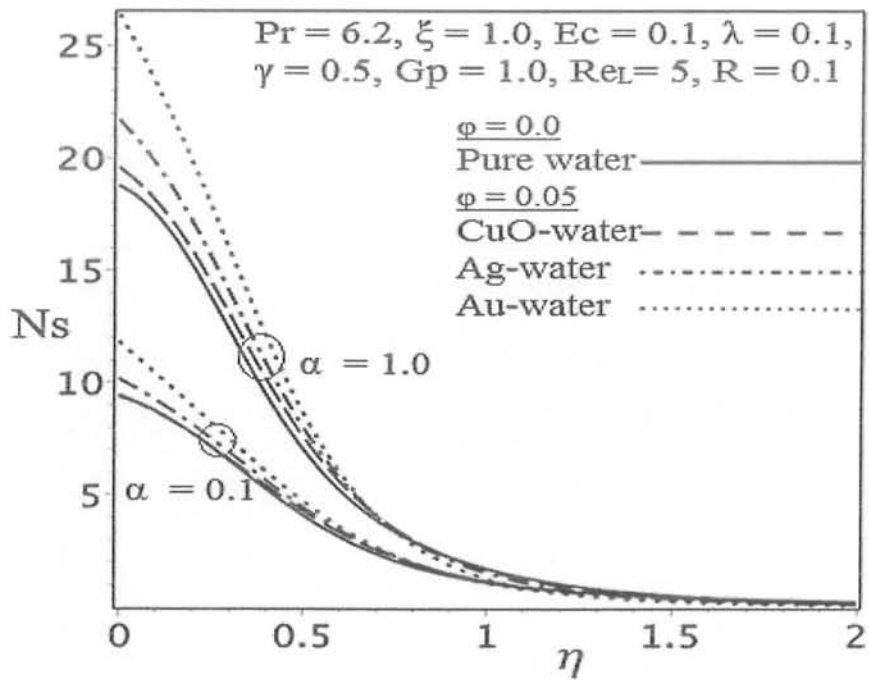


Fig. (6.8a)

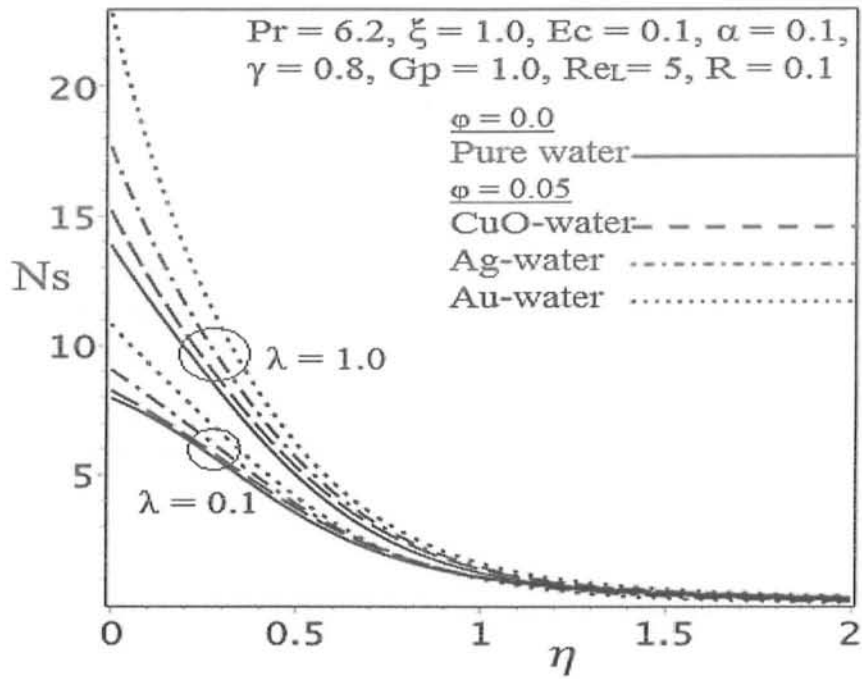


Fig. (6.8b)

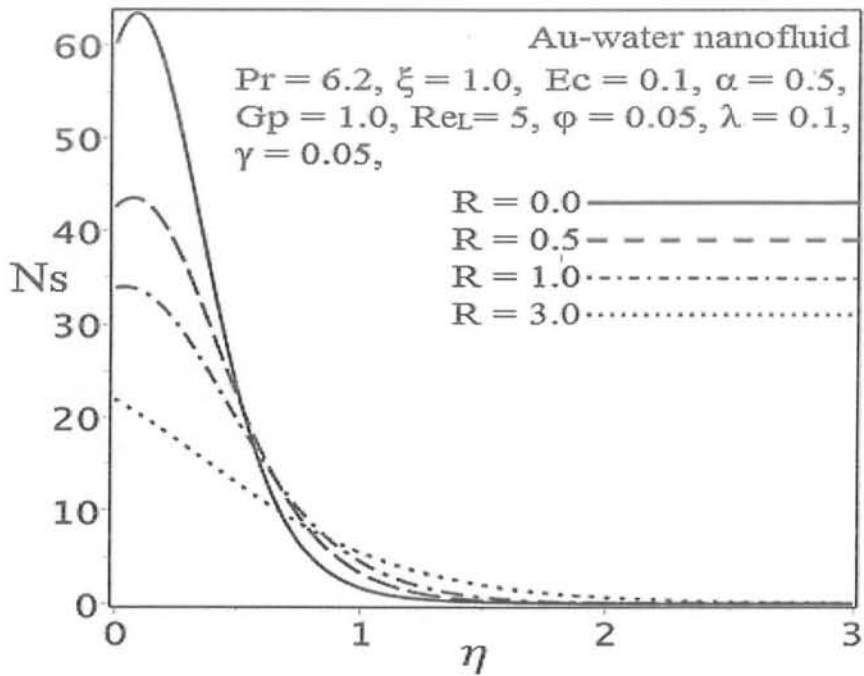


Fig. (6.8c)

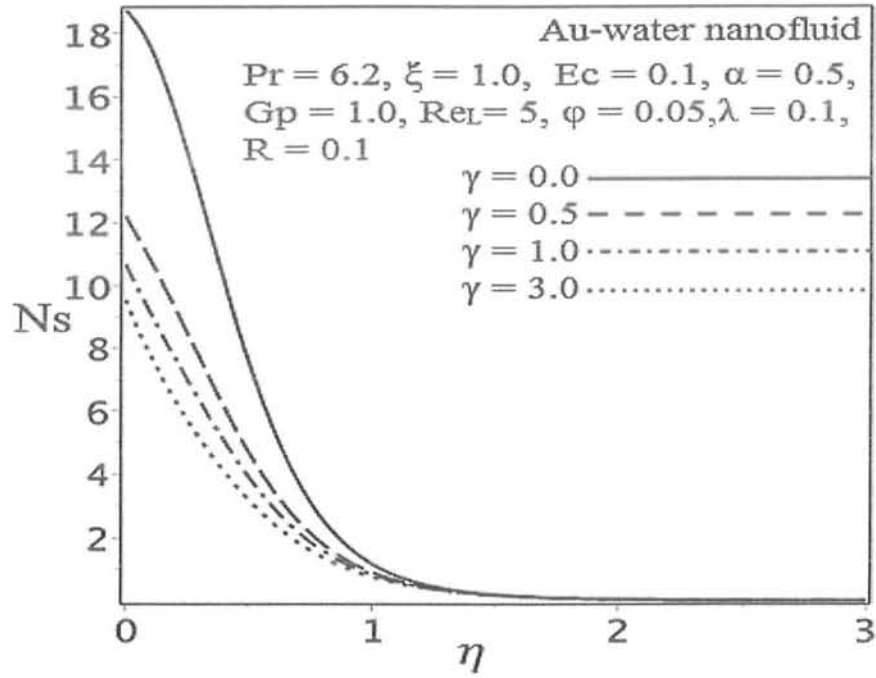


Fig. (6.8d)

Figs. (6.8a – d): Variation of non-dimensional entropy N_s with η for various values of

- 6.8a: Stretching ratio α with variant ϕ ,
- 6.8b: Rotation parameter λ with variant ϕ ,
- 6.8c: Radiation parameter R for *Au – water* nanofluid
- 6.8d: Thermal slip parameter γ for *Au – water* nanofluid

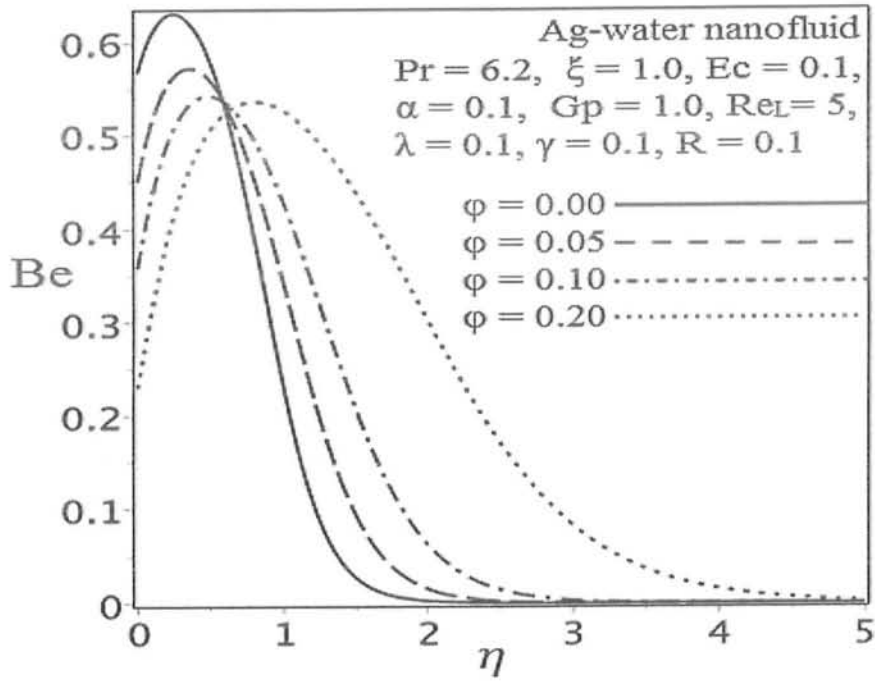


Fig. (6.9a)

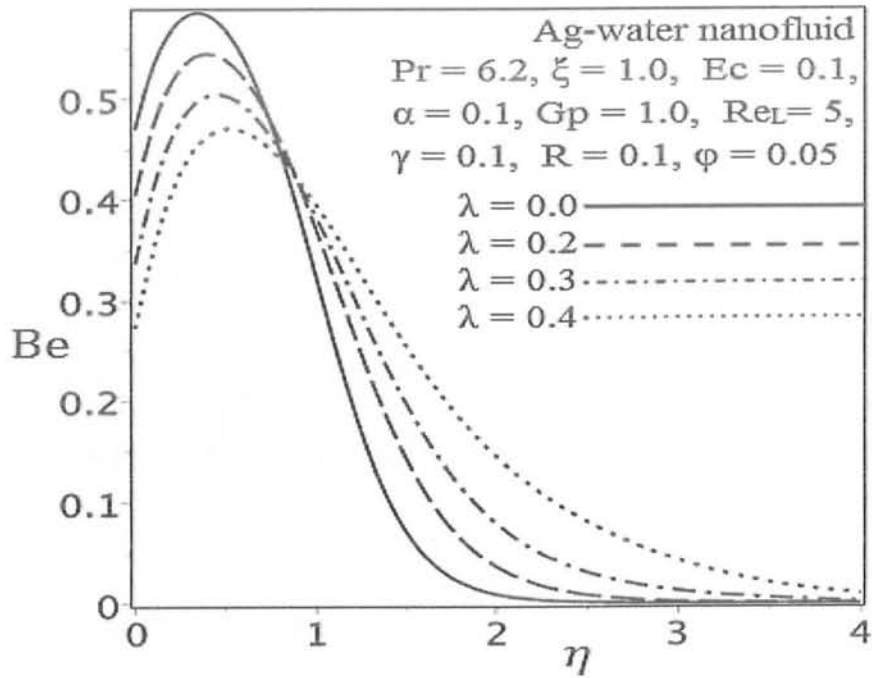


Fig. (6.9b)

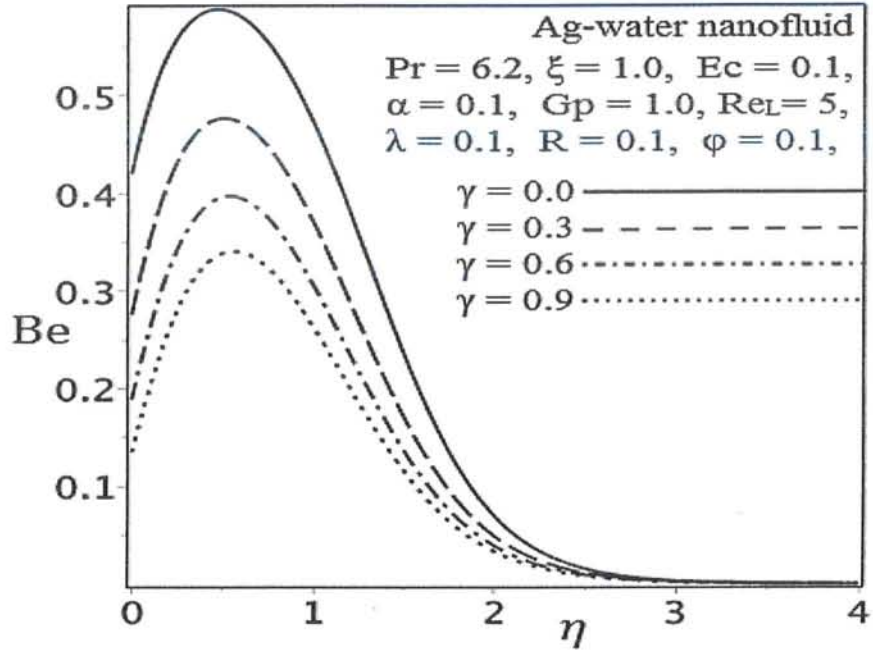


Fig. (6.9c)

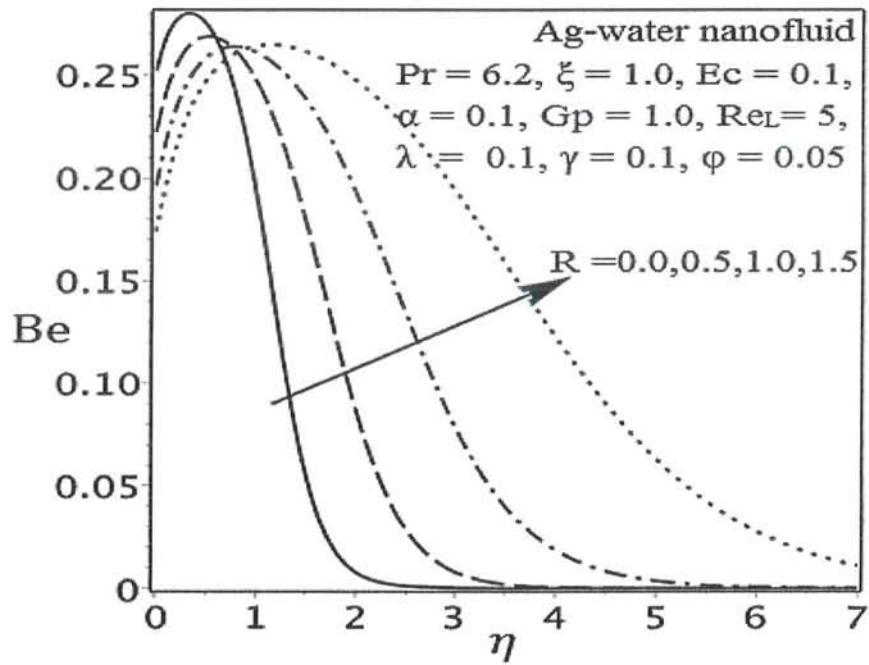


Fig. (6.9d)

Figs. (6.9a – d): Variation in Bejan number Be for $Ag - water$ nanofluid versus η for a number of values of
 (6.9a): Volumetric particle fraction ϕ , (6.9b): Rotation parameter λ ,
 (6.9c): Thermal slip parameter γ and (6.9d): Radiation parameter R

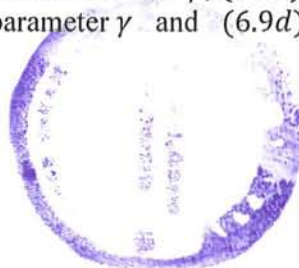


Table (6.1) : Thermophysical properties of components [37,41,71]

Properties\Constituents	Pure Water (H ₂ O)	Copper Oxide (CuO)	Silver (Ag)	Gold (Au)
Density (ρ) Kg/m ³	997.1	6320	10500	19282
Specific Heat (C_p) J/Kg.K	4179.0	531.80	235	129
Thermal Conductivity (K) W/m.K	0.6130	76.50	429	310
Prandtl Number (Pr)	6.20	-	-	-

Table (6.2) : Some values of skin friction $\frac{-1}{(1-\varphi)^{2.5}} f''(0)$ for different α, φ and λ ($\xi = 1$)

α	φ	λ	CuO – water	Ag – water	Au – water
0.2	0.1	0.1	1.439062	1.622119	1.952601
0.4			1.463823	1.650249	1.986626
0.8			1.512321	1.705339	2.053318
0.4	0.05	0.3	1.193378	1.289055	1.470078
	0.10		1.405179	1.587051	1.913332
	0.20		1.890299	2.243735	2.845455
0.1	0.1	0.1	1.426559	1.607938	1.935525
		0.2	1.435977	1.622451	1.958643
		0.3	1.475830	1.671245	2.015266

Table (6.3): Some values of skin friction $\frac{-1}{(1-\varphi)^{2.5}} g''(0)$ for different α, φ and λ ($\xi = 1$)

α	φ	λ	CuO – water	Ag – water	Au – water
0.2	0.1	0.1	0.392851	0.446147	0.540948
0.4			0.657307	0.742941	0.896425
0.8			1.367363	1.543227	1.859320
0.4	0.05	0.3	0.849122	0.918982	1.049185
	0.10		1.000676	1.132415	1.365173
	0.20		1.346223	1.601324	2.029512
0.1	0.1	0.1	0.291401	0.333606	0.408087
		0.2	0.502023	0.578347	0.707599
		0.3	0.701687	0.796675	0.952935

Table (6.4): Some values of heat flux $\frac{-K_{nf}}{K_f} \theta'(0)$ for different parameters.

α	φ	λ	R	γ	Ec	CuO – water	Ag – water	Au – water
0.2	0.12	0.12	3.0	0.35	0.1	0.751492	0.694231	0.607870
0.4						0.807038	0.744718	0.649656
0.8						0.857051	0.779106	0.655999
0.3	0.05	0.25	3.5	0.2	0.05	0.660311	0.635492	0.595055
	0.10					0.766276	0.717220	0.646809
	0.20					1.066497	0.961989	0.830519
0.5	0.15	0.1	2.5	0.1	0.15	1.036446	0.895974	0.690249
		0.2				0.999352	0.851231	0.636142
		0.3				0.944484	0.786040	0.559482
0.5	0.05	0.05	1.0	0.4	0.1	0.895639	0.868432	0.819410
			2.0			0.757133	0.732036	0.687604
			4.0			0.598638	0.577659	0.541613
0.1	0.15	0.2	2.0	0.3	0.2	0.679486	0.531044	0.312707
				0.6		0.582817	0.460683	0.274573
				0.9		0.510229	0.406786	0.244729
0.3	0.15	0.15	3.0	0.5	0.1	0.783793	0.713536	0.608851
					0.2	0.661078	0.562304	0.410449
					0.3	0.538363	0.411073	0.114624

Table (6.5): Comparison of skin friction $-f''(0)$ for various estimates of α
 $(\varphi = 0 = \lambda = \gamma = R)$

α	Wang [4] (perturbation Method)	Ariel [6] (Homotopy Perturbation Method)	Butt et al [77] (Homotopy Analysis Method)	Present (Numerical Method)
0.0	1	1	1	1
0.1	1.020902	1.017027	1.020260	1.023843
0.2	1.041804	1.034587	1.039495	1.042584
0.3	1.062705	1.052470	1.057955	1.060655
0.4	1.083607	1.070529	1.075788	1.078171
0.5	1.104509	1.088662	1.093095	1.095213
0.6	1.125411	1.106797	1.109947	1.111838
0.7	1.146312	1.124882	1.126398	1.128093
0.8	1.167214	1.142879	1.142489	1.144014
0.9	1.188116	1.160762	1.158254	1.159630
1.0	1.209018	1.178511	1.173721	1.174965

Table (6.6): Comparison of skin friction $-g''(0)$ for various estimates of α
 $(\lambda = 0 = \varphi = \gamma = R)$

α	Wang [4] (Perturbation Method)	Ariel [6] (Exact Solution)	Butt et al [77] (Homotopy Analysis Method)	Present (Numerical Method)
0.0	0	0	0	0
0.1	0.058198	0.066847	0.073099	0.067831
0.2	0.116395	0.148737	0.158231	0.150139
0.3	0.174593	0.243360	0.254347	0.244929
0.4	0.232791	0.349209	0.354347	0.350823
0.5	0.290988	0.465205	0.476290	0.466801
0.6	0.349186	0.590529	0.600833	0.592074
0.7	0.407384	0.724532	0.733730	0.726008
0.8	0.465581	0.866683	0.874551	0.868084
0.9	0.523779	1.016539	1.022922	1.017861
1.0	0.581977	1.173721	1.178511	1.174965

6.6 Conclusions

Three dimensional rotating nanofluid flow in presence of thermal slip , thermal radiation and with entropy generation is investigated over a stretching surface. Important extractions can be arranged as

- i) Particle volume fraction φ and rotation parameter λ both decrease velocity boundaries for velocity $f'(\eta)$ and $g'(\eta)$. Au-water has leading behaviour for decrement among three nano fluids.
- ii) Stretching ratio α increases velocity boundary in case of $f'(\eta)$ but has an opposite behaviour in case of $g'(\eta)$.
- iii) Skin friction along $x - axis$ as well as along $y - axis$ increase with particle volume fraction φ , rotation parameter λ and stretching ratio α . Au-water nano fluid contributes the most and Cu – water fluid contributes the least in growth.
- iv) Particle volume fraction φ , Eckert number Ec and thermal radiation R all increase the thermal boundary while stretching ratio α and thermal slip γ decrease the thermal boundary for all three nanofluids under investigation.
- v) Heat flux along the surface amplifies with stretching ratio α and particle volume fraction φ while the same reduces with rotation parameter λ , thermal radiation R , thermal slip γ and Eckert number Ec for all three nano fluids used here at.
- vi) Entropy generation is enhanced by stretching ratio α , particle volume fraction φ and rotation parameter λ while the same is contracted by thermal radiation R and slip parameter γ .
- vii) Dominancy of entropy production because of heat transfer can be shifted to the dominancy due to other factors (radiation + fluid friction) by a certain contribution of either of the particle volume fraction φ , rotation parameter λ , thermal slip parameter γ and thermal radiation R .

viii) The factor responsible for entropy generation near the surface is normally heat transfer and factors responsible for entropy generation beyond the surface are thermal radiations and fluid frictions.

ix) Comparison of our computed results with those already published literature provides the guaranty of numerical scheme launched in this study.

Chapter 7

Slip flow of a chemically reacting rotating hybrid nanofluid with uniform heat source/ sink

7.1 Introduction

This unit is committed to investigate and compare the enhancement of flow and heat/ mass transfer between rotating nanofluid and a newly discovered hybrid or nested nanofluid. A particular amount of volumetric fraction of more than one type of nano particles offers better transporting results as compare to same total amount of volumetric particle fraction of nano subdivisions of same material. Three dimensional stretching surface representing real world situation is engaged to consider rotating hybrid nanofluid $Cu-(CuO/water)$. RK-Fehlberg procedure [48] is incorporated to extract numerical solutions. Effects of necessary factors like rotation, volumetric particle fraction, heat source/sink, velocity slip and chemical reaction parameters on flow and heat/ mass transfer are studied and analysed via graphs and tables.

7.2 Mathematical formulation

Consider a highly elastic horizontal $xy - plane$ which is being stretched in two mutually normal directions of x and y -axis with constant stretching rates " a " and " b " with fixed origin. Copper (Cu) and Copper Oxide (CuO) nano particles with base fluid water are involved for the investigation. In order to constitute $CuO - water$ nano fluid, a volume fraction φ_1 of 0.1 vol. of CuO is dispersed in pure water and thermal equilibrium is achieved. This solid particle fraction φ_1 is fixed throughout the problem. In order to optimise our desired results second particle volume fraction φ_2 of Cu nano particles will be distributed in $CuO - water$ nanofluid to form our targeted hybrid nanofluid $Cu-(CuO/water)$. The steady laminar fluid is lying in space with limitation $Z \geq 0$. Nanofluid is revolving about vertical $axis$ such that the angular

velocity Ω of the fluid is constant. $u_w = ax$ and $v_w = by$ are respectively stretching velocities of $xy - plane$ in directions of x and y -axis. Temperature of fluid along wall T_w and concentration along wall C_w are constants.

7.2.1 Governing equations

Here the mathematics representing the flow consists of Eqs. of continuity, motion, energy and concentration as follow [78, 79]

$$\frac{\partial u}{\partial x} + \frac{\partial v}{\partial y} + \frac{\partial w}{\partial z} = 0, \quad (7.1)$$

$$u \frac{\partial u}{\partial x} + v \frac{\partial u}{\partial y} + w \frac{\partial u}{\partial z} - 2\Omega v = \nu_{hnf} \frac{\partial^2 u}{\partial z^2}, \quad (7.2)$$

$$u \frac{\partial v}{\partial x} + v \frac{\partial v}{\partial y} + w \frac{\partial v}{\partial z} + 2\Omega u = \nu_{hnf} \frac{\partial^2 v}{\partial z^2}, \quad (7.3)$$

$$u \frac{\partial T}{\partial x} + v \frac{\partial T}{\partial y} + w \frac{\partial T}{\partial z} = \alpha_{hnf} \frac{\partial^2 T}{\partial z^2} + \frac{Q_0}{(\rho C_p)_{hnf}} (T - T_\infty), \quad (7.4)$$

$$u \frac{\partial C}{\partial x} + v \frac{\partial C}{\partial y} + w \frac{\partial C}{\partial z} = D_{hnf} \frac{\partial^2 C}{\partial z^2} - k_1 (C - C_\infty)^n, \quad (7.5)$$

where ν_{hnf} , α_{hnf} , and D_{hnf} are momentum diffusivity (kinematic viscosity), thermal diffusivity and concentration diffusivity respectively of hybrid nanofluid and k_1 denotes constant rate of first order chemical reaction.

Corresponding endpoint conditions are

$$\left. \begin{aligned} u(x, y, 0) - u_w &= k v \frac{\partial u}{\partial z}(x, y, 0), \\ v(x, y, 0) - v_w &= k v \frac{\partial v}{\partial z}(x, y, 0), \\ T(x, y, 0) &= T_w, \quad C(x, y, 0) = C_w \\ u \rightarrow 0, \quad v \rightarrow 0, \\ T \rightarrow T_\infty, \quad C \rightarrow C_\infty \end{aligned} \right\} \text{when } z \rightarrow \infty. \quad (7.6)$$

7.2.2 Relations of effective physical measures

The relations of effective thermo physical properties for hybrid nanofluid are as follows [78]

$$\left. \begin{aligned} \rho_{hnf} &= [(1 - \varphi_2)\{(1 - \varphi_1)\rho_f + \varphi_1 \rho_{s_1}\}] + \varphi_2 \rho_{s_2} & , D_{hnf} &= (1 - \varphi_2)(1 - \varphi_1)D_f, \\ (\rho C_p)_{hnf} &= [(1 - \varphi_2)\{(1 - \varphi_1)(\rho C_p)_f + \varphi_1 (\rho C_p)_{s_1}\}] + \varphi_2 (\rho C_p)_{s_2}, & \mu_{hnf} &= \frac{\mu_f}{(1 - \varphi_1)^{5/2}(1 - \varphi_2)^{5/2}}, \end{aligned} \right\} \quad (7.7 a, b)$$

and by extended Maxwell model (Hamilton-Crosser model) [9,19]

$$\frac{K_{hnf}}{K_f} = \frac{K_{s_2} + (m-1)K_f - (m-1)\varphi_2(K_f - K_{s_2})}{K_{s_2} + (m-1)K_f + \varphi_2(K_f - K_{s_2})}, \quad (7.7 c)$$

provided that

$$\frac{K_{nf}}{K_f} = \frac{K_{s_1} + (m-1)K_f - (m-1)\varphi_1(K_f - K_{s_1})}{K_{s_1} + (m-1)K_f + \varphi_1(K_f - K_{s_1})}. \quad (7.7 d)$$

The parameters are defined in nomenclature.

In last two Eqs. m is defined by

$$m = \frac{3}{\Psi}, \quad (7.8)$$

Ψ being the sphericity of the nano particle and is given by

$$\Psi = \frac{\text{surface area of the sphere}}{\text{volume of the particle}}, \quad (7.9)$$

when $\Psi = 1$, nano particles are perfect spheres which implies $m = 3$ and then the Hamilton-

Crosser model takes the form

$$\frac{K_{hnf}}{K_f} = \frac{K_{s_2} + 2K_f - 2\varphi_2(K_f - K_{s_2})}{K_{s_2} + 2K_f + \varphi_2(K_f - K_{s_2})}, \quad (7.10)$$

along with

$$\frac{K_{nf}}{K_f} = \frac{K_{s_1} + 2K_f - 2\varphi_1(K_f - K_{s_1})}{K_{s_1} + 2K_f + \varphi_1(K_f - K_{s_1})}. \quad (7.11)$$

Here K_f , K_{nf} , K_{hnf} are thermal conductivities of base fluid, nano fluid and hybrid nano fluid respectively. φ_1 and φ_2 are particle volume fractions for Copper Oxide (CuO) and Copper (Cu) nano particles respectively.

7.2.3 Similarity relations

The following shifts are used in problem to transform the system from dimensional to non-dimensional status [4, 6, 77, 79]

$$u = axf'(\eta), v = ayg'(\eta), w = -\sqrt{av_f}(f(\eta) + g(\eta)), \eta = z\sqrt{\frac{a}{v_f}}, R_c = \frac{k_1(C-C_\infty)^{n-1}}{a},$$

$$\theta(\eta) = \frac{T-T_\infty}{T_w-T_\infty}, H(\eta) = \frac{C-C_\infty}{C_w-C_\infty}, Sc = \frac{v_f}{D_f}, \delta = \frac{Q_0}{a(\rho C_p)_f}, Pr = \frac{(\rho C_p)_f}{K_f}, \quad (7.12 a, b)$$

here $f'(\eta)$ and $g'(\eta)$ are non-dimensional velocities of flow in x- and y-directions respectively. $\theta(\eta)$ and $H(\eta)$ are non-dimensional temperature and non-dimensional concentration respectively, Sc represents Schmidt number, δ the heat source/sink parameter and R_c is the chemical reaction constraint.

Invoking Eqs. (7.7) - (7.12), we see from Eq. (7.1) that mass is conserved and Eqs. (7.2) to (7.5) are converted in to a set of differential Eqs. which are ordinary in nature as

$$f''''(\eta) - (1 - \varphi_1)^{\frac{5}{2}}(1 - \varphi_2)^{\frac{5}{2}}[(1 - \varphi_2) \left\{ (1 - \varphi_1) + \varphi_1 \left(\frac{\rho_{s_1}}{\rho_f} \right) \right\} + \varphi_2 \left(\frac{\rho_{s_2}}{\rho_f} \right)] [(f'(\eta))^2 - f''(\eta)(f(\eta) + g(\eta)) - 2\lambda\xi g'(\eta)] = 0, \quad (7.13)$$

$$g''''(\eta) - (1 - \varphi_1)^{\frac{5}{2}}(1 - \varphi_2)^{\frac{5}{2}}[(1 - \varphi_2) \left\{ (1 - \varphi_1) + \varphi_1 \left(\frac{\rho_{s_1}}{\rho_f} \right) \right\} + \varphi_2 \left(\frac{\rho_{s_2}}{\rho_f} \right)] [(g'(\eta))^2 - g''(\eta)(f(\eta) + g(\eta)) + 2\left(\frac{\lambda}{\xi}\right)f'(\eta)] = 0, \quad (7.14)$$

$$\frac{K_{hnf}}{K_f} \theta''(\eta) + Pr \left[\left((1 - \varphi_2) \left\{ (1 - \varphi_1) + \varphi_1 \left(\frac{(\rho C_p)_{s_1}}{(\rho C_p)_f} \right) \right\} + \varphi_2 \left(\frac{(\rho C_p)_{s_2}}{(\rho C_p)_f} \right) \right) (f + g)\theta'(\eta) + \delta\theta(\eta) \right] = 0, \quad (7.15)$$

$$H''(\eta) + \frac{Sc}{(1 - \varphi_1)(1 - \varphi_2)} [(f(\eta) + g(\eta))H'(\eta) - R_c H(\eta)] = 0. \quad (7.16)$$

Boundary conditions (7.6) of flow, temperature and concentration after using transformations (7.12a, b) take the following non-dimensional form as

$$\left. \begin{aligned} f(0) = 0, \quad g(0) = 0, \quad f'(0) = 1 + Kf''(0), \quad g'(0) = \alpha + Kg''(0), \\ \theta(0) = 1, \quad H(0) = 1, \quad \theta(\infty) = 0, \quad H(\infty) = 0, \quad f'(\infty) = 0, \quad g'(\infty) = 0. \end{aligned} \right\} \quad (7.17)$$

Here K is velocity slip parameter and is given by

$$K = k\sqrt{av_f}, \quad (7.18)$$

with k as slip length.

An interesting fact arising here is that when we put $\varphi_1 = 0 = \varphi_2 = \lambda$, our flow Eqs. (7.13) and (7.14) coincide with the problems of Ariel [6] and Ullah *et al* [7] and the concentration Eq. (7.16) reduces to that of Ferdows *et al.* [79] with an addition of non-dimensional function $g(\eta)$. Further when we take $\alpha = 0 = K = \delta$ in energy Eq. (7.15), it lowers down to that of Wang [31] with addition of non-dimensional function $g(\eta)$.

7.3 Physical quantities of interest

Skin friction along x-axis Cf_x , skin friction along y-axis Cf_y , heat flux at wall q_w and mass flux q_m are the quantities of our special interest. All these are given by [78, 79]

$$Cf_x = \frac{\mu_{hnf} \left(\frac{\partial u}{\partial z} \right)_{z=0}}{\rho(ax)^2}, \quad Cf_y = \frac{\mu_{hnf} \left(\frac{\partial v}{\partial z} \right)_{z=0}}{\rho(ax)^2}, \quad q_w = -K_{hnf} \left(\frac{\partial T}{\partial z} \right)_{z=0}, \quad q_m = -D_{hnf} \left(\frac{\partial C}{\partial z} \right)_{z=0}. \quad (7.19)$$

The non-dimensional skin frictions for hybrid nano fluid are

$$(Re_x)^{\frac{1}{2}} Cf_x = \frac{1}{(1-\varphi_1)^{2.5}(1-\varphi_2)^{2.5}} f''(0), \quad \xi^{-1} (Re_x)^{\frac{1}{2}} Cf_y = \frac{1}{(1-\varphi_1)^{2.5}(1-\varphi_2)^{2.5}} g''(0). \quad (7.20)$$

Further, Nusselt number and Sherwood number in reduced forms are

$$\frac{(Re_x)^{\frac{-1}{2}} x q_w}{K_f(T_w - T_\infty)} = \frac{-K_{hnf}}{K_f} \theta'(0), \quad \frac{(Re_x)^{\frac{-1}{2}} x q_m}{D_f(C_w - C_\infty)} = -(1 - \varphi_1)(1 - \varphi_2)H'(0). \quad (7.21)$$

Where $Re_x = \frac{u_w x}{v_f}$ is the confined Reynolds number.

7.4 Solution method

Eqs. (7.13) to (7.16) along with limitations (7.17) are tackled with a numerical procedure RKF45 [48-50] with shooting process. The procedure adopted is as follows:

$$\text{Let } B_1 = \frac{1}{(1-\varphi_1)^{5/2}(1-\varphi_2)^{5/2}}, \quad B_2 = (1-\varphi_2) \left\{ (1-\varphi_1) + \varphi_1 \left(\frac{\rho_{s1}}{\rho_f} \right) \right\} + \varphi_2 \left(\frac{\rho_{s2}}{\rho_f} \right),$$

$$B_3 = (1-\varphi_2) \left\{ (1-\varphi_1) + \varphi_1 \left(\frac{(\rho C_p)_{s1}}{(\rho C_p)_f} \right) \right\} + \varphi_2 \left(\frac{(\rho C_p)_{s2}}{(\rho C_p)_f} \right), \quad B_4 = (1-\varphi_1)(1-\varphi_2), \quad (7.22 \text{ a, b})$$

and

$$f = y_1, \quad f' = y_2, \quad f'' = y_3, \quad f''' = y_3', \quad (7.23)$$

$$g = y_4, \quad g' = y_5, \quad g'' = y_6, \quad g''' = y_6', \quad (7.24)$$

$$\theta = y_7, \quad \theta' = y_8, \quad \theta'' = y_8', \quad (7.25)$$

$$H = y_9, \quad H' = y_{10}, \quad H'' = y_{10}'. \quad (7.26)$$

Then the system of Eqs. (7.13) – (7.16) reduces to a system of 1st order ordinary differential Eqs. as

$$\begin{bmatrix} y_2 \\ y_3 \\ y_3' \\ y_5 \\ y_6 \\ y_6' \\ y_8 \\ y_8' \\ y_{10} \\ y_{10}' \end{bmatrix} = \begin{bmatrix} y_1' \\ y_2' \\ \frac{B_2}{B_1} [y_2^2 - (y_1 + y_4)y_3 - 2\lambda\xi y_5] \\ y_4' \\ y_5' \\ \frac{B_2}{B_1} [y_5^2 - (y_1 + y_4)y_6 + \left(\frac{2\lambda}{\xi}\right)y_2] \\ y_7' \\ \frac{-Pr}{\left(\frac{\kappa_{hnf}}{\kappa_f}\right)} [B_3(y_1 + y_4)y_8 + \delta y_7] \\ y_9' \\ \frac{Sc}{B_4} [R_c \cdot y_9 - (y_1 + y_4)y_{10}] \end{bmatrix}, \quad (7.27)$$

with initial conditions as follows

$$\begin{bmatrix} y_0(1) \\ y_0(2) \\ y_0(3) \\ y_0(4) \\ y_0(5) \\ y_0(6) \\ y_0(7) \\ y_0(8) \\ y_0(9) \\ y_0(10) \end{bmatrix} = \begin{bmatrix} 0 \\ 1 + K, y_0(3) \\ p_1 \\ 0 \\ \alpha + K, y_0(6) \\ p_2 \\ 1 \\ p_3 \\ 1 \\ p_4 \end{bmatrix}. \quad (7.28)$$

α is stretching ratio parameter while p_i are shooting parameters for $i = 1,2,3,4$. These parameters are dealt as in unit 4. Convergence criterion of 10^{-6} is fixed for computation of results in this study.

7.5 Results and discussion

Pictorial/ tabular results and related discussions are the subject of this section. The main objective here is to examine the flow for hybrid rotating nano fluid. The comparison of thermal conductivities for pure water, nano fluid (*CuO – water*) and hybrid nano fluid (*Cu – CuO/water*) is displayed in Fig.(7.1). From this figure it is depicted that despite identical particle volume fractions, the thermal conductivity due to hybrid nano fluid is the greater. How hybrid nano fluid influences the flow velocity? The answer to this question can easily be inferred from Fig.(7.2). As irrespective of Suriya et al.[78] there is no magnetic field involved here to accelerate nano particles, so the hybrid nano fluid slows down the fluid velocity. Other factors reducing fluid velocity are density and dynamic viscosity which are increased by hybridity and so velocity is reduced. Rotation of fluid decreases the boundaries of its linear velocity in both $x -$ and $y -$ directions. This fact is demonstrated in Figs. (7.3) and (7.4). These Figs. also describe that hybrid nano fluid velocity is always less than nano fluid velocity. The reason is obvious as inclusion of more massive particles declines normal fluid flow. In Fig.(7.5), comparison of temperature profile among pure water, nano fluid and hybrid nano fluid is

visualized. We see that under same conditions and equal total amounts of particle volume fraction, the hybrid nano fluid attains more temperature than nano fluid. As in previous problems, rotation boosts the thermal boundary layer thickness, this behaviour remains the same as can be seen in Fig. (7.6). Further, rapid rise in temperature is due to hybrid nano fluid. A bird eye view on Fig. (7.7) explores that the hybrid nano fluid enhances the thermal boundary and this enhancement is proportional to surge in heat source/sink parameter δ . From Fig. (7.8) it can be perceived that with a rise in rotation, concentration increases. Here the effects of hybridity on the concentration are opposite and intending concentration towards surface. Variations due to Schmidt number Sc , chemical reaction R_c in concentration and hybridity can be visualized in Figs. (7.9) and (7.10). The Schmidt number, the chemical reaction and the hybridity all sweep the concentration towards the surface of the rotating system. In Fig. (7.11), heat transfer rate across the surface versus rotation parameter λ is extracted. We note that heat transfer rate declines with increase in rotation and velocity slip. A considerable growth in heat transfer rate across surface is noted for hybrid nano fluid as compared to nano fluid. In previously explored problems, there is no stretching along $y - axis$ i.e., when α i.e., stretching ratio along $y - axis$ to the stretching ratio along $x - axis$ is zero or negligible, the tangential stress along $x - axis$ as well as along $y - axis$ increases with increase in rotation. But here case is different. When stretching ratio α is non-zero and lies in the interval $0 < \alpha < 1$, with increase in rotation the tangential stress along x -axis is observed declining down to specific value while same stress along y -axis still increases likewise examined earlier. This phenomenon for $\alpha = 0.5$ can be detected in Figs. (7.12a) and (7.12b). Here velocity slip impulsively decreases tangential stress along $x - axis$ as well as along $y - axis$ while hybridity enhances skin friction in both directions. Fig. (7.13) explicitly explores that velocity slip parameter K and rotation parameter λ are reducing Sherwood number.

In *Table (7.1)* thermo physical properties of constituents of nano and hybrid nano fluids are tabulated. In *Table (7.2)* the same properties have been calculated for nano and hybrid nano base fluids for different particle volume fractions φ_2 . Here values for $\varphi_2 = 0$ correspond to the nano base fluid and values for $\varphi_2 > 0$ for hybrid nano based fluid. We observe that the thermal conductivity, density and dynamic viscosity of nano fluid are all positively affected by hybridity while volume heat capacity is lowered.

From data arranged in *Table (7.3)*, we extract that rotation parameter λ and stretching ratio parameter α enhance skin frictions in both $x -$ and $y -$ directions. Physical interpretation behind it is the collision of nano particles with the surface either it is by rotation or by relative stretching increase or both and so skin friction is increased. Slip parameter K reduces skin friction which is obvious from the fact that smaller the friction between fluid and surface implies a greater slip and vice versa. Hybridity of fluid is up surging these skin frictions. This may be due to inclusion of more massive particles and due to collisions of more than one type of particles having different properties like mass, density etc and thus continuing a series of nested collisions and thus resulting in more skin friction. From data *Table (7.4)*, rotation parameter λ , velocity slip parameter K and heat source/sink parameter δ all contribute in lowering heat transfer rate at the wall. In fact, rotation, velocity slip and heat source/sink all cause a rise in temperature profile $\theta(\eta)$ and obviously heat flux at surface is reduced. On the other hand stretching ratio parameter α causes a rise in surface heat flux. The reason behind it is that a proliferation in stretching ratio indicates a reduction in temperature profile and so surface heat flux tends to a high value. Finally, from this table it is depicted that hybridity rises heat transfer rate at wall. It is because inclusion of more than one type of nano particles having greater thermal conductivities and different masses and densities collide each other continuously and thus play role in accelerating heat transfer at the surface. From *Table (7.5)*, it is clear that mass transfer Nusselt number at

surface increases with increase in Schmidt number Sc , stretching ratio α and chemical reaction parameter R_c . While the same reduces with increase in velocity slip parameter K and rotation λ . Results are compatible with graphical results of Fig. (7.13). Further the hybridity of the fluid decreases the Sherwood number at the surface.

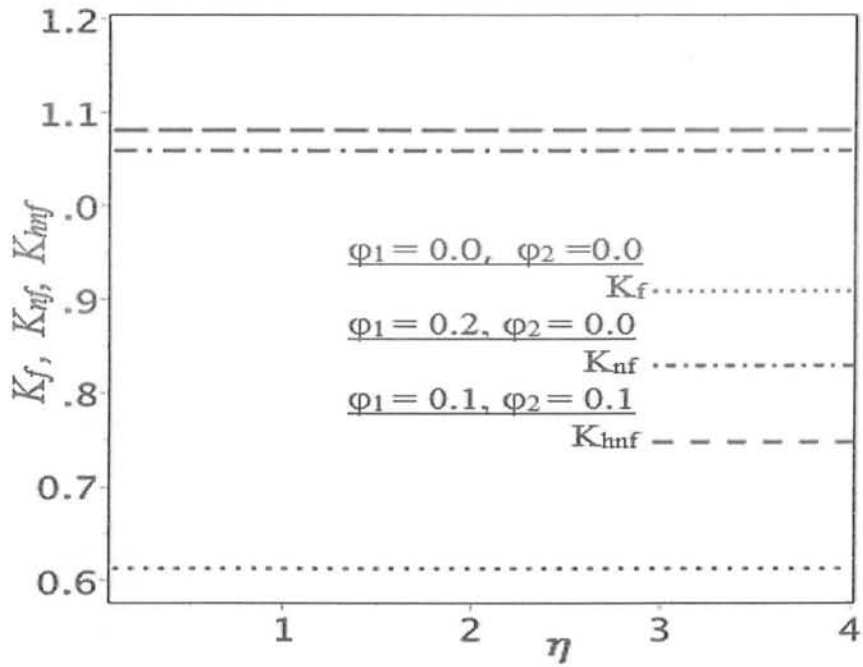


Fig. (7.1): Comparison of thermal conductivities of pure water (K_f), nanofluid (K_{nf}) and hybrid nanofluid (K_{hnf})

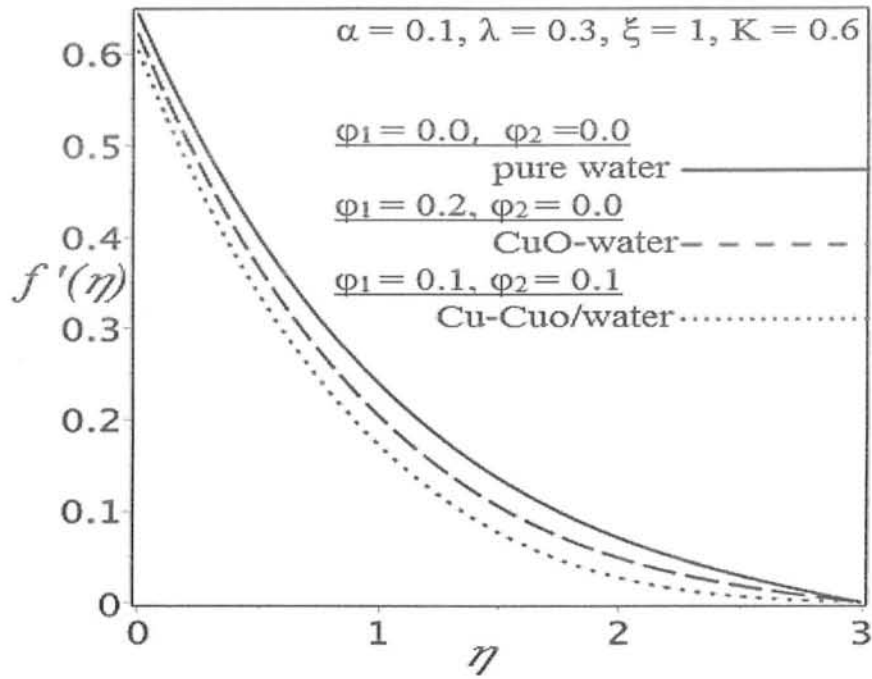


Fig. (7.2): Comparison of velocity profile $f'(\eta)$ for pure water, nanofluid ($CuO - water$) and hybrid nanofluid ($Cu - CuO/water$)

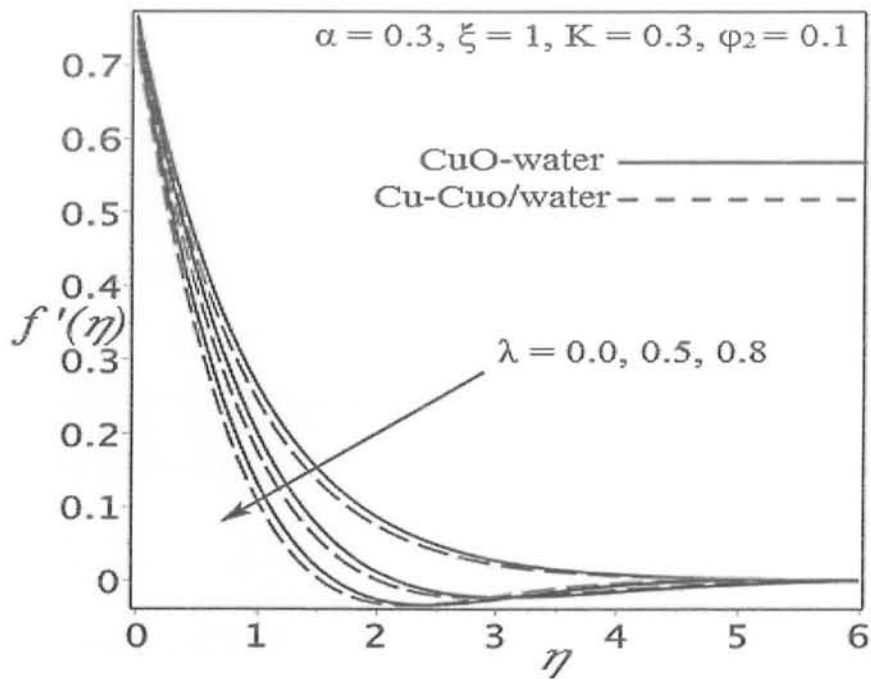


Fig. (7.3): Variations due to rotation parameter λ in dimensionless velocity component $f'(\eta)$ for nanofluid ($CuO - water$) and hybrid nanofluid ($Cu - CuO/water$)

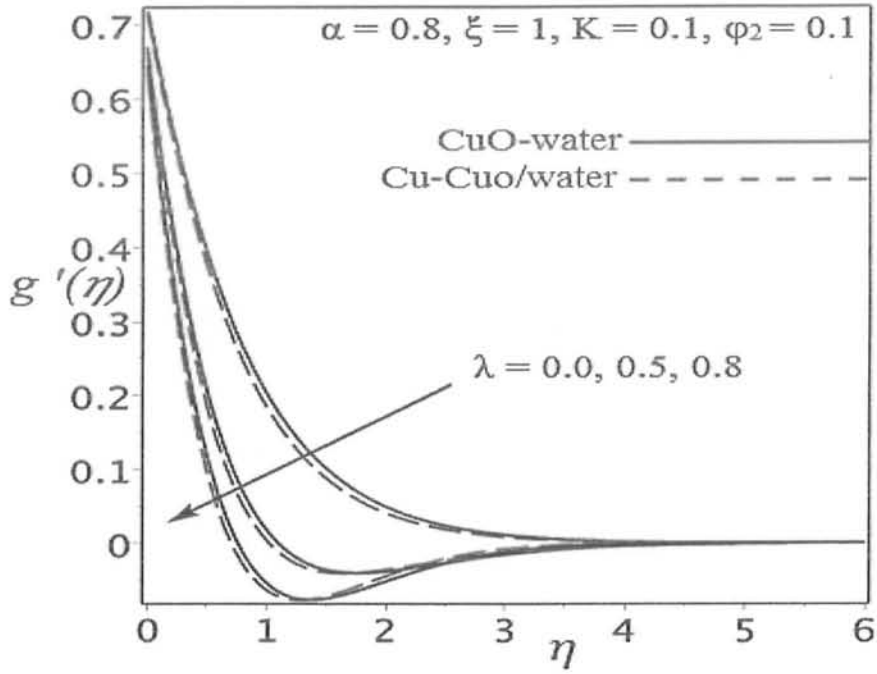


Fig. (7.4): Variations due to rotation parameter λ in dimensionless velocity component $g'(\eta)$ for nanofluid (CuO – water) and hybrid nanofluid (Cu – CuO/water)

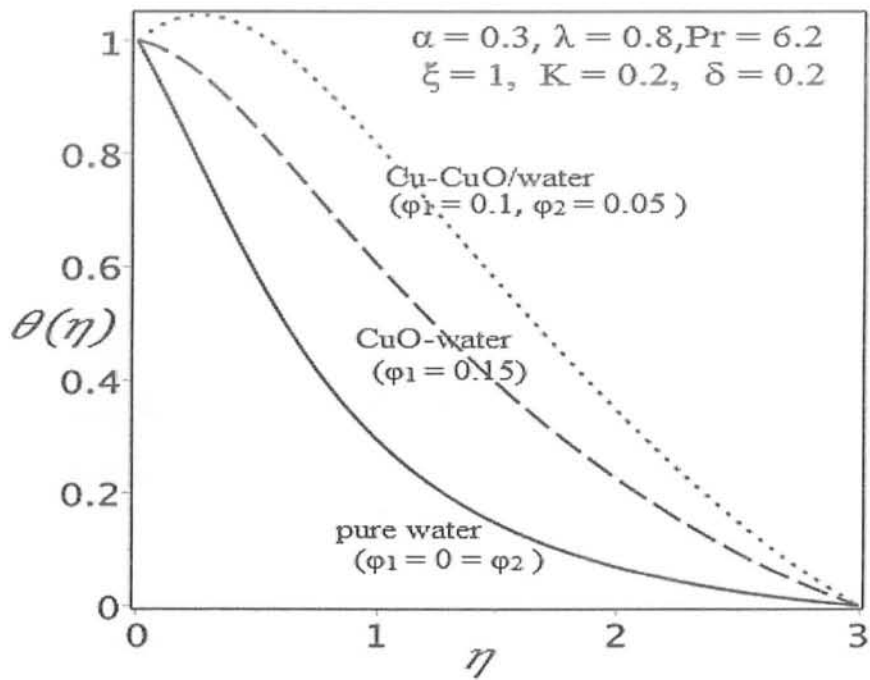


Fig. (7.5): Comparison of temperature profile $\theta(\eta)$ for pure water, nanofluid (CuO – water) and hybrid nanofluid (Cu – CuO/water)

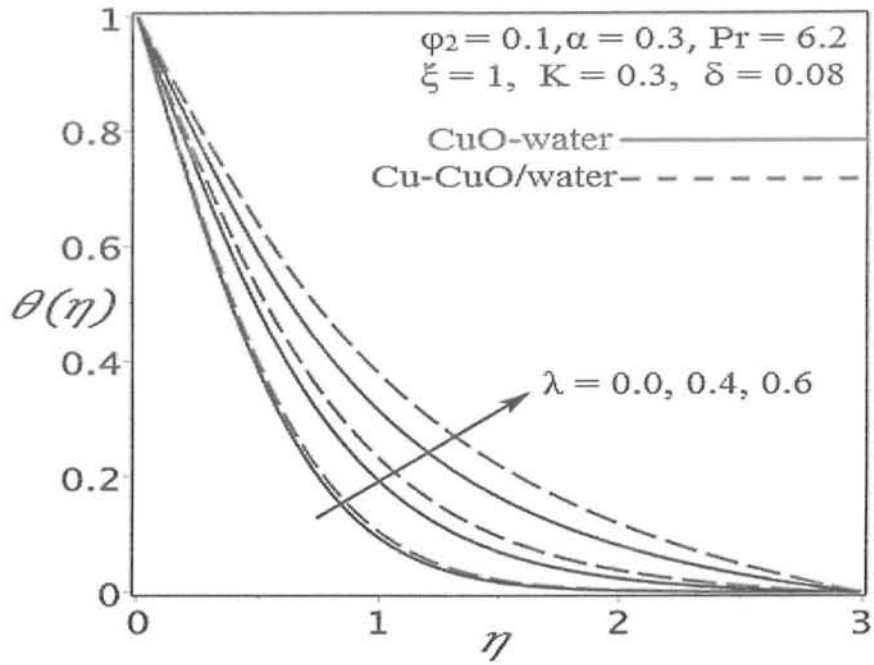


Fig. (7.6): Effects of rotation parameter λ on temperature profile $\theta(\eta)$ for nanofluid ($CuO - water$) and hybrid nanofluid ($Cu - CuO/water$)

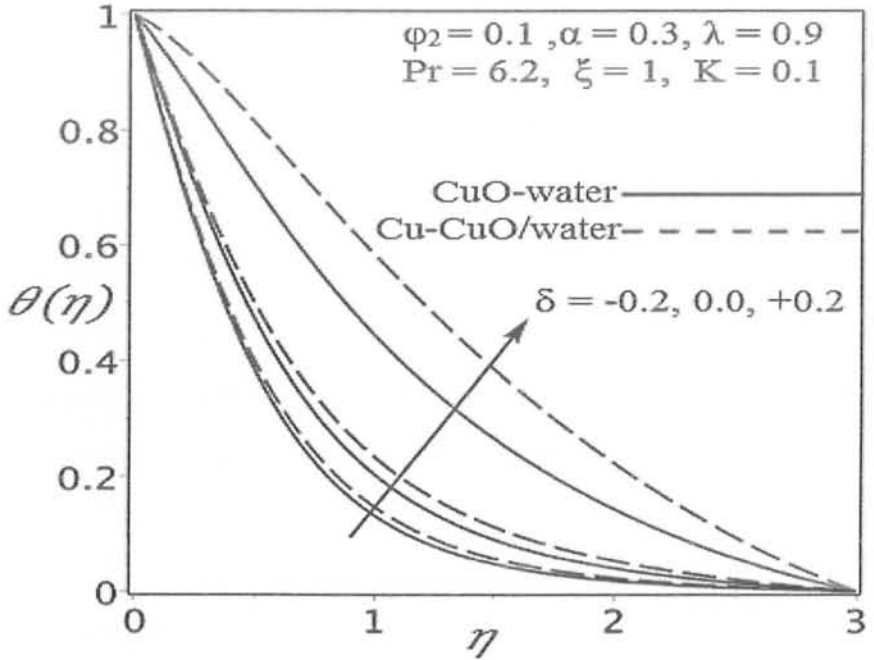


Fig. (7.7): Variations due to heat sink/source parameter δ in dimensionless temperature $\theta(\eta)$ for nanofluid ($CuO - water$) and hybrid nanofluid ($Cu - CuO/water$)

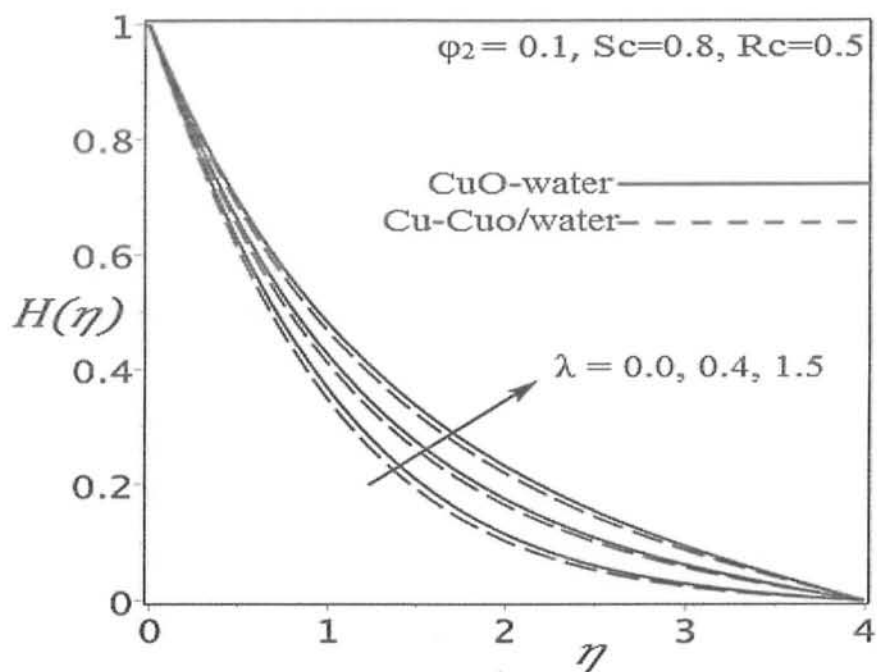


Fig. (7.8): Effects of rotation parameter λ on concentration profile $H(\eta)$ for nanofluid ($\text{CuO} - \text{water}$) and hybrid nanofluid ($\text{Cu} - \text{CuO/water}$)

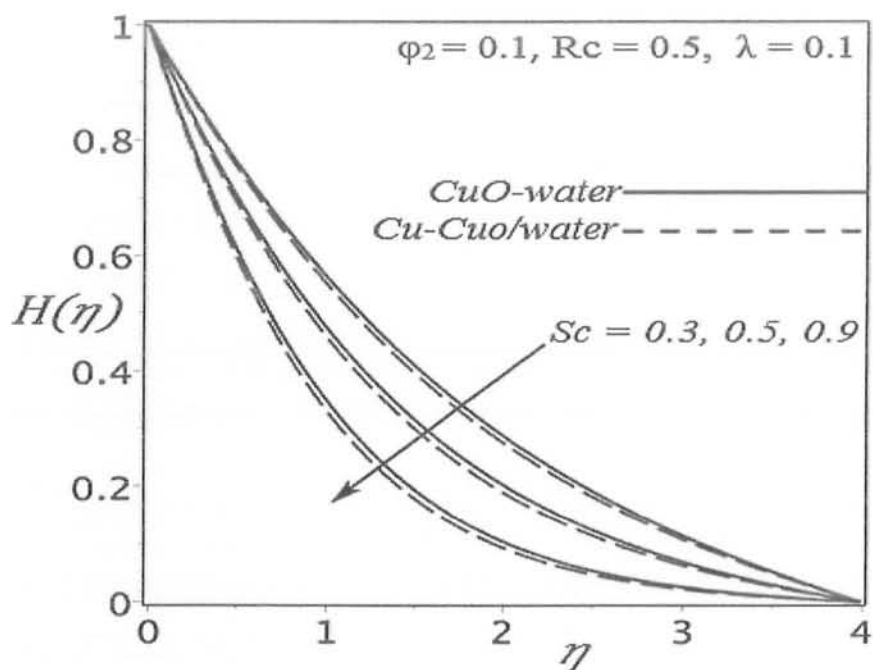


Fig. (7.9): Concentration profile $H(\eta)$ versus η for some estimates of Schmidt number Sc

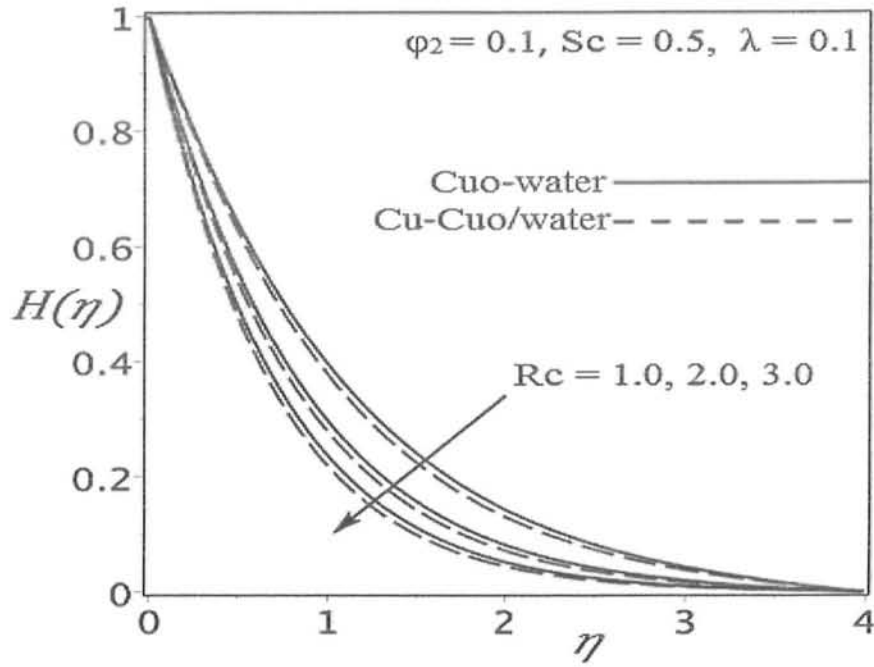


Fig. (7.10): Concentration profile $H(\eta)$ versus η for different values of chemical reaction parameter R_c

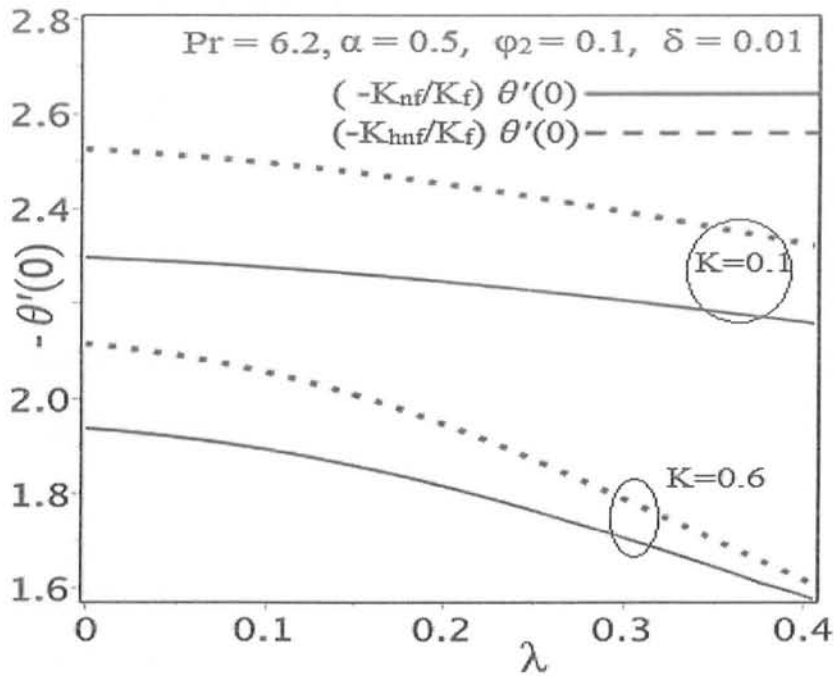


Fig. (7.11): Heat flux across the surface versus rotation parameter λ for nano fluid ($CuO - water$) and hybrid nano fluid ($Cu - CuO/water$)

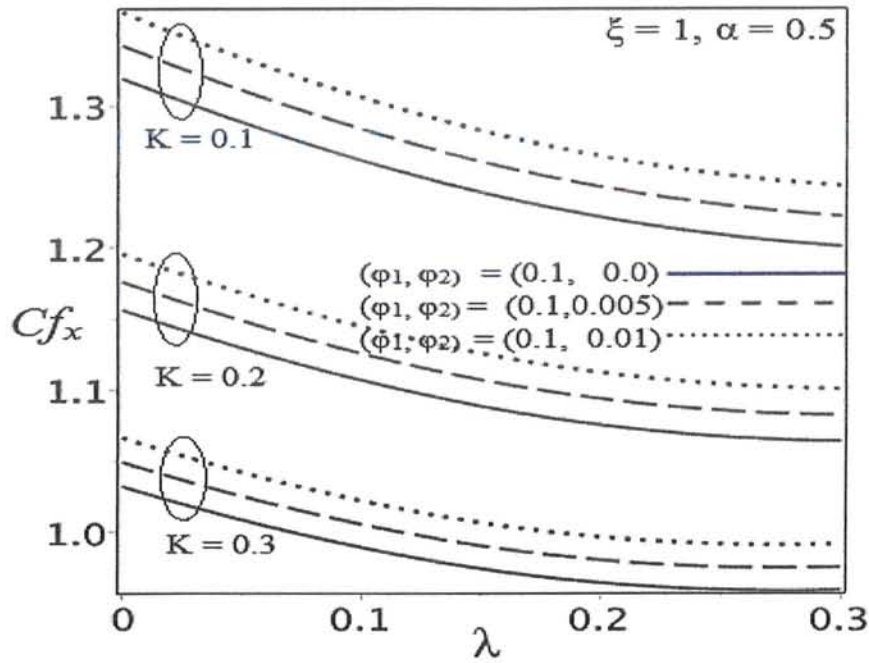


Fig. 7.12a

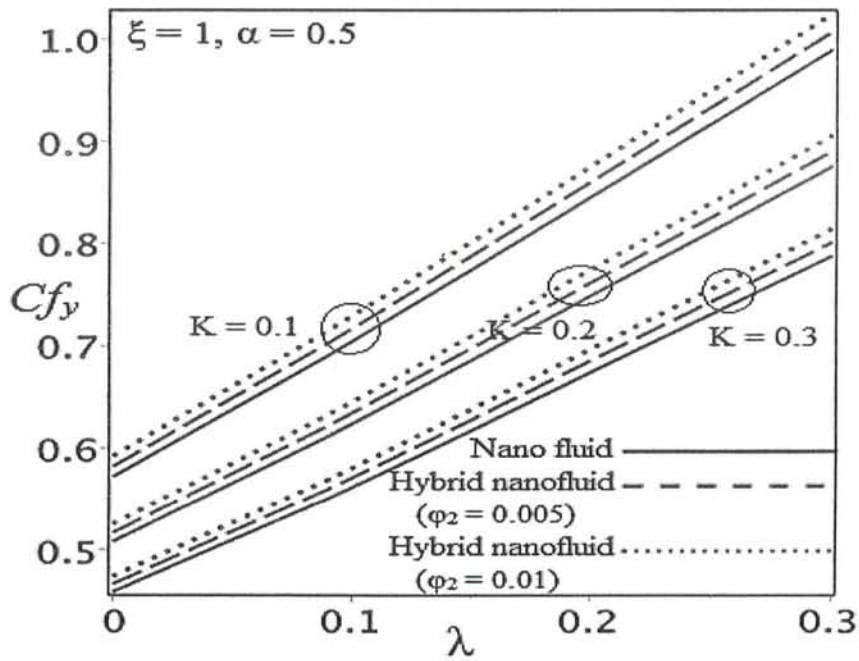
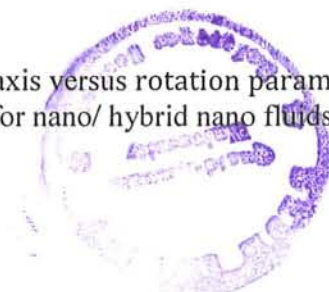


Fig. 7.12b

Figs. (7.12a, b): Skin frictions in the direction of x-axis and y-axis versus rotation parameter λ for various estimates of linear velocity slip parameter K for nano/ hybrid nano fluids



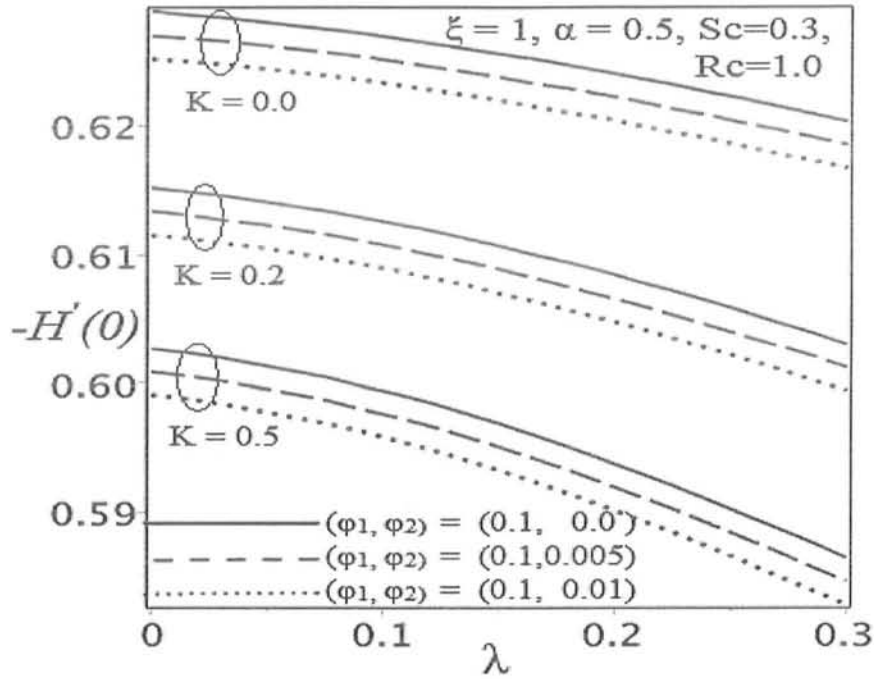


Fig. (7.13): Reduced concentration at wall $-H'(0)$ versus rotation parameter λ for various estimates of velocity slip parameter K for nano/ hybrid nano fluids

Table (7.1) : Thermo physical properties of constituents [23, 37]

Properties\Constituents	Pure Water (H_2O)	Copper (Cu)	Copper Oxide (CuO)
Density (ρ) Kg/m^3	997.1	8933	6320
Dynamic Viscosity (μ_f) $Kg/m.s$	0.000891	-	-
Specific Heat (C_p) $J/Kg.K$	4179.0	385.0	531.8
Thermal Conductivity (K) $W/m.K$	0.6130	400	76.50
Prandtl Number (Pr)	6.2	-	-

Table (7.2) : Thermo physical properties of nano and hybrid nano fluids at 25°C

($\varphi_1 = 0.1$)				
Properties → Particle volume fractions ↓ for hybrid nanofluid	Thermal Conductance $W/m.K$	Density Kg/m^3	Dynamic Viscosity $Kg/m.s$	Volume Heat Capacity $(J/m^3) \times 10^6$
	(K_{hnf})	(ρ_{hnf})	μ_{hnf}	$(\rho C_p)_{hnf}$
$\varphi_2 = 0.00$	$0.8120 = K_{nf}$	$1529.39 = \rho_{nf}$	$0.001160 = \mu_{nf}$	$4.0862904 = (\rho C_p)_{nf}$
$\varphi_2 = 0.05$	0.9394	1899.57	0.001318	4.053936
$\varphi_2 = 0.10$	1.0808	2269.75	0.001509	4.0215819

Table (7.3): Effects of reflected parameters on reduced skin frictions $-f''(0)$ & $-g''(0)$ for nano and hybrid nanofluids ($\xi = 1, \varphi_1 = 0.1$)

λ	K	α	$\frac{-1}{(1-\varphi_1)^{2.5}} f''(0)$	$\frac{-(1-\varphi_1)^{-2.5}}{(1-\varphi_2)^{2.5}} f''(0)$		$\frac{-1}{(1-\varphi_1)^{2.5}} g''(0)$	$\frac{-(1-\varphi_1)^{-2.5}}{(1-\varphi_2)^{2.5}} g''(0)$	
				$\varphi_2 = 0.05$	$\varphi_2 = 0.1$		$\varphi_2 = 0.05$	$\varphi_2 = 0.1$
0.1	0.2	0.1	1.08451	1.27470	1.48283	0.23453	0.27870	0.32590
0.2			1.10263	1.29903	1.51300	0.41479	0.49712	0.58379
0.3			1.15645	1.36507	1.59067	0.57678	0.68154	0.79355
0.2	0.1	0.4	1.22437	1.44574	1.68562	0.72070	0.85306	0.99566
	0.2		1.07981	1.26973	1.47735	0.64095	0.75588	0.88062
	0.3		0.96955	1.13659	1.32047	0.57915	0.68116	0.79253
0.15	0.15	0.2	1.15462	1.36016	1.58399	0.40770	0.48345	0.56474
		0.4	1.15663	1.36213	1.58605	0.60733	0.71711	0.83599
		0.6	1.16031	1.36620	1.59064	0.85747	1.01095	1.17771

Table (7.4): Effects of reflected parameters on heat flux at the surface for nano and hybrid nano fluids ($Pr = 6.2, \varphi_1 = 0.1$)

λ	K	α	δ	$-\left(\frac{K_{hnf}}{K_f}\right)\theta'(0)$	$-\left(\frac{K_{hnf}}{K_f}\right)\theta'(0)$	
					$\varphi_2 = 0.05$	$\varphi_2 = 0.1$
0.1	0.1	0.5	0.01	2.27701	2.38434	2.49750
0.2				2.24639	2.34669	2.45298
0.3				2.20646	2.29714	2.39384
0.15	0.2	0.3	0.03	1.93068	2.00532	2.08674
	0.4			1.76126	1.81925	1.88602
	0.6			1.62707	1.67156	1.72641
0.2	0.1	0.2	0.05	1.84531	1.90363	1.96692
		0.4		2.07703	2.15993	2.24807
		0.6		2.26470	2.36256	2.46607
0.1	0.3	0.5	0.02	2.06932	2.15818	2.25495
			0.04	2.03095	2.11490	2.20652
			0.06	1.99195	2.07081	2.15708

Table (7.5): Effects of various parameters on concentration at wall for nano and hybrid nano fluids ($\varphi_1 = 0.1$)

λ	K	α	Sc	R_c	$-(1 - \varphi_1) H'(0)$	$\frac{-(1 - \varphi_1)}{(1 - \varphi_2)^{-1}} H'(0)$	
						$\varphi_2 = 0.02$	$\varphi_2 = 0.05$
0.1	0.1	0.5	0.2	0.5	0.41474	0.40894	0.40059
0.2					0.41149	0.40566	0.39729
0.3					0.40729	0.40143	0.39304
0.2	0.1	0.5	0.3	1.0	0.61530	0.60806	0.59757
	0.2				0.60841	0.60117	0.59069
	0.3				0.60275	0.59552	0.58506
0.3	0.3	0.2	0.2	0.2	0.63284	0.62565	0.61508
		0.4			0.64298	0.63573	0.62506
		0.8			0.65728	0.64985	0.63895
0.3	0.3	0.6	0.1	0.5	0.31716	0.31198	0.30445
			0.2		0.40136	0.39543	0.38698
			0.3		0.47889	0.47219	0.46275
0.2	0.2	0.4	0.1	1.0	0.37252	0.36727	0.35956
				2.0	0.46953	0.46382	0.45538
				3.0	0.55339	0.54714	0.53785



7.6 Conclusions

Three dimensional rotating hybrid nano fluid with heat source/sink, mass concentration, velocity slip and chemical reaction is analysed on a plane stretching surface. Important findings are as follows:

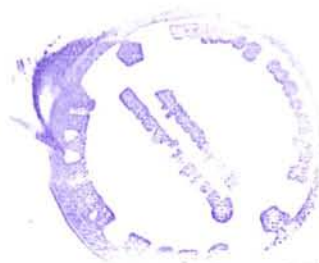
- 1) Hybridity decrease velocity profile but increase temperature profile. Also it boosts the rate of heat transfer at surface.
- 2) Rotation drops linear velocity viscous boundary and heat transfer rate. It increases the thermal boundary of hybrid nano fluid and reduces the concentration at surface.
- 3) For stretching ratio $\alpha \in (0,1)$, a rise of rotation parameter λ implies a rise in skin friction along $y - axis$ while skin friction along $x - axis$ is found to deprive itself down to a specific value.
- 4) Heat source/sink parameter δ increases thermal boundary of hybrid nano fluid.
- 5) The linear velocity slip parameter K lowers tangential stresses and mass concentration of hybrid nano fluid at wall.
- 6) Sc the Schmidt number and R_c the chemical reaction both boost the mass concentration at the surface.

References

- 1) Crane L J., Flow past a stretching plate, *Z Angew Math Phys.*, 1970; 21,445-447.
- 2) Siddappa B., Khapate BS., Rivlin-Ericksen fluid flow past a stretching plate, *Rev Roum Sci Techn M-c Appl.*, 1976; 21, 497-505.
- 3) McLeod J. B., Rajagopal K. R., On the uniqueness of flow of a Navier-Stokes fluid due to a stretching boundary, *Arch Rat Mech Anal.*, 1987; 98, 385-393.
- 4) Wang CY., The three dimensional flow due to a stretching flat surface, *Phys Fluids.*, 1984; 27,1915-1917.
- 5) Rajagopal K.R., Na T.Y., Gupta A.S., Flow of a viscoelastic fluid over a stretching sheet, *Rheol Acta.*, 1984; 23, 213-215.
- 6) Ariel P. D., The three-dimensional flow past a stretching sheet and the homotopy perturbation method, *Comput Math Appl.*, 2007; 54, 920–925.
- 7) Ullah H., Islam S., Idrees M., Fiza M., Zaman A., The three dimensional flow past a stretching sheet by extended optimal homotopy asymptotic method, *Sci Int (Lahore).*, 2014; 26(2), 567-576.
- 8) Choi U. S., Eastman, J. A., Enhancing thermal conductivity of fluids with nanoparticles, *ASME Int Mech Eng Congress & Exposition.*, San Francisco.,1995.
- 9) Hamilton R.L., Crosser O.K., Thermal conductivity of heterogeneous two-component systems, *Ind Eng Chem Fundam.*,1962; 1, 182-191.
- 10) Choi, S., *Nanofluid Technology: Current status and future research*, Energy Technology Division Argonne National Laboratory Argonne, IL 60439.
- 11) Buongiorno J., Convective transport in nanofluids, *ASME J Heat Transf.*, 2006; 128,240-250.
- 12) Wong K.F.V., Leon O.D., Applications of nanofluids: current and future, *Adv Mech Eng.*,

2010; Article ID 519659.

- 13) Pak BC, Cho YI., Hydrodynamic and heat transfer study of dispersed fluids with submicron metallic oxide particles, *Exp Heat Transf.*,1998; 11,151-170.
- 14) Wang X., Xu X., Choi S.U.S., Thermal conductivity of nanoparticle-fluid mixture, *J Thermo phys Heat Transf.*, 1999; 13,474-480.
- 15) Li Q., Xuan Y., Experimental investigation on transport properties of nanofluids, *Heat Transf Sci Tech.*, 2000; (ed. Wang Buxuan), Beijing: HEP., 757-762.
- 16) Xuan Y., Li Q., Heat transfer enhancement of nanofluids, *Int J Heat Fluid Flow.*, 2000; 21,158-164.
- 17) Li Q., Xuan Y.M., Convective heat transfer and flow characteristics of Cu–water nanofluids, *Sci China, Series E.*, 2002; 45, 408–416.
- 18) Lee S., Choi S.U.S., Application of metallic nanoparticle suspensions in advanced cooling systems, Argonne National Laboratory Energy Technology Division 9700 S. (U.S.A)
- 19) Kakac S., Pramuanjaroenkij A., Review of convective heat transfer enhancement with nanofluids, *Int J Heat Mass Transf.*,2009; 52, 3187-3196.
- 20) Nadeem S., Mehmood R., Akbar N. S., Optimized analytical solution for oblique flow of a Casson-nano fluid with convective boundary conditions, *Int J Therm Sci.*, 2014; 78, 90–100.
- 21) Aladag, B., Halelfadl S., Doner N., Mare T., Duret S., Estelle P., Experimental investigations of the viscosity of nanofluids at low temperatures, *Appl Energy.*, 2012, 97, 876-880.
- 22) Bachok N., Ishak A., Pop I., Stagnation-point flow over a stretching/shrinking sheet in a nanofluid, *Nanoscale Res Lett.*, 2011; 6, 623.
- 23) Bachok N., Ishak A., Pop I., Flow and heat transfer characteristics on a moving plate in a nanofluid, *J Heat Mass Transf.*, 2012; 55, 642-648.
- 24) Bachok N., Ishak A., Nazar R., Senu N., Stagnation-point flow over a permeable stretching/shrinking sheet in a copper-water nanofluid, *Bound Value Probl.*, 2013; 39,



- 25) Vajravelua K., Kumarb BVR., Analytical and numerical solutions of a coupled non-linear system arising in a three-dimensional rotating flow, *Int J NonLinear Mech.*, 2004; 39,13-24.
- 26) Nazar R., Amin N., Pop I., Unsteady boundary layer flow due to a stretching surface in a rotating fluid, *Mech Res Comm.*, 2004; 31,121-128.
- 27) Kumari M., Nath G., Transient rotating flow over a moving surface with a magnetic field, *Int J Heat Mass Transf* 2005; 48, 2878-2885.
- 28) Kumari M., Grosan T., Pop I., Rotating flow of power-Law fluids over a stretching surface, *Tech Mech.*, 2006; 26, 11-19.
- 29) Kumari M., Nath G., Flow and heat transfer in a stagnation point flow over a stretching sheet with a magnetic field, *Mech Res Comm.*, 1999; 26, 469-478.
- 30) Zaimi K., Ishak A., Pop I., Stretching surface in rotating viscoelastic fluid, *Appl Math Mech -Engl. Ed.*, 2013, 34, 945-952.
- 31) Wang CY., Stretching a surface in a rotating fluid, *J Appl Math Phys (ZAMP)*., 1988; 39,177-185.
- 32) Ascher U., Mattheij R., Russell R., Numerical solution of boundary value problems for ordinary differential equations, *SIAM Classics in Appl Maths.*, 1995; 13, 327-357.
- 33) Ascher U., Petzold L., *Computer Methods for Ordinary Differential Equations and Differential-Algebraic Equations*, SIAM, Philadelphia., (1998).
- 34) Noghrehabadi A., Ghalambaz M., Samimi A., Approximate solution of laminar thermal boundary layer over a thin plate heated from below by convection, *J Comput Appl Research Mech Engg.*, 2013; 2, 54-57.
- 35) Anderson H. I., Slip flow past a stretching surface, *Acta Mechanica.*, 2002; 158, 121 - 125.
- 36) Aminreza N., Rashid P., Mohammad G., Effect of partial slip boundary condition on the flow and heat transfer of nanofluids past stretching sheet prescribed constant wall temperature, *Int J Therm Sci.*, 2012; 54, 253-261.

- 37) Sharma R., Ishak A., Pop I., Partial slip flow and heat transfer over a stretching sheet in a nano fluid, *Math Prob Engg.*, 2013; Article ID 724547.
- 38) Rosensweig R.E., Heating magnetic fluid with alternating magnetic field, *J Magn Magn Mater.*, 2002; 252, 370-374.
- 39) Nadeem S., Mehmood R., Motsa S.S., Numerical investigation on MHD oblique flow of Walter's B type nano fluid over a convective surface, *Int J Therm Sci.*, 2015; 92: 162-172.
- 40) Debnath L., On unsteady MHD boundary layers in a rotating flow, *Recent Research in Unsteady Boundary Layers*, Les Presses De L'Universit e Laval Quebec., (1972).
- 41) Sheikholeslami M., Hatami M., Ganji D.D., Nanofluid flow and heat transfer in a rotating system in the presence of a magnetic field, *J Mol Liq.*, 2014; 190, 112-120.
- 42) Takhar H. S., Nath G., Unsteady flow over a stretching surface with a magnetic field in a rotating fluid, *Z Angew Math Phys.*, 1998; 49, 989-1001.
- 43) Subhas A. M., Siddheshwar P.G., Nandeppanava M. M., Heat transfer in a viscoelastic boundary layer flow over a stretching sheet with viscous dissipation and non-uniform heat source, *Int J Heat Mass Transf.*, 2007; 50, 960-966.
- 44) Bataller R. C., Viscoelastic fluid flow and heat transfer over a stretching sheet under the effects of a non-uniform heat source, viscous dissipation and thermal radiation, *Int J Heat Mass Transf.*, 2007; 50, 3152-3162.
- 45) Kumaran V., Banerjee A.K., Vanav Kumar A., and Pop I., Unsteady MHD flow and heat transfer with viscous dissipation past a stretching sheet, *Int Commun Heat Mass*, 2011; 38, 335-339.
- 46) Sheikholeslami M., Ashorynejad H. R., Ganji D. D., Kolahdooz A., Investigation of Rotating MHD Viscous Flow and Heat Transfer between Stretching and Porous Surfaces Using Analytical Method, *Math Prob Engg.*, 2011; Article ID 258734.
- 47) Khan Z. H., Khan W. A., Qasim M., and Shah I. A., MHD stagnation point ferrofluid flow

- and heat transfer toward a stretching sheet, *IEEE T NanoTechnol.*,2014;13.
- 48) Fehlbberg E., Low-order classical Runge-Kutta formulas with step size control and their application to some heat transfer problems, NASA technical report,1969; R-315, Washington D.C.
- 49) John H., Mathews and Kurtis K. Fink, *Numerical Methods using MATLAB*, ISBN: 0-13-065248-2.
- 50) Press W.H., Flannery B.P., Teukolsky S.A., Vetterling W.T., Cambridge University Press, Cambridge, England., 1992; 704–716.
- 51) Timofeeva E.V., Routbort, J.L., Singh, D., Particle shape effect on thermophysical properties of alumina nanofluids, *J Appl Phys.*, 2009; 106, Article ID 014304.
- 52) Halelfadl S., Estelle P., Aladag B., Doner, N., Mare T., Viscosity of carbon nanotubes water-based nanofluids: Influence of concentration and temperature, *Int J Therm Sci.*, 2013; 71, 111-117.
- 53) Hongjie Dai., Carbon nanotubes opportunities and challenges, *Surf Sci.*, 2002; 500, 218–241.
- 54) Nan C.W., Shi Z., Lin Y., A simple model for thermal conductivity of carbon nanotube-based composites, *Chem Phys Lett.*, 2003; 375, 666–669.
- 55) Xue Q. Z., Model for thermal conductivity of carbon nanotube-based composites, *Physica B.*, 2005; 368, 302–307.
- 56) Wang J., Zhu J., Zhang X., Chen Y., Heat transfer and pressure drop of nanofluids containing carbon nanotubes in laminar flows, *J Exp Therm Fluid Sci.*, 2013; 44, 716–721.
- 57) Choongho Y., Li S., Zhen Y., Deyu L., Arunava M., Thermal conductance and thermopower of an individual single-wall carbon nanotube, *Nano Lett.*, 2005; Vol. 5, No. 9.



- 58) Hong H., Wright B., Wensel J., Jin S., Rong Ye X., Roy W., Enhanced thermal conductivity by the magnetic field in heat transfer nanofluids containing carbon nanotube, *Synthetic Met.*, 2007; 157, 437- 440.
- 59) Xie H., Lee H., Youn W., Choi M., Nanofluids containing multiwalled carbon nanotubes and their enhanced thermal properties, *J Appl Phys.*, 2003; 94 (8), 4967–4971.
- 60) Kim P., Shi L., Majumdar A., McEuen P. L., Thermal transport measurements of individual multiwalled nanotubes, *Phys Rev Lett.*, 2001; 87, 215502.
- 61) Kamali R., Binesh A.R., Numerical investigation of heat transfer enhancement using carbon nanotube-based non-Newtonian nanofluids, *Int Commun Heat Mass Transf.*, 2010; 37, 1153–1157.
- 62) Silotia P., Dabas S., Saxena A., Tewari S., On the Thermal conductivity of single-walled carbon nanotube ropes, *Soft Nanoscience Letters.*, 2013; 3, 7-10.
- 63) Bellman, R.E., Kalaba, R.E., *Quasilinearisation and nonlinear boundary-value problems*, Elsevier, 1965; New York.
- 64) Trefethen, L. N., *Spectral Methods in MATLAB*, 2000; SIAM.
- 65) Motsa, S.S., A new spectral local linearization method for nonlinear boundary layer flow problems, *J Appl Math.*, 2013; p. 15, ID 423628.
- 66) Motsa, S.S., Makukula, Z.G., Shateyi, S., Spectral local linearization approach for natural convection boundary layer flow, *Math Probl Eng.*, 2013; ID 423628, 92, 162-172.
- 67) Ishak A., Thermal boundary layer flow over a stretching sheet in a micropolar fluid with radiation effect, *Meccanica.*, 2010; 45(3), 367–373.
- 68) Aziz A., Hydrodynamic and thermal slip flow boundary layers over a flat plate with constant heat flux boundary condition, *Commun Nonlinear Sci.*, 2010;15, 573–580.



- 69) Mukhopadhyay. S., Gorla R.S.R., Effects of partial slip on boundary layer flow past a permeable exponential stretching sheet in presence of thermal radiation, *Heat Mass Transfer.*, 2012; 48, 1773–1781.
- 70) Mukhopadhyay. S., Slip effects on MHD boundary layer flow over an exponentially stretching sheet with suction/blowing and thermal radiation, *Ain Shams Eng J.*, 2013; 4, 485–491.
- 71) Kameswaran P.K., Sibanda P., Murti A. S. N., Nanofluid flow over a permeable surface with convective boundary conditions and radiative heat transfer, *Math Probl Eng.*, 2013; Article ID 201219.
- 72) Haq R.U., Nadeem S., Khan Z.H. , Akbar N.S., Thermal radiation and slip effects on MHD stagnation point flow of nanofluid over a stretching sheet, *Physica E* 65, 2015; 17-23.
- 73) Bejan A., Entropy generation minimization, CRC Press 1996; Boca Raton.
- 74) Sheikholeslami M., Ganji D.D., Entropy generation of nanofluid in presence of magnetic field using Lattice Boltzmann Method, *Physica A* 417, 2015; 273–286
- 75) Mahmoodi M., Kandelousi Sh. Analysis of the hydrothermal behaviour and entropy generation in a regenerative cooling channel considering thermal radiation, *Nucl Eng Des.*, 291, 2015; 277-286.
- 76) Ellahi. R, Hassan M., R., Zeeshan. A., Shape effects of nanosize particles in Cu-H₂O nanofluid on entropy generation, *Heat Mass Transfer.*, 2015; 81, 449–456.
- 77) Butt A.S., Asif A., Investigation of entropy generation effects in magnetohydrodynamic three-dimensional flow and heat transfer of viscous fluid over a stretching surface, *J Braz Soc Mech Sci Eng.*, 2015; 37, 211–219.
- 78) Suriya U. D. S., Anjali S.P.D, Numerical investigation on three dimensional hybrid Cu – Al₂ O₃/ water nanofluid flow over a stretching sheet with effecting Lorentz force subject to Newtonian heating, *Can J Phys.*, 2015; 0799.

79) Ferdows M., Al-Mdallal Q. M., Effects of order of chemical reaction on a boundary layer flow with heat and mass transfer over a linearly stretching sheet, AJFD., 2012; 2(6), 89-94.

